FLORIDA INTERNATIONAL UNIVERSITY

Miami, Florida

CROSS-DISCIPLINARY IMAGE-BASED APPROACHES FOR HERITAGE ANALYSIS AND PRESERVATION

A dissertation submitted in partial fulfillment of

the requirements for the degree of

DOCTOR OF PHILOSOPHY

in

CIVIL ENGINEERING

by

Mohammad Ibrahim Abu-Haifa

2023

To: Dean John L. Volakis
College of Engineering and Computing

This dissertation, written by Mohammad Ibrahim Abu-Haifa, and entitled Cross-Disciplinary Image-Based Approaches for Heritage Analysis and Preservation, have been approved in respect to style and intellectual content, and it is referred to you for judgment.

We have read this dissertation and recommend that it be approved.

_____
Armin Mehrabi

_____
David Garber

_____
Nipesh Pradhananga

_____
Seung Jae Lee, Major Professor

Date of Defense: June 26, 2023

The dissertation of Mohammad Ibrahim Abu-Haifa is approved.

_____
Dean John L. Volakis
College of Engineering and Computing

_____
Andrés G. Gil
Vice President for Research and Economic Development
and Dean of the University Graduate School

Florida International University, 2023

DEDICATION

To my parents, whose unconditional love, sacrifice, and guidance have been my source of strength and inspiration throughout my life. Your wisdom, values, and hard work have instilled in me a passion for lifelong learning and a commitment to excellence that will always guide me in my endeavors.

To my lovely wife, Hala, whose patience, understanding, and companionship sustained me through the ups and downs of this journey. Your love and support have given me the courage to pursue my dreams and overcome every obstacle on my way.

To my son, Ibrahim, whose innocent smile, playful spirit, and curious mind have filled my life with joy, purpose, and wonder. You are my inspiration, my motivation, and my greatest achievement. Every moment with you is a reminder of the preciousness of life and the importance of leaving a positive impact on the world for future generations.

To my brother, sisters, family, friends, and mentors who stood by me every step of the way. This journey would not have been possible without your unwavering support, encouragement, and belief in me.

I humbly dedicate this dissertation to all of you, with profound gratitude and appreciation for everything you have done to make me the person and the scholar I am today. May this work contribute to the advancement of knowledge and the betterment of society in meaningful ways, and may it inspire others to pursue their dreams with passion, perseverance, and dedication. Here's to the future, and the many exciting possibilities it holds.

ACKNOWLEDGMENTS

I would like to express my sincere gratitude to my major professor, Dr. Seung Jae Lee, for his unwavering support, encouragement, and guidance throughout my doctoral journey. His expertise, insights, and mentorship have been instrumental in shaping my research and professional development. Sometimes ‘thanks’ is not enough to express our feelings, but he should know that I am truly grateful for working under his supervision.

I extend my heartfelt thanks to my committee members, Drs. Armin Mehrabi, David Garber, and Nipesh Pradhananga, for accepting to evaluate this dissertation, and for their valuable feedback, constructive criticism, commitment, support, and inspiration throughout my research journey. I would also like to thank my current and former colleagues for their help during this journey.

I am highly appreciative of the Dissertation Year Fellowship (DYF) and Doctoral Evidence Acquisition (DEA) Fellowship provided by the University Graduate School at FIU, which enabled me to focus on my research, complete my dissertation successfully, and gain invaluable academic and research experience.

Lastly, I would like to acknowledge the generous support of the funding agencies that provided financial assistance for my research, including the National Center for Preservation Technology and Training of the US National Park Service (NPS) under award P19AP00141, and the US National Science Foundation (NSF) under award 1635378, which helped me to carry out my research and publish my findings. The views and opinions expressed in this dissertation are those of the author and do not reflect the position of the funding agencies. Also, thanks to Miss Priya Tripathi for providing Figure 4.2.

ABSTRACT OF THE DISSERTATION

CROSS-DISCIPLINARY IMAGE-BASED APPROACHES FOR HERITAGE ANALYSIS AND PRESERVATION

by

Mohammad Ibrahim Abu-Haifa

Florida International University, 2023

Miami, Florida

Professor Seung Jae Lee, Major Advisor

Preserving our cultural heritage requires ensuring the protection and maintenance of its tangible aspects such as historic structures and artworks. Therefore, their comprehensive analysis is a critical step towards their preservation. This study focuses on two key areas: unreinforced masonry structures and the craquelure patterns found in historic paintings by presenting two novel image-based analysis frameworks with the goal of developing more effective methods for preservation and restoration. The first framework utilizes image processing techniques, impulse based dynamics, and discrete element method, resulting in a streamlined methodology for efficient vulnerability assessment of masonry structures. The framework involves using several techniques such as image segmentation, polygon approximation, and geometric analysis methods. The splitting and Douglas-Peuker polygon approximation methods are adopted to enhance computational efficiency of the analysis. Even if the splitting method slightly outperforms Douglas-Peuker method, results show that both methods can simplify brick shapes with a high-fidelity level. This framework is applied on a real single-wythe masonry structure, Stylite Tower in Jordan, to examine its applicability, by investigating the impact of an earthquake of a magnitude 7

Richter on the structure, which can provide critical domain knowledge that can be useful for disaster preparedness.

This dissertation also highlights a phenotypic trait of historic paintings. This approach uses image processing techniques to convert the craquelure image into binary image, where the islands are presented in white pixels and the cracks in black. Then, geometric analysis is conducted by converting each island into a polygon and finding its area and perimeter. The obtained data are plotted in a log-log scale, where the *x*-axis represents perimeter/area and the *y*-axis represents the area, and the probability distribution of the data are determined in terms of bivariate ellipses. Results show that image processing helps in investigating dating and provenance of craquelure patterns, as they have a phenotypic trait, which can aid historians preserving ancient artworks. Also, it is noted that when historic paintings are from the same origin and time period, they are more likely to exhibit similar craquelure behavior.

Overall, the research makes significant contributions to the fields of engineering and art preservation.

TABLE OF CONTENTS

CHAPTER PAGE

LIST OF TABLES

TABLE PAGE

LIST OF FIGURES

FIGURE PAGE

CHAPTER 1 . INTRODUCTION

This dissertation explores the use of image-based analysis for the evaluation and preservation of two types of cultural heritage materials - historic masonry structures and paintings with craquelure patterns. The research questions addressed in this dissertation are how image-based analysis can be used to study the structural aspects of masonry structures and the visual aspects of craquelure patterns on historic paintings. Despite their differences in nature and materiality, these two heritage materials share a common need for evaluation and preservation, and the use of image-based analysis offers a promising approach to meet these needs.

1.1 Analysis of Masonry Structures

1.1.1 Masonry as structural material

Masonry is a commonly used structural material that consists of units made from materials such as brick, stone, or concrete blocks and bound together using a joint material like mortar (Praseeda et al. 2015). Mortar is typically made of cement, sand, and water (Muhit et al. 2014). One of the primary advantages of masonry is its strength, durability, and fire resistance, making it a popular choice in construction (Hendry 2001). Masonry structures are known for their load-bearing capacity (Bakeer 2016), and they are used to support walls, foundations, and arches among other structural elements (Zhang et al. 2018). Facades are another popular application of masonry, where the material's weight and durability make for long-lasting and protective facades (Ferreira et al. 2014). It is also used in the construction of retaining walls for soil stabilization and flood protection (Pulatsu et al. 2021).

Masonry's thermal mass can also aid in energy efficiency by stabilizing interior temperatures, and reducing the need for heating or cooling (Ismaiel et al. 2022; Zedan et al. 2016). Although the initial cost of masonry construction can be high (Marques and Lourenço 2014), it is often seen as a long-lasting and low-maintenance option (Abdelrahman et al. 1993; Nayak and Dutta 2016). The fire-resistant nature of masonry also makes it ideal for constructing fire-resistant walls and partitions, chimneys, and fireplaces, as it can effectively withstand high temperatures (Lawrence and Gnanakrishnan 1987; Russo and Sciarretta 2013). The compressive strength and rigidity of masonry make it an excellent choice for resisting vertical loads (Cavaleri et al. 2005; Zampieri et al. 2020). However, because masonry is not a flexible material, its ability to resist lateral forces is limited and requires additional measures to prevent collapse during natural disasters, such as earthquakes (Kappos et al. 2002; Yi et al. 2006).

There are several types of masonry, each with unique properties and characteristics. Brick masonry is the most common type of masonry and is made from clay that is formed into rectangles and then baked at high temperatures (Furtado et al. 2020). Stone masonry involves using natural stones, such as granite, limestone, or sandstone, to create walls and other structures. This type is common in monumental and historic heritage (Angiolilli et al. 2021; Juhásová et al. 2008). Finally, concrete block masonry is another type of masonry material, which uses precast concrete blocks to build walls and other structures. This type is common in building the partitions and façades (Brocken and Nijland 2004).

1.1.2 Historic masonry structures

Historic masonry structures are a vital part of human history and our built environment, serving as testaments to the artistic and architectural achievements of different cultures. These structures were constructed using different types of masonry materials and are known for their durability, strength, and inherent beauty. They have stood the test of time and have witnessed major historical events, serving as visual records for future generations (Krentowski et al. 2023).

Historic masonry structures are considered as cultural assets that have a scientific value, as they provide valuable historical, engineering, and architectural information, which enables researchers and engineers to better understand the techniques and materials used in the past (Binda et al. 1997). These structures have been the focus of many preservation and restoration projects, not only to maintain their integrity but also to understand better the techniques that enabled their original builders to create such long-lasting structures, which have remained durable over centuries (Klusáček et al. 2021; Wilmers 2012).

Historic masonry structures are also substantial evidence of the cultural, economic, social, and intellectual foundation that contributes to the formation of society and the development of civilization (Hendry 2001; Kemp 2006; Trigger et al. 1983). In many cases, these structures may hold great significance to the people who occupied them, served as places of religious worship, or city halls, museums, and other government buildings, or the birthplaces of significant personalities in history (D'Amato and Sulla 2021). Therefore, they often serve as landmarks that draw visitors from around the world, contributing to economic development through tourism revenues (Petroman et al. 2020; Vicente et al.

2018). Thus, they are significant to world heritage preservation, and maintaining and conserving them is a responsibility shared by the present and future generations.

1.1.3 Bonds in masonry structures

Bonds are an essential aspect of masonry structures and considered one of the significant building components that provide strength and durability (Sarangapani et al. 2005). The bond is the arrangement of masonry units (e.g., bricks or stones) in a specific sequence to form a structural pattern. Bonds strengthen the masonry structure by transferring the load from one unit to the other and distribute the stress evenly to reduce cracking or failure. Hence, good bonding is critical for the stability, safety, and resistance of the structure as it creates a robust and stable connection between masonry units to resist the stresses and movements that occur in a structure (Zhang and Beyer 2019). Without proper bonding, a masonry structure can experience cracks, movements, and shifting, and loss of load-bearing capacity, even when subject to minor stresses (Hossain et al. 2016). Therefore, the appropriate selection and execution of bonds are crucial in ensuring the safety and longevity of the structure, as their significance in masonry structures cannot be overstated (Foraboschi 2019).

Different types of bonds have been used throughout history to create stable and aesthetically appealing masonry structures. Some types of bonds include the common bond, stretcher or running bond, English bond, Flemish bond, and stack bond (Reid 2004). Figure 1.1 illustrates how the bricks are arranged in these types. Each bond type has unique advantages and limitations in terms of functionality, strength, and appearance, as well as effects on structural behavior and stability (Ahiwale et al. 2023). Therefore, selecting the

appropriate bond depends on the intended use of the structure, its location, design, size, and shape (Basha et al. 2022).

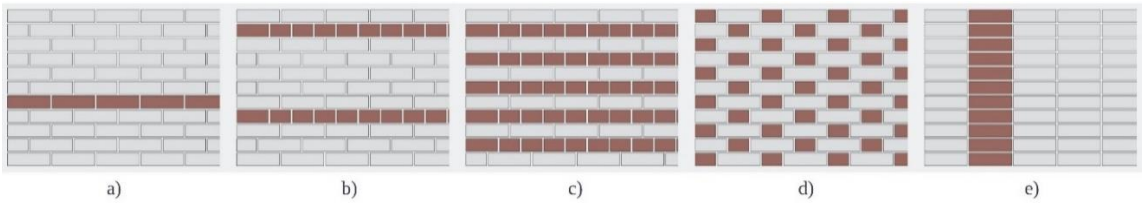

Figure 1.1. Several types of bonds in masonry walls; a) running, b) common, c) English, d) Flemish, and e) stack (Archtoolbox 2023); Images reused with written permission from Archtoolbox.

1.1.4 Vulnerability assessment of masonry structures

Despite its strength and durability, masonry structures are still susceptible to a range of risks that can affect their integrity and stability, lead to their failure, reduce their longevity, and increase the chances of harm (Micelli and Cascardi 2020). These risks can include natural hazards such as earthquakes, floods, and windstorms, as well as human-made risks such as poor maintenance, lack of proper building codes enforcement, or terrorist attacks (Micelli and Cascardi 2020; Nayak and Dutta 2016). The mortar and the bricks are both known to be "quasi-brittle materials" whose mechanical performance could be affected under seismic loadings, making unreinforced masonry structures extremely vulnerable to earthquakes. Due to the lack of a strong connection between structural elements and the insufficient stiffness of horizontal floors, unreinforced masonry structures are also very vulnerable to lateral cyclic loads that include the combined in-plane and out-of-plane collapse mechanism and out-of-plane bending behavior of walls (Bruneau 1994; Roca et al. 2010; Valluzzi and Sbrogiò 2019). Figure 1.2 shows the distribution of unreinforced masonry structures in relation to other structural systems in European nations.

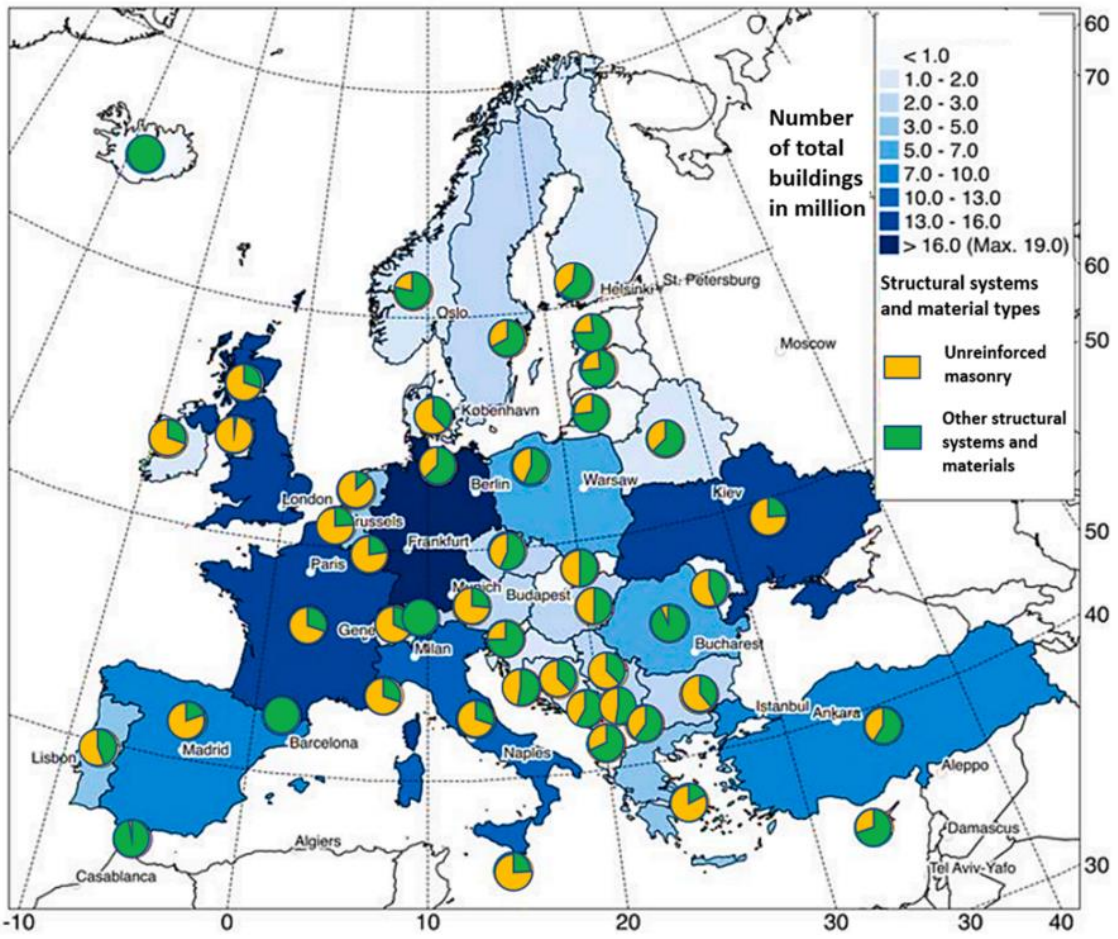

Figure 1.2. An approximate map of the distribution of unreinforced masonry structures and the number of all buildings in European countries (Shabani et al. 2021).

As masonry structures age, they also become more susceptible to risks such as structural deterioration, foundation settlement, and deformation (Tumialan et al. 2001). Given the risks that can affect masonry structures, it is essential to conduct vulnerability assessments to evaluate their overall safety and risk. A vulnerability assessment is an essential part of the risk management process, providing a systematic and comprehensive evaluation of the structure's potential vulnerability, identifying its critical components, and assessing the likelihood and potential consequences of risk scenarios taking place to create an effective risk management strategy to reduce these risks (Moret 2014). This can ensure that masonry

structures continue to stand the test of time, preserving cultural heritage, and protecting people's safety (Asteris et al. 2019; Shabani et al. 2021).

By conducting a vulnerability assessment, engineers can evaluate the building's structural capacity and functionality, its level of maintenance, and the degree of seismic risk in the location (Shabani et al. 2021). Through this process, engineers can identify the critical components, which may need reinforcement or rehabilitation, as well as where maintenance or retrofitting work is necessary to reduce the risks and maintain the structure's integrity. By doing this, the safety and longevity of masonry structures can be taken care of, helping to ensure their safeguard for future generations.

1.1.5 Numerical simulations for masonry structures

Numerical simulations are an effective tool for the evaluation of risks in masonry structures. Numerical simulations are virtual models that replicate the behavior of real-world masonry structures under different conditions, such as earthquake loading, wind loads, and extreme weather conditions, among others (Brunelli et al. 2021; Pellegrini et al. 2023; Penna et al. 2016; Vemuri et al. 2018). One of the key advantages of numerical simulations is their ability to provide accurate and detailed information on the behavior of different components of masonry structures, such as walls and arches to identify potential failure points, opportunities for structural upgrading, and recommendations for structural strengthening, retrofitting, and maintenance to reduce risks and manage the overall safety (Wang et al. 2018a). They can evaluate the capacity, functionality, and efficiency of the structure, as they can run through multiple scenarios, which is especially useful for assessing risks of natural hazards such as earthquakes (Brunelli et al. 2021). Compared to

traditional physical testing, numerical simulations are cost-efficient, fast, and provide a high-level of accuracy (Diz et al. 2015). They also offer a dynamic visualization of structural response (Kaya et al. 2023), which makes it easier for engineers and stakeholders to understand and determine the potential consequences of decisions made on the structure.

There are two main types of numerical simulation methods that can be used to assess the vulnerability of masonry structures. These include i) the finite element method (FEM), and ii) the discrete element method (DEM) (Lourenço 2002). FEM is used in assessing the vulnerability of masonry structures by analyzing stress and deformation of masonry structures under different loads (Theodossopoulos and Sinha 2013). FEM models masonry walls as a continuous material with finite numbers of elements (Lee and Hashash 2015). FEM has a well-established theoretical background with a significant number of previous studies on its application in masonry structure for (Tzamtzis and Asteris 2003). However, FEM in masonry structures is limited in the sense that it doesn’t model the interaction between individual blocks (Lee and Hashash 2015). It also cannot account for the complex behavior of joints and connection elements, which can affect masonry walls' performance under loads (Lemos 2007). On the other hand, DEM can be used to model the behavior of masonry walls as a system of discrete interacting elements, by simulating the behavior of each individual brick (Abu-Haifa and Lee 2022). The method can also predict the behavior of masonry walls under various loading conditions, including static, dynamic, and seismic loads (Pulatsu et al. 2016). The main advantage of DEM is its ability to model the complex behavior of masonry structures, including their realistic geometric shapes and material heterogeneity (Pulatsu et al. 2016). In addition, DEM can simulate the interaction of individual blocks, joints, and cracks, providing more accurate and detailed results of

masonry wall performance under different conditions (Abu-Haifa and Lee 2022). However, the selection of the appropriate simulation method highly depends on the research question, the purpose of the analysis, the complexity of the structure, and the data available (D'Altri et al. 2020).

As DEM gives more accurate and realistic simulation results, it has been widely used to model and analyze the behavior of masonry structures, and it is increasingly becoming common in several applications. These applications include structural analysis, failure mechanism investigation, material characterization, and optimization studies. For the analysis, it has been used to study the strength and deformation of several elements in the structure such as arches and vaults (Fang et al. 2018), domes (Paris et al. 2020), and wall panels (Baraldi et al. 2018). Furthermore, it has been employed in masonry structures to investigate the formation and propagation of cracks, slip of bond interfaces (Bui et al. 2021; Pulatsu et al. 2016), debonding of connections (Petersen 2009), and the mechanisms of aging and deterioration of historic buildings under different load scenarios (Pulatsu et al. 2016). DEM can also provide valuable information about the micromechanical behavior of masonry structures by analyzing the behavior of individual bricks (Pepe et al. 2020), assessing their fracture and deformation properties (Pulatsu et al. 2020), and exploring the material parameters of masonry structures such as tensile strength (Pulatsu et al. 2019), shear strength (Cuong et al. 2022; Petersen 2009), and elastic modulus (Radi et al. 2019). Lastly, optimization studies have been conducted using DEM to find the optimal design of masonry structures under various performance criteria such as safety, cost, and energy use (Boni et al. 2019).

1.1.6 Imaging techniques in masonry structures

In the past, the assessment of masonry structures involved mainly visual inspection, which is subjective and limited in its ability to identify early-stage damage. Non-destructive testing (NDT) techniques based on various sensing modalities have thus been developed and employed to overcome this limitation in monitoring the structural health of masonry constructions (Martínez-Soto et al. 2021). Among these NDT techniques, imaging techniques have emerged as a powerful tool for monitoring the health of masonry structures. The use of imaging techniques allows for non-invasive and non-contact damage detection over a large area by providing high-resolution and high-sensitivity imaging data (Popovics 2003). Imaging methods have shown great potential for detecting and characterizing various types of damage to masonry structures, including cracks, voids, and delamination, as well as for assessing the overall condition of these structures (Kassotakis and Sarhosis 2021). The use of imaging techniques in masonry structures for health monitoring is considered as a promising area of research since they have the potential to improve the safety and longevity of masonry structures (Loverdos et al. 2021).

The use of imaging techniques in masonry structures for health monitoring has several advantages as they: 1) are non-destructive, meaning that they do not require any physical alteration of the masonry structure being monitored (Popovics 2003). This makes it a useful tool for assessing the condition of culturally significant structures that cannot be altered, 2) can detect defects that are not visible to the naked eye, which can help prevent structural damage (Qiu 2020), and 3) can be used to monitor the health of the structures over time, which can help prevent costly repairs and maintenance (Pla-Rucki and Eberhard 1995).

However, each imaging technique has its advantages and limitations, making them useful in a variety of applications. Some of the most commonly used imaging techniques in health monitoring of masonry structures include infrared thermography (IRT), ground penetrating radar (GPR), ultrasonic testing (UT), X-ray imaging, digital image correlation (DIC), photogrammetry, acoustic emission testing, and laser scanning (Gupta et al. 2022; Kumar et al. 2019; Luo et al. 2021; Stavroulaki et al. 2016; Verstrynge et al. 2021).

Studies showed that numerical simulations can still be improved through the implementation of imaging techniques due to the detailed information that they can provide. For example, structure from motion (SfM) is a photogrammetric approach that uses digital images to reconstruct the 3D geometry of masonry structures (Schonberger and Frahm 2016). Through SfM, a series of images taken from different angles are used to triangulate common points and produce a 3D point-cloud of the structure, which can then be used to generate a 3D model of the structure (Iglhaut et al. 2019). Figure 1.3 presents an example for the use of SfM on the 3D reconstruction of a masonry bridge. The resulting 3D models can then be used to extract information such as brick sizes, shapes, and orientations, which cannot be easily obtained otherwise (Kassotakis et al. 2021). Once the 3D model is constructed, FEM and/or DEM simulations can be performed by using the model as an input (Kassotakis and Sarhosis 2021). This will automate the analysis, thus decrease the modeling time, and increase the model's accuracy and reliability, which lead to more accurate predictions of the strength, deformation, and damage evolution of masonry structures (Kassotakis et al. 2022). SfM also has the potential to incorporate quantitative image analysis to provide information on the structure’s surface roughness, efflorescence, voids and damage locations, and alteration patterns, which can also be input

directly into the FEM and/or DEM models to simulate more realistic boundary conditions for the walls (Ellenberg et al. 2014; Valero et al. 2019; Wang et al. 2019a).

Figure 1.3. A 3D dense point cloud for Jevington Church reconstructed using SfM (Green et al. 2014); Image reused with written permission from the publisher.

1.2 Craquelure Analysis of Historic Paintings

1.2.1 Craquelure patterns as a painting fingerprint

Craquelure is the network of fine cracks that develops on the surface of a painting over time as the paint dries and ages. Figure 1.4 presents an example of the cracks developed in the Mona Lisa with a typical pattern of small islands. The pattern of craquelure is unique to each painting and can be used to help authenticate it (Stork 2009). Craquelure analysis of historic paintings involves heritage material and its evaluation (like masonry structures). While masonry is an architectural material, and craquelures are a patina found on paintings, both are part of our cultural heritage and, as such, can provide perspective and insights into

our history. Additionally, both masonry and paintings with craquelure patterns can provide insights into the age, origin, and evolution of the structures or paintings. Performing craquelure analysis of paintings and risk assessment of masonry structures can play a crucial role in the historic preservation of our heritage environment. This is through their role in preserving the dates and origins of artworks and helping scholars to make informed decisions on the most appropriate preservation strategies. This can range from preventative measures such as changing the humidity and temperature of their storage environment, to recommendations for repairs and maintenance that can help to extend the life of the structure.

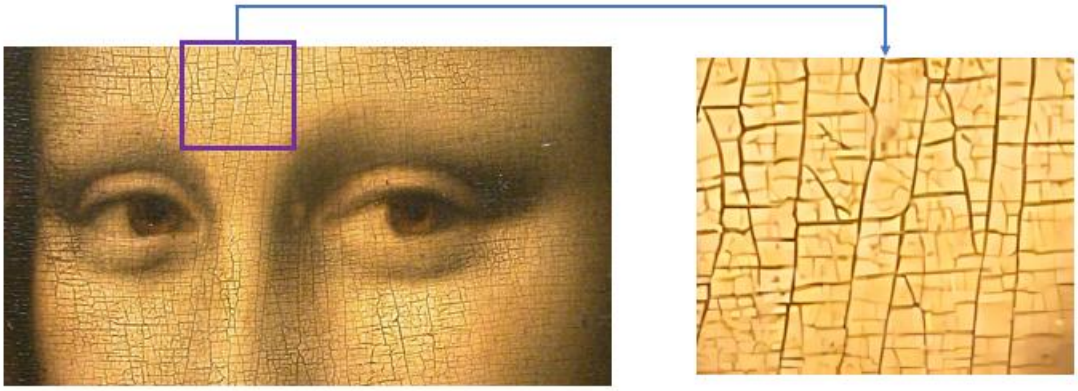

Figure 1.4. Crack pattern in the Mona Lisa with small islands.

In general, craquelure analysis is a non-destructive method of analysis that can provide valuable information about the age, authenticity, and provenance of paintings (Bucklow 1998). For example, if a painting is alleged to be a work by a particular artist, but the craquelure pattern does not match that of other known works by the artist, then it is likely a forgery (Taylor et al. 2015). Craquelure can also be used to date paintings, as the pattern changes over time, predict their origins as a country has its specific style and materials, and understand the artists' intentions (Bucklow 1999; Civil et al. 2002; Krzemień et al. 2016).

The descriptive method is a valuable tool for art historians to analyze painting craquelures using visual inspection to identify and describe the characteristics of craquelure patterns (Bucklow 1997). To use the descriptive method, art historians first need to carefully examine the painting.

Art historians look for some signs that may help such as:

- The materials used in the painting, such as the type of paint, canvas, or wood.
- The techniques used in the painting, such as the use of perspective, shading, and composition.
- The overall style of the painting, such as whether it is realistic, abstract, or somewhere in between.
- Any clues that can help identify the artist, such as a signature or a date.
- Any clues that can help date the painting, such as the fashions of the people depicted or the historical events that are depicted.

Additionally, they look for some characteristics of craquelure patterns including i) size and shape of the cracks, ii) direction of the cracks, iii) density of cracks, and iv) pattern of the cracks. These characteristics can provide clues about the type of paint used, the artist's painting technique, the age of the painting, the way the painting was stretched and hung, and the environment in which the painting was created or restored. For instance, once art historians have identified the characteristics of the craquelure pattern, they can then compare the pattern to the patterns of known works by the artist. If the craquelure pattern of a painting matches the patterns of other known works by the artist, then it is more likely

that the painting is authentic (Barron and Sharma 2020). However, it is important to remember that the descriptive method is just one tool that art historians use.

1.2.2 Image processing in craquelure analysis

In recent years, there has been a growing interest in using craquelure patterns for art authentication and dating. This is due in part to the development of new technologies that can help to analyze and visualize craquelure patterns. These technologies can be used to create detailed maps of craquelure patterns, which can then be compared to the patterns of known works of art (Kim et al. 2022). However, the use of craquelure patterns for art authentication and dating is still a developing field, but it has the potential to be a valuable tool for art historians and conservators (Bucklow 2020).

Image processing is a powerful tool that can be used to improve the accuracy and efficiency of craquelure analysis, and for art historians and conservators who are working to study and preserve paintings (Sidorov and Yngve Hardeberg 2019). Image processing can be used in craquelure analysis in several ways. For example, craquelure cracks can be difficult to see with the naked eye, especially on old paintings. Image processing can be used to enhance the visibility of craquelure cracks, making them easier to study (Abas 2004). Also, it can quantify the characteristics of craquelure cracks such as their size, shape, direction, and density (Kim et al. 2022). This information can be used to help identify the artist of a painting, to date a painting, and to authenticate a painting. Finally, image processing can help identify forgeries and to study the evolution of an artist's painting technique over time by comparing craquelure patterns between different paintings (Polak et al. 2017).

1.3 Objective and Scope

This dissertation focuses on two heritage subjects concerning unreinforced masonry structures and ancient paintings. The overall objective of this research is to develop an automated approach for analyzing 2D images of masonry structures to evaluate potential risks they face. Additionally, it aims to examine images of cracks found in art paintings in order to differentiate between genuine and counterfeit works, as well as determine the geographical origin of the painting. Although this study represents the initial stage in pursuit of its broader objective, it specifically concentrates on single-wythe masonry structures and a limited dataset of craquelure images. Future advancements in this research endeavor will lead to the creation of proficient tools that can be employed effectively in heritage preservation efforts. This study specifically aims to:

1. Develop a streamlined "Imaging-to-Simulation" framework, the first of its kind to use imaging results as an input for discrete element analysis of single-wythe masonry structures. This will transform visual recognition data into critical domain knowledge that we can use for disaster preparedness, which can improve the capabilities of the preservation practice for hazard vulnerability assessment. In this framework, the interactions between individual bricks are explicitly considered and the brick images are used as the input for the 3D polyhedral DEM simulation of the 3D masonry structures. A notable aspect of this framework is the utilization of a restricted set of images as input for reconstructing the 3D DEM model.
2. Investigate whether craquelure is a self-similar structure and whether the self-similarity characteristic is a distinctive feature of a craquelure pattern. In order to

accomplish this, a unique framework by Lee et al. (2022) proposed for mineral particles and is applied and modified to describe the islands that are encompassed by the painting cracks. The materials and methods used to create the islands in craquelure are the same, and all islands have the same origin and a shared history of drying and aging. These commonalities support to speculate that those islands might exhibit a phenotypic trait that is self-similar on various dimensions. In this study, image processing techniques are applied in an automated manner to segment images of craquelure and extract the geometric characteristics of each distinct island within the craquelure pattern. Subsequently, statistical analysis is performed on the resulting imaging data to explore the viability of employing these statistical features for distinguishing between craquelure patterns originating from different sources or origins. By leveraging image processing and statistical analysis, this investigation aims to contribute to the potential use of such techniques in differentiating between craquelure patterns based on their origins.

In addition, this dissertation has three significant aspects:

1. This study is the first of its kind to use one image per wall as an input and the outcomes of the image analysis for use as an input to the discrete element simulation. This deviation from other imaging techniques involving a larger number of input images, like SfM, distinguishes the novelty of this approach. Therefore, the outcomes will lead to an innovation in the digital reconstruction of 3D masonry structures and the preservation practice for effective hazard

vulnerability assessment of historic masonry structures as a part of unreinforced masonry structures.

2. This study maintains computational efficiency by simplifying the brick geometries to *n*-sided polygons, where *n* is much lower than the original required number of vertices, without affecting the simulation accuracy.
3. This study implements impulse-based dynamics, which is computationally more efficient than the conventional DEM, thus will significantly enhance the capabilities in the preservation practice for hazard vulnerability assessment. The ability of the country to retain its historic masonry heritage will benefit from this.
4. This dissertation improves the accuracy and efficiency of craquelure pattern analysis by employing image processing techniques. The analysis results of the craquelure images are used to improve the prediction of painting provenance.

1.4 Dissertation Organization

This dissertation is mainly composed of two parts. The first part of the dissertation (Chapter 2 and Chapter 3) aims to automatically develop a model for the simulation of risk assessment procedures of historic masonry structures, while the second part (Chapter 4) applies image processing techniques to identify features in craquelure patterns that aid in the preservation by helping identify the painting origins and historical period. This dissertation is written in the format of ‘paper-based dissertation’, where each individual chapter of this dissertation has either been published in a peer-reviewed journal, or currently under review for publication. However, minor changes have been made to the nomenclature and abbreviations in order to ensure consistency throughout the dissertation.

Additionally, a unified references list is provided at the end of the dissertation encompassing all chapters.

Chapter 1 provides a general introduction about masonry structures, image processing, numerical modeling, and craquelure analysis of paintings.

Chapter 2 discusses the work presented in Abu-Haifa and Lee (2022), which presents a streamlined image-based modeling-to-simulation framework for planar masonry walls. This framework can convert one masonry image into a 3D masonry model by using image processing, polygon approximation methods, and the scalable vector graphics (SVG) format as the final modeling format that is used in the DEM simulation. In this chapter, impulse-based dynamic simulation method is adopted to study the impact of an artificial earthquake on the developed model. This study also provides a comparison between two polygon approximation methods: the splitting and Douglas–Peucker methods.

Chapter 3 discusses the work presented in Abu-Haifa and Lee (2023). In this chapter, the developed framework in Chapter 2 is developed by considering a whole single-wythe masonry structure in the image-based modeling process. Here, the developed discrete element bricks are exported as ‘objects’ not ‘scalable vectors’, to fully automate the 3D modeling process. Similarly, the collapse scenarios from the input masonry wall images are estimated using impulse-based dynamics. The proposed framework is tested on a real existing single-wythe masonry structure, Stylite Tower in Jordan, to examine its applicability. Results show that an earthquake of a magnitude 7 on the Richter scale could potentially lead to the collapse of Stylite Tower.

In Chapter 4, image-based analysis of craquelure patterns in historic paintings is presented. This chapter shows that it's possible to apply the phenotypic trait of mineral particles with the enhancement of image processing to help in better describing the painting origins and ages. The method was tested on a dataset of paintings from different origins and time periods, and the results showed that paintings with the same origin and have a small age gap (e.g., same century) are most likely to share similar craquelure behavior. The findings of the chapter suggest that craquelure patterns can be used quantitatively as a reliable tool for determining the origin of paintings, and that the method could be used to help art historians and conservators to authenticate and provenance paintings.

Chapter 5 summarizes the major findings and contributions of this study toward improved heritage preservation practices. Also, some of the future recommendations for further improvement of the study are presented in this chapter.

CHAPTER 2 . IMAGE-BASED MODELING-TO-SIMULATION OF MASONRY WALLS

2.1 Introduction

Masonry structures represent a significant subpopulation of our built environment as well as the historic heritage. Many masonry structures have been damaged by various natural hazards including earthquakes, thermal stresses, foundation settlements, etc. (Micelli and Cascardi 2020; Nayak and Dutta 2016; Tumialan et al. 2001). For instance, Figure 2.1 shows masonry walls damaged by the 2016 Pawnee earthquake in Oklahoma and 2010 Canterbury earthquakes in New Zealand (Clayton et al. 2016; Dizhur and Ingham 2015).

(a) (b)

Figure 2.1. Masonry wall damaged by earthquake excitations: (a) the 2016 magnitude 5.8 Pawnee earthquake in Oklahoma (Clayton et al. 2016) and (b) the 2010 magnitude 7.1 Canterbury earthquakes in New Zealand (Dizhur and Ingham 2015); Image reused with the written permission from T. Clayton and D. Dizhur.

Some masonry structures were built as a part of critical infrastructure and often located in harsh environments exposed to surge, high winds, and other severe conditions. For example, Figure 2.2 compares 1934 and 2015 photos of Fort Jefferson, a masonry fortress built in the 1840s on the Dry Tortugas Island for coastal defense. A structural damage is

clearly visible near the cannon embrasure in the 2015 photo. The damage accumulation even accelerates due to the impact of changing climate that transforms the hazard type and intensity (National Park Service 2014) and it is important to predict the aggravating impact on the masonry structures.

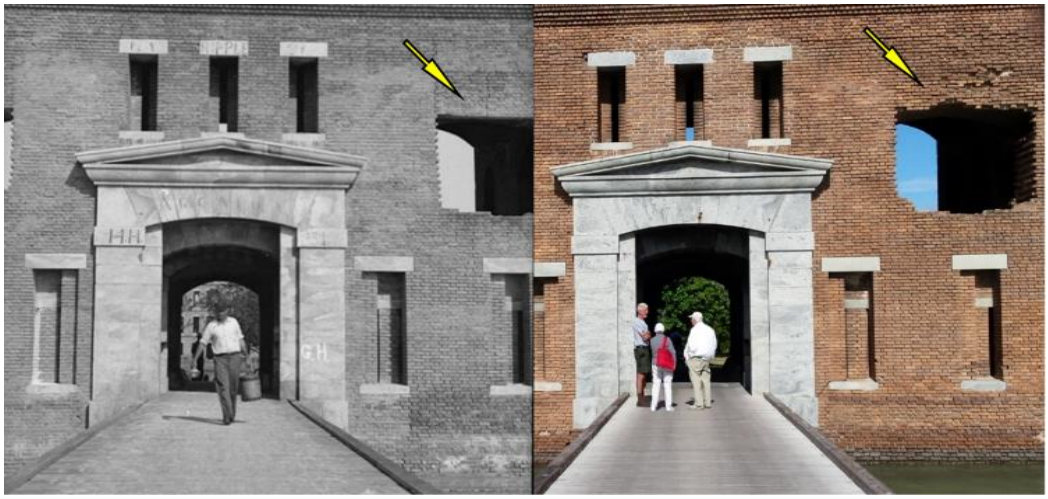

Figure 2.2. Fort Jefferson in 1934 (Peterson 1934) and 2015 (photo taken by Dr. Seung Jae Lee); The figure on the left is a public domain image from the Library of US Congress.

Masonry structures are inherently heterogeneous in the sense that they comprise the masonry units (i.e., bricks, blocks, and stones) and joints (i.e., mortar). Therefore, examining the composite properties as well as properties of units and joints helps to better assess the hazard vulnerability of masonry structures (Ghiassi et al. 2019). With recent advances of the image acquisition techniques, the research community has adopted image-based investigations to visually examine the sanity of masonry structure (Dunphy and Sadhu 2022; Loverdos and Sarhosis 2022; Nghiem et al. 2015), stochastically characterize the modulus of elasticity and the lateral capacity of unreinforced masonry walls (Falsone and Lombardo 2007; Gonen et al. 2021), quantify the texture irregularity of masonry walls (Almeida et al. 2016), detect cracks in masonry structures (Chaiyasarn et al. 2018), estimate

the homogenized elastic properties for quasi-periodic masonry structures (Sejnoha et al. 2008), and derive homogenized failure surfaces using a random media material-scale technique (Cavalagli et al. 2013).

The structure from motion (SfM) is a photogrammetric range-imaging technique that develops a 3D digital model using a set of images. With a reasonably large number of photos taken around an object, the SfM creates a dense point cloud that represents the object geometry with a high level of fidelity (Koutsoudis et al. 2014). Researchers proposed several SfM-based approaches for masonry structures (Pepe and Costantino 2020). For example, SfM has been employed to obtain the complex geometry of masonry structures (D'Altri et al. 2018), to quantify the impact of geometric uncertainty on the structural behavior of masonry arches (Kassotakis et al. 2021), and to monitor the temporal changes in the masonry facades (Liu et al. 2022b). The ground-based terrestrial laser scanning (TLS) also has been popularly used to capture the surface geometry of masonry structures (Błaszczak-Bąk et al. 2020; Nowak et al. 2022; Suchocki et al. 2018), to assess the behavior of historic masonry arch bridge (Batar et al. 2021), to perform the diagnosis of masonry building damage (Nowak et al. 2020), to measure damage on the masonry surface layers (Dais et al. 2021), and to track the moisture movement in the structures (Suchocki et al. 2018).

Recently, unmanned aerial vehicles (UAV) were introduced, and the integration of the imaging techniques into UAV was studied to better capture the geometry of masonry structures (Pepe and Costantino 2021). The UAV-based imaging approach was adopted to capture the geometry of masonry structure elements such as arch and pilaster (Pepe and

Costantino 2021), to evaluate the structural damage and material degradation (Biscarini et al. 2020; Cavalagli et al. 2020), to detect cracks on the surface of masonry structures (Ellenberg et al. 2016), and to study the behavior of masonry structures under lateral loading (Santini et al. 2022). Automatic edge detection from the point cloud data was also studied to identify the boundary of masonry walls, e.g., building openings. To this end, voxelization was performed on the point cloud, and the building opening was detected using an algorithm such as known-nearest-neighbors (Truong-Hong et al. 2013). The ground penetrating radar (GPR) was jointly used with terrestrial photogrammetry techniques to develop a realistic 3D digital model of masonry bridge. The GPR supplemented the information hard to obtain from the surface image of structures, e.g., the damages developed inside the masonry structure and displacements of the supports (Stavroulaki et al. 2016). In addition, a mobile-based brick detection method and deformation analysis were also proposed (Lindenbergh and Pietrzyk 2015; Riveiro et al. 2016). Recent developments adapting the Deep learning (DL) and Convolutional Neural Networks (CNN) techniques are gaining popularity in the image analysis of masonry structures (Chaiyasarn et al. 2021; Pushkar et al. 2018; Wang et al. 2018b, 2019b). For example, Dais et al. (2021) leveraged CNN to detect the cracks in the masonry images.

The techniques discussed above could be used to capture the surface geometry of masonry structures as-is. However, it is equally important to characterize the extent to how the masonry structure is vulnerable to anticipated hazards. For example, Cheomseongdae observatory located in Gyeongju, Korea, is one of the oldest stargazing masonry structures constructed in AD 647. Cheomseongdae recently survived the 2016 Gyeongju earthquake of magnitude 5.4 without major collapse, but a permanent displacement of 2 cm was

observed at the roof level (Park et al. 2019). Then we can ask ourselves what earthquake magnitude would make it collapse and how we can better underpin it. Numerical modeling can be employed to address these questions by simulating the structural behavior subjected to predictable hazards. Researchers could use the imaging data for the modeling, but most studies were limited to capturing the overall geometry of masonry structure without presenting the discrete nature of masonry structures. For example, a continuum-mechanics framework, e.g., the finite element method (FEM), was adopted for the image-based structural analysis of masonry structure (Castellazzi et al. 2015; Ioannides et al. 2012; Micelli and Cascardi 2020; Truong-Hong et al. 2013). In the FEM analysis, the interactions between individual masonry bricks, i.e., the discrete nature, could not be explicitly simulated, thus inherent limitations in assessing the hazard vulnerability that can lead to collapse. The discrete element method (DEM) is a suitable choice for the analysis of masonry structures as it explicitly considers the discrete nature by modeling the individual bricks and their interactions. The DEM has been widely adopted to analyze and predict the behavior of masonry structures (Bui et al. 2017; DeJong and Vibert 2012; Dell'Endice et al. 2021; Ghaboussi 1988; Lemos and Campos Costa 2016; Malomo et al. 2019; Masi et al. 2020; Pulatsu et al. 2018; Tóth et al. 2009). However, limited efforts were made to develop a 'image-based' DEM analysis due to the challenge to streamline the brick detection from masonry images to explicitly present the individual bricks in a DEM model. Recently, the concept of streamlined image-based DEM analysis was introduced (Ham et al. 2017) to estimate the potential risks associated with anticipated hazards at hurricane-prone construction sites.

The objective of this study is to introduce a streamlined image-based modeling-to-simulation framework for DEM analysis of planar masonry walls. In this framework, a photographic image is directly used as an input for the discrete element modeling of individual bricks and the simulation of the masonry behavior to an anticipated hazard is seamlessly conducted. This study focuses more on the image-based modeling part because the DEM simulation of masonry structures (the latter part) has been extensively studied in the research community as discussed above. The following section discusses the details of the proposed image-based modeling-to-simulation framework.

2.2 Image-based Modeling-to-Simulation Framework for Masonry Walls

An overview of the streamlined image-based modeling-to-simulation framework for vulnerability assessment of masonry structures is provided in Figure 2.3; (I) with raw photographic image obtained, (II) image segmentation of the masonry structure is performed, i.e., bricks in the images are detected; (III) the geometry of each brick is then extracted from the segmented image; (IV) the shape of each brick is approximated to a simpler polygon for computationally manageable DEM simulation; and (V) the 3D masonry model is constructed and the rigid body dynamic simulation is performed using DEM.

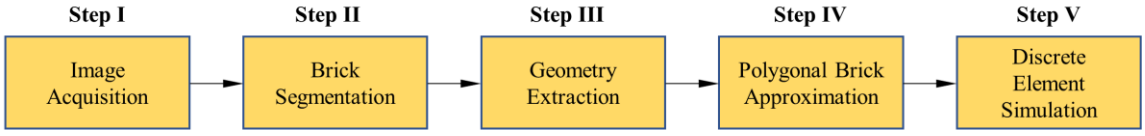

Figure 2.3. The proposed streamlined 'image-based modeling-to-simulation' framework.

MATLAB codes (MathWorks 2021a) are developed and integrated to streamline Step II to IV. Step V leverages the Blender (The Blender Foundation 2021a), a free and open-source

3D computer graphics software which the Bullet physics engine (Coumans 2020) is integrated into. The Bullet physics engine is an impulse-based dynamic simulation code which enables a 3D discrete element simulation of rigid polyhedral bodies. The following sections discuss each step of the framework applied for masonry wall images.

2.2.1 Image Acquisition (Step I)

A set of masonry images used in this study is shown in Figure 2.4. The masonry walls have regular or irregular brick shapes with a periodic or random arrangement.

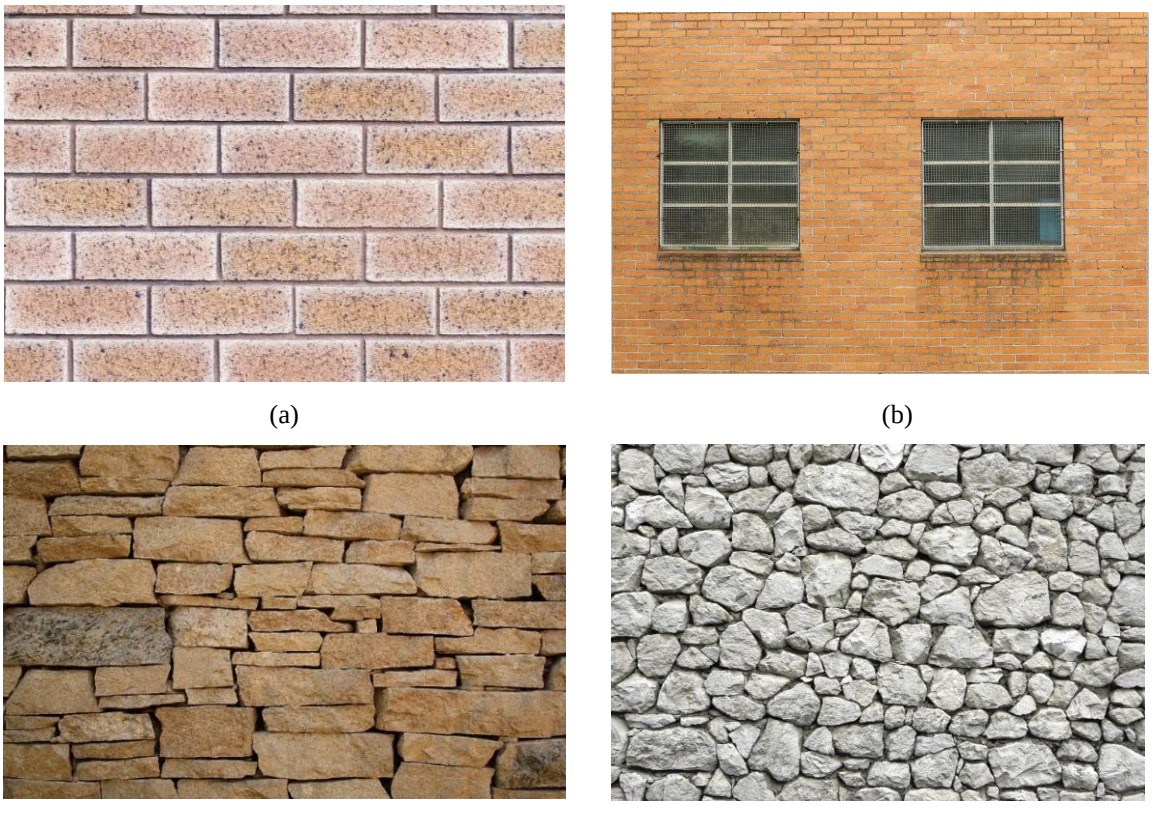

(a) (b)

(c) (d)

Figure 2.4. Masonry images used in this study: (a) A wall with a periodic arrangement of rectangular bricks (Shaun 2020); (b) A masonry wall with openings (Paine 2018); (c) A masonry wall with irregular-shaped bricks (Belemmi 2012); and (d) A rubble masonry wall with irregular-shaped bricks (Buzzle 2021).

2.2.2 Brick Segmentation (Step II)

The segmentation involves partitioning of an image into meaningful objects. This process labels every pixel in an image based on specific characteristics such as intensity, color, and texture. The results are sets of segments or contours. The image segmentation of masonry walls is to detect bricks and distinguish those from joints (mortar). Manual segmentation is impractical if there are many bricks in a masonry image as it is labor-intensive and time-consuming. Therefore, various algorithms were developed to automate the process. These algorithms typically used a converted black and white binary image from the original photo, thereby the bricks were represented as white pixels and the mortar was represented as black pixels. This study utilizes the Image Segmenter app (MathWorks 2021b) in the MATLAB image processing toolbox for the binary image-based segmentation of the masonry images. Several segmentation methods are implemented in the app, among which this study selectively adopts the flood fill, auto cluster, and active contour methods: The flood fill is a technique that segments areas with similar intensity values by which it determines regions connected to the seed points in a multi-dimensional array depending on a start node, a target color, and a replacement color (Lee and Kang 2010). The auto cluster and active contours are iterative methods that segment target image into foreground and background elements (Lei et al. 2019; Peng et al. 2009; Wang et al. 2017). This step conducts informed iterations to segment images in a cumulative manner, i.e., the methods are applied one at a time until bricks are properly segmented from each other.

When the raw image is first converted to a binary image for segmentation, some impurities may be generated as shown in Figure 2.5a and b. Black pixels are considered as mortar and

white pixels are considered as brick in the segmentation. Therefore, the code may recognize the small white impurities surrounded by black pixels as a part of brick or a small individual brick (Figure 2.5a). Likewise, the small black impurities surrounded by white pixels may be recognized as part of mortar (Figure 2.5b), which may create segmentation errors and may confuse the geometry extraction in later steps. A threshold method is developed to remove the white impurity pixels (Figure 2.5a) and a filling method (MathWorks 2021c) is used to remove the black impurity pixels (Figure 2.5b) before the final segmentation. The flowchart for the threshold method is shown in Figure 2.6 which is implemented in MATLAB. The step 1 in this threshold approach finds all clusters of white pixels, then counts the number of boundary pixels for each cluster. In the step 2, based on the number of boundary pixels of the white clusters, an initial guess is made regarding the threshold value for the smallest brick size. In the step 3, the algorithm removes all white pixel clusters with fewer boundary pixels than the threshold value. For example, if the smallest brick in the image is represented by 50 boundary pixels, a good initial guess of threshold value can be a number less than 50. If 30 is set as the threshold value, all white pixel clusters less than 30 boundary pixels are removed. In the steps 4 and 5, the algorithm checks if all white impurity pixels are removed while no real bricks are removed. If impurity exists, the threshold value is raised. If bricks are removed, the threshold value is lowered. This is an informed iteration process until all white impurities in the images are removed. Similarly, the fill method is used to remove the small black impurity pixels by filling all holes in the white clusters, in which a hole is defined as a set of black pixels that cannot be properly removed by filling in the background area starting from the edge of the image.

(a) (b)

Figure 2.5. Impurities in the binary images: (a) white impurity pixels in mortar (black) and (b) black impurity pixels in bricks (white).

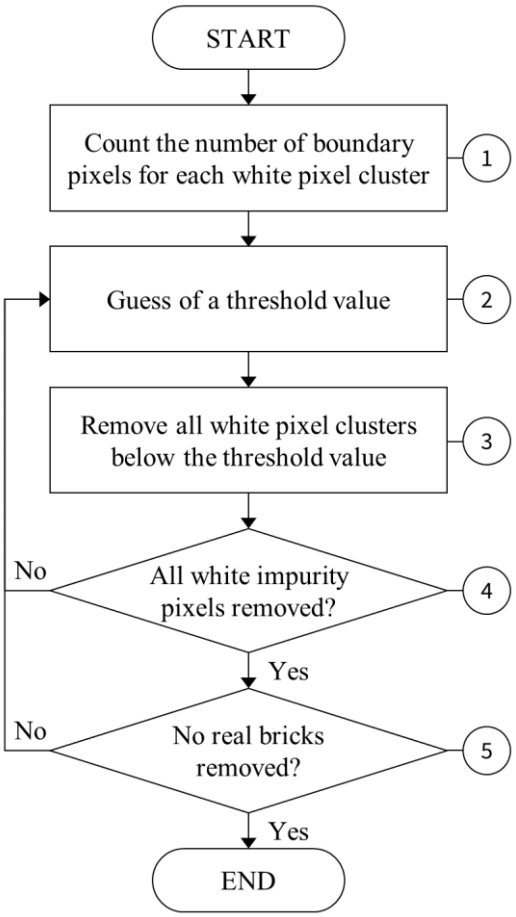

Figure 2.6. Flowchart for the threshold method to remove white impurity pixels; The step numbers are shown in the circles.

The resulting binary images after these impurity removals and the final image segmentation are shown in Figure 2.7 which indicates that the segmented regions and their boundaries are clearly identified. The bricks are shown in different colors, indicating the bricks are

properly segmented and recognized as individual objects. This study uses a 64-bit Windows 11 operating system with Intel Core i7-8565U Processor (1.8 GHz) and 8.0 GB of random-access memory (RAM). The time taken to extract the final segmented images is about 1 to 4 minutes: 1.3, 2.8, 2.3, and 3.8 minutes for Figure 2.7a, b, c, and d, respectively. The difference in time is attributed to the image resolution, size/number/shape of bricks, and difference in color contrast between bricks and mortar regions.

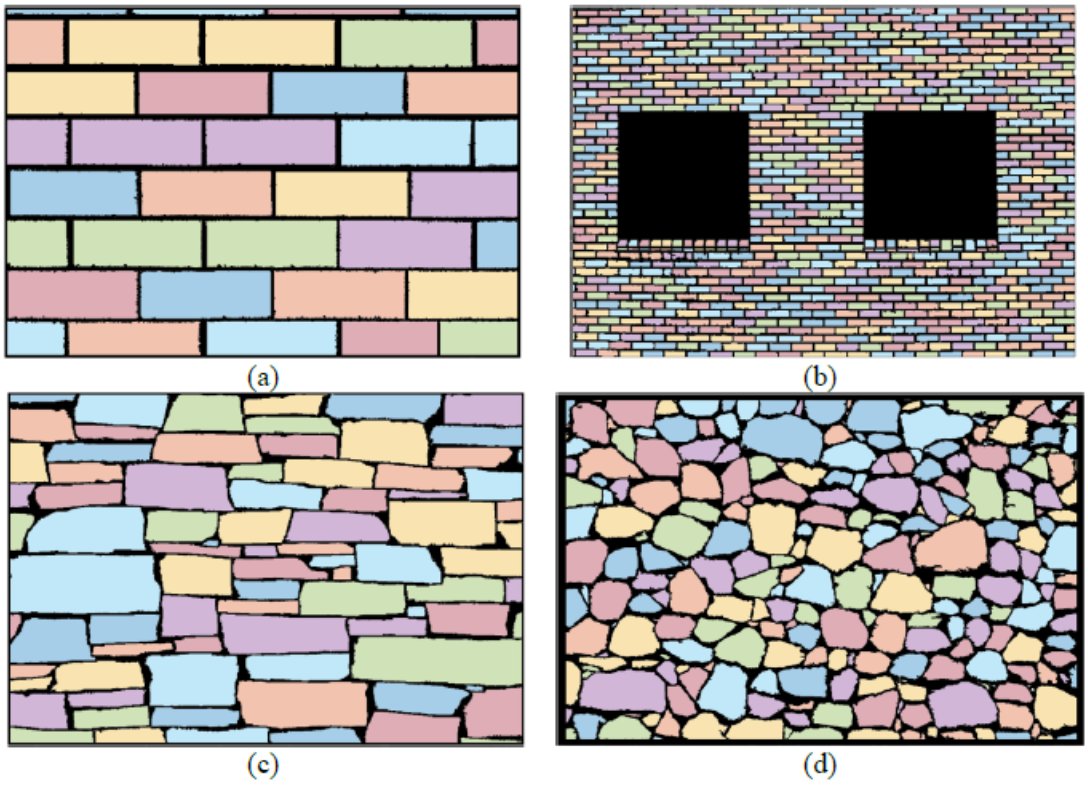

Figure 2.7. Segmented masonry wall images of: (a) Figure 2.4a, (b) Figure 2.4b, (c) Figure 2.4c, and (d) Figure 2.4d.

2.2.3 Geometry Extraction (Step III)

In Step III, the brick geometry is obtained by extracting the coordinates of each segmented brick's boundary vertices, for which the MATLAB boundary tracing function is used (MathWorks 2023a). Figure 2.8 shows an example where the captured brick geometry is

represented by a polygon with 576 vertices (in green). Figure 2.9 shows the result after the geometry extraction of all bricks (highlighted in green). These bricks (composed of black and white pixels) are converted into a set of irregular shaped polygons with boundary vertices.

Table 2.1 shows the average number of the vertices to represent each brick in Figure 2.9. Each brick polygon in Figure 2.9a is represented by more than 600 vertices because the bricks in the image are large (thus more pixels) despite simple rectangular shapes. Compared to Figure 2.9b and d, the larger brick size in the image results in a greater number of pixels and more vertices representing each brick. Likewise, the brick images in Figure 2.9c are overall the second largest, thereby the number of vertices is greater than Figure 2.9b and d.

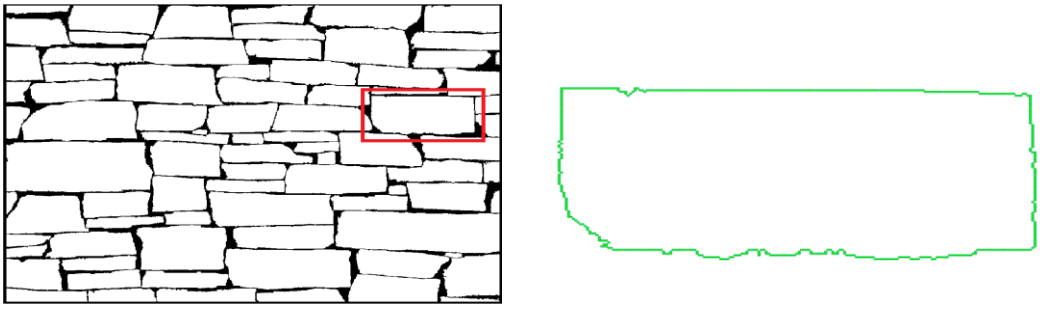

Figure 2.8. A brick represented as a polygon; the 576 vertices are shown as green points.

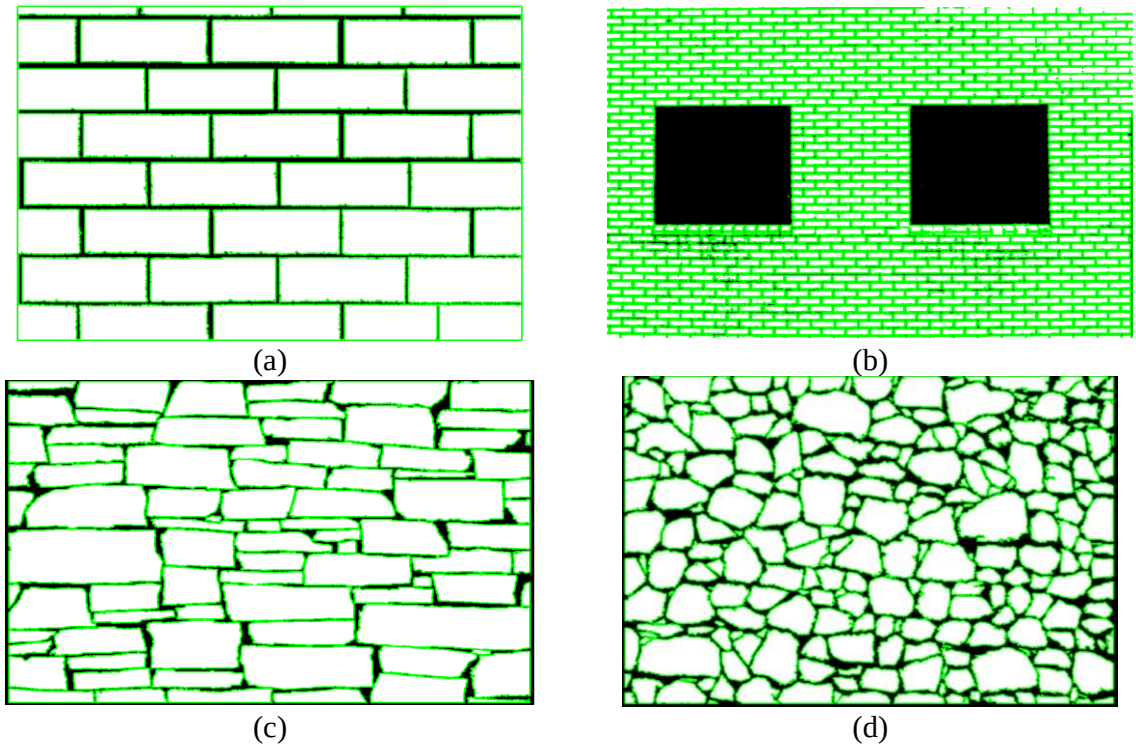

Figure 2.9. Extracted geometries from the masonry images (shown in green lines) of: (a) Figure 2.4a, (b) Figure 2.4b, (c) Figure 2.4c, and (d) Figure 2.4d.

Table 2.1. Average number of vertices to represent each brick.

	Figure 2.9a	Figure 2.9b	Figure 2.9c	Figure 2.9d
Avg. number of vertices	623.47	89.54	362.73	187.1

Considering individual brick is going to be presented as a polyhedral discrete element in Step V for rigid body dynamic simulations, it is necessary to represent the brick element with a reasonable number of vertices to maintain the overall computational cost manageable. The computational cost for contact detection in DEM significantly increases with the number of vertices of the discrete elements (Lee 2014). While the brick shape in Figure 2.9a can be reasonably represented with 4 vertices, modeling it with more than 600 vertices is clearly impractical. Therefore, shape approximation is considered to remove the redundant vertices and lower the computational cost required to run the discrete element analysis of modeled masonry walls. This shape approximation is conducted in Step IV.

2.2.4 Approximation of Brick Shapes to Simpler Polygons (Step IV)

This step approximates the brick shapes to simpler polygons. This study adopts two polygon approximation methods by Douglas and Peucker (1973), and Pikaz and Dinstein (1995) referred to as the splitting method.

The Douglas-Peucker (DP) method adopts an iterative end-point fitting approach that reduces the number of points according to a user-specified tolerance per the maximum Euclidean distance between a vertex and the approximated line. On the other hand, the splitting method iteratively divides the shape into two parts by finding a line that connects the two farthest points on the boundary. Therefore, the splitting method finds the point in each divided part that has the maximum perpendicular distance from the line. This process is repeated until the polygon is simplified to the specified target number of vertices. This study employs the MATLAB functions with the DP and splitting methods (Bone 2023; Schwanghart 2021). We apply these methods to simplify the brick shapes to a polygon with fewer vertices based on a predefined target. The approximation target compared to the original brick shape is evaluated in the sense of R^2 as in Equation (1), where X_i and Y_i are the coordinates of each boundary point of the original brick geometry obtained from Step III, while $\overline{X}$ and $\overline{Y}$ are the mean of the X and Y coordinates, respectively, for all boundary points of the original geometry. The number of points that represent the original shape of the brick is n, and d_i is the distance from each point of the original brick geometry to the closest boundary point on the approximated polygon.

$$R^2(\%) = \quad 1 - \frac{\sum_{i=1}^{n} d_i^2}{\sum_{i=1}^{n} |X_i - \bar{X}||Y_i - \bar{Y}|} \qquad (1)$$

The approximation algorithm (i) first tries with 4 vertices for the approximation and therefore simplifies the brick to a 4-sided polygon, (ii) evaluates R^2 and checks if the target R^2 is obtained. If not, (iii) an iteration is performed with an increased number of vertices until the R^2 value from the approximated polygon is greater than or equal to the target R^2 value. This approximation and evaluation are performed for every brick in the image. Figure 2.10 shows the approximated bricks from Figure 2.9a and c with the target of 98%. Both methods can reasonably approximate all bricks into an *n*-sided polygon with a much fewer number of vertices.

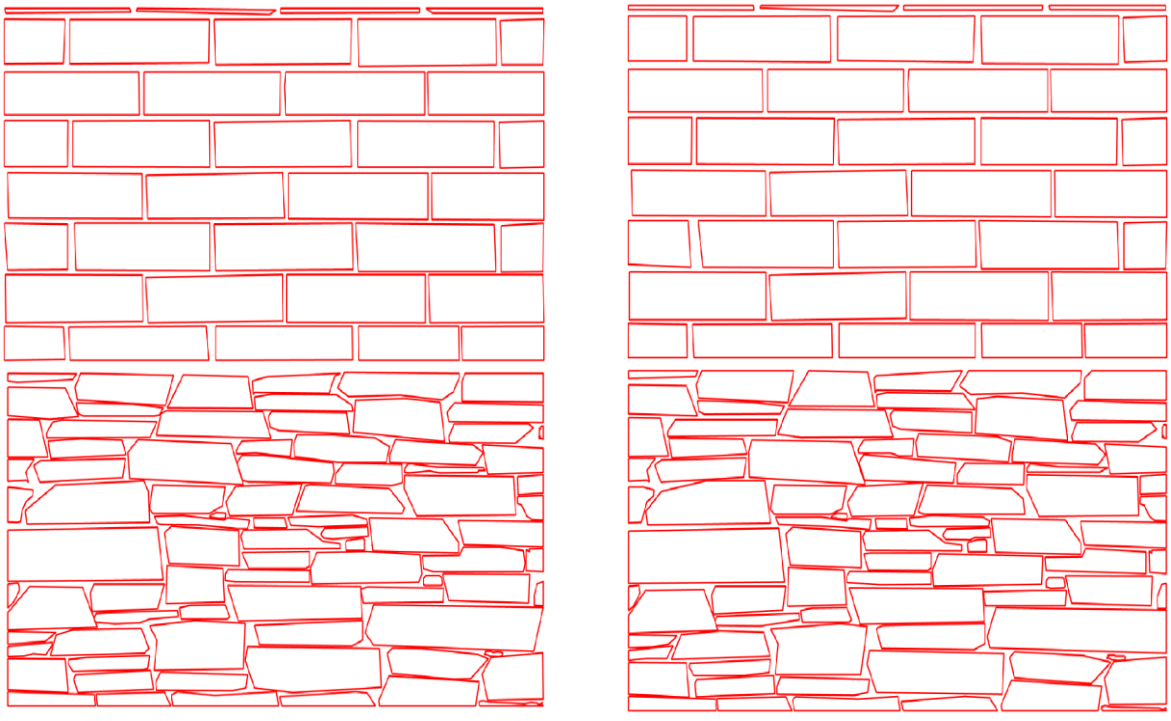

(a) (b)

Figure 2.10. Approximated brick shape (Figure 2.9a and c) to a simpler polygon with 98% target after applying the (a) DP and (b) Splitting methods.

The performance of the DP and splitting methods are compared in detail in Figure 2.11. A range of 98% to 99.5% target is considered. The number of vertices used to represent each polygon clearly tends to increase with the target R^2. The splitting method produces polygons with a slightly fewer number of vertices than the DP method, thus a better performance. However, both methods can represent the original shape with reasonably fewer vertices. Figure 2.9c and d tend to have a larger number of vertices after the approximation because of the more complex brick shapes that increases the number of vertices required to achieve the target R^2 value. Nevertheless, the proposed algorithm produces an accurate representation of these complex shapes with a reasonably small number of vertices less than about 10. Consequently, this approximation lowers the computational cost required for the 3D discrete element simulation in Step V. As the splitting method performs better, it is adopted to develop the 3D model for Step V.

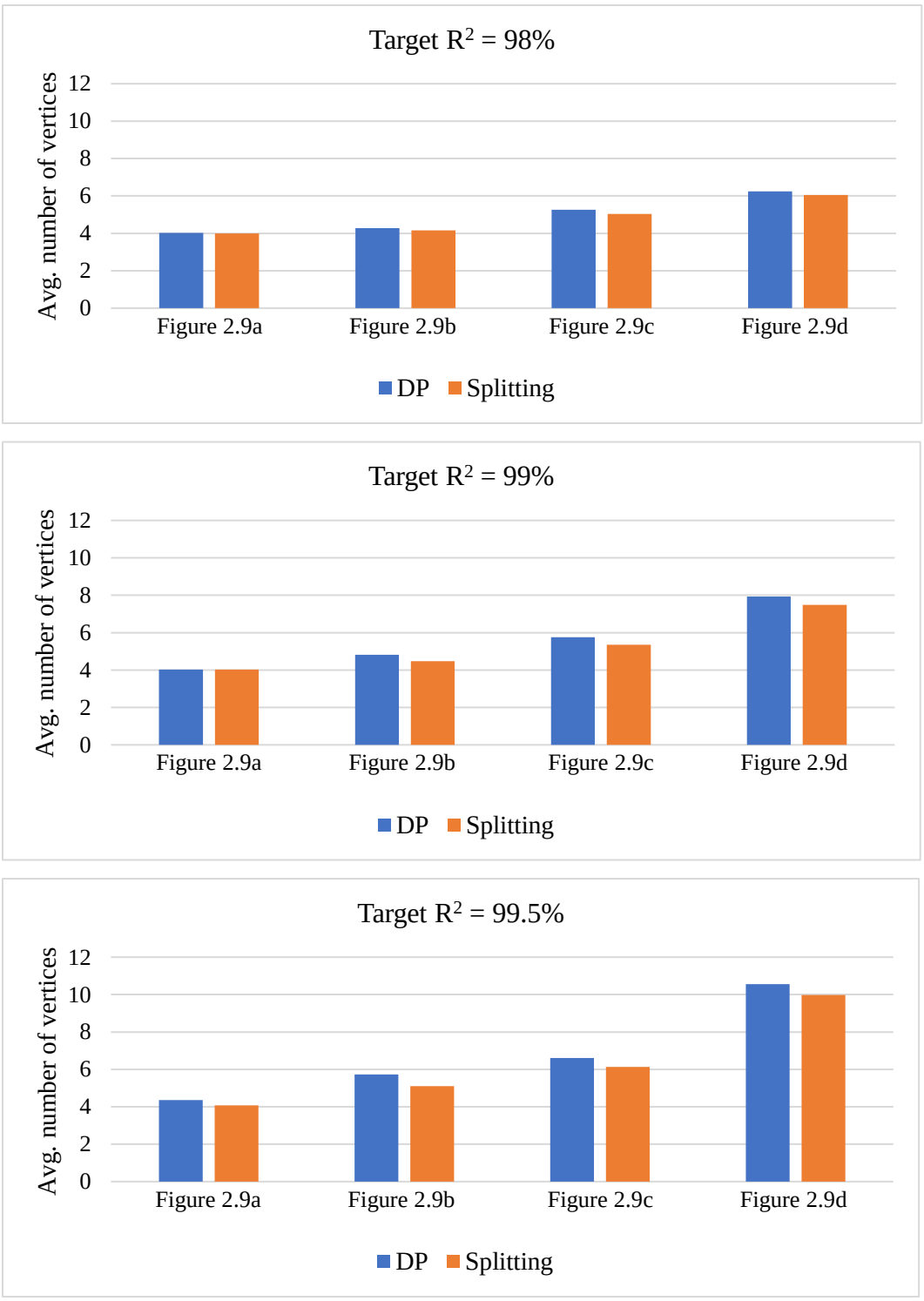

Figure 2.11. Average number of vertices of the approximated brick polygons by the DP and Splitting methods obtained at a different target R^2.

2.2.5 Discrete Element Simulation (Step V)

Step V first interprets each brick polygon obtained from Step IV into a scalable vectors graphics (SVG) format. SVG is an XML-based format that allows users to develop high-quality graphical models with a high level of geometric accuracy (Bowler et al. 2001). The SVG format can contain the information of shapes and their attributes (e.g., polygon geometry), which is different from bitmap image formats (e.g., PNG and JPEG) that consist of a fixed set of dots. The brick polygons in the SVG format are then imported to graphics software for 3D modeling. The Blender is used in this study which is a free and open-source 3D computer graphics software. The 2D polygons are extruded to 3D polyhedrons with a specified thickness in the Blender.

A set of physics engines including the Bullet (Coumans 2020) is integrated in Blender which enables a seamless modeling-to-simulation using the discrete element method (DEM). It is worth noting that DEM referred in this study is the DEM defined in a broader sense as proposed by Cundall and Hart (1992), not the original DEM by Cundall and Strack (1979) that was proposed as the 'distinct' element method. Cundall and Hart (1992) proposed that all numerical methods are collectively referred to as the 'discrete' element method (DEM) if the following two conditions are met: "(a) allows finite displacements and rotations of discrete bodies, including complete detachment, and (b) recognizes new contacts automatically as the calculation progresses." Cundall and Hart (1992) also discussed that there are four classes of DEM conforming to the definition, and one of those is the momentum-exchange method. The Bullet physics engine is an impulse-based dynamic simulation code for rigid polyhedral bodies which is based on the momentum-

exchange method (Augarde et al. 2021). This impulse-based (and velocity-based) dynamic simulation method is computationally more efficient compared to the original force-based (and acceleration-based) 'distinct' element method, and therefore it enables a faster dynamic discrete element simulation. This study adopts the impulse-based dynamic simulation method for the simulation of the masonry wall collapse. Please note the 'impulse-based method' does not mean the loading is impulsive, but which was named as the primary variable is the collision impulse, not the contact force. Impulse is defined as a time integral of force per the impulse-momentum theorem. Accordingly, the time integration scheme is different in the numerical methods: the impulse-based dynamic simulation method uses the first-order accurate symplectic Euler time integration, but the conventional DEM adopts the explicit central different time integration scheme. A detailed comparison of the impulse-based dynamic simulation method with the original DEM is provided in Lee and Hashash (2015).

The effect of mortar between bricks is modeled by setting up the constraints which can be seen as the virtual springs adopted to model the mechanical properties between the rigid bodies. Figure 2.12 visualizes the modeled constraints to present the mortar effects between modeled bricks. For example, the constraints can be modeled so that adjacent rigid bodies do not move towards each other but can be separated when the breaking threshold is exceeded. However, unlike the conventional DEM, the primary variable in the impulse-based dynamic simulation is the velocity and the collision impulse (that are computed from the change of relative velocities of the interacting bodies). Therefore, instead of directly manipulating the position properties of rigid bodies to satisfy the specified constraints, the velocity constraints are implemented to limit the freedom of movement of the objects that

are interacting with each other. This constraints-based modeling has been broadly adopted in the computer graphics community to create the complex interactions including springs, hinges, pulleys, etc. (Bender et al. 2014; Erleben et al. 2005; Sauer and Schömer 1998). This study models a set of linear and rotational constraints in the volume between the bricks to present the mortar effects. The Bullet Constraint Builder (Kostack 2021), a Blender add-on, is adopted for the constraint modeling. The interactions of neighboring bricks are simulated through the modeled constraints and the bricks are separated based on the modeled breaking threshold. The compressive, shear, and tensile breaking thresholds of the modeled constraints are 10 N/mm^2, 0.3 N/mm^2, and 2 N/mm^2, respectively. The brick and mortar properties are modeled based on the data in literature (Alecci et al. 2013; Chiang et al. 2008; Dorji et al. 2021; Zhang et al. 2022). Figure 2.13 shows the developed 3D masonry walls where each brick is modeled as a polyhedral discrete element.

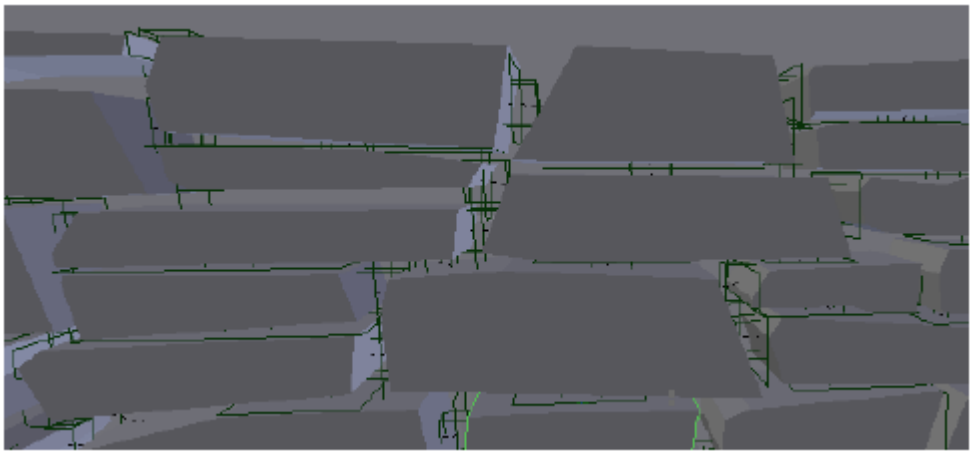

Figure 2.12. Modeled constraints to represent the mortar effects (in solid lines).

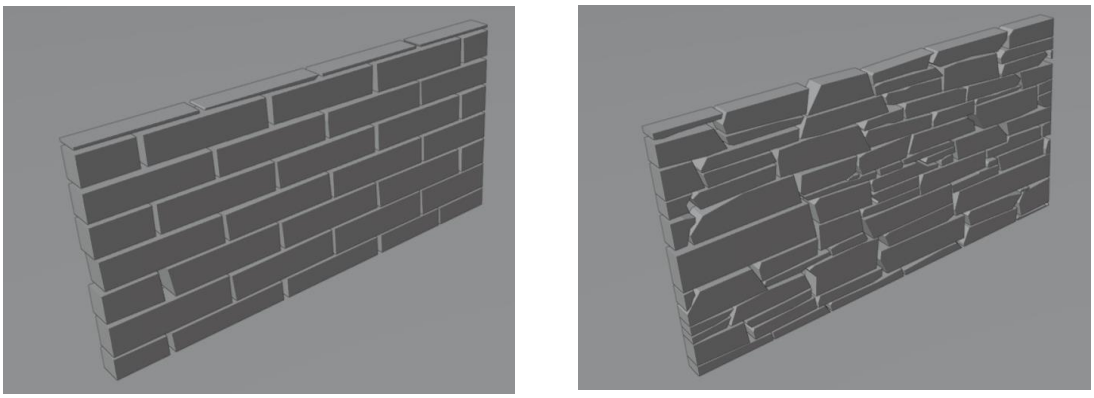

Figure 2.13. Masonry bricks modeled as a set of polyhedral discrete elements.

Figure 2.14 demonstrates a DEM simulation of the modeled masonry wall in Figure 2.13. The modeled wall is first attached to a single-story house, then a synthetic earthquake is created with the Bullet Constraints Builder and applied to the house model. The impulse-based dynamic simulation is then performed for the DEM simulation of the masonry wall collapse. A magnitude 5.8 earthquake is applied for 20 seconds in the out-of-plane direction of the wall, and the collapse of the modeled masonry wall is realistically simulated as in Figure 2.14.

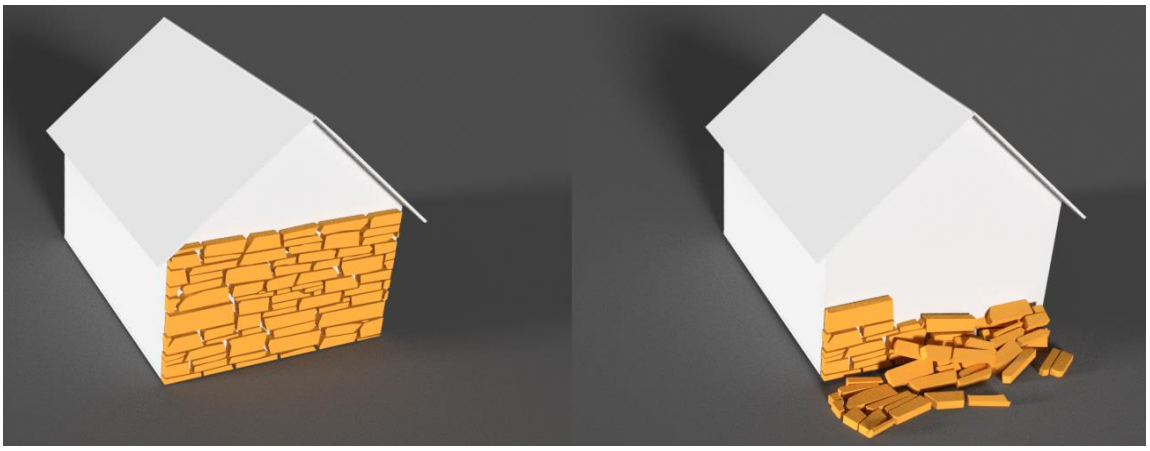

Figure 2.14. DEM simulation of a masonry wall collapse before and after earthquake excitation.

2.3 Concluding Remarks

This study presents an image-based modeling-to-simulation framework for discrete element analysis of masonry structure. A continuum-mechanics framework such as the finite element method (FEM) has been introduced in published literature for an image-based analysis of masonry structure, but the individual bricks in the masonry structure were not explicitly presented in the approaches. Consequently, the interactions of individual bricks could not be realistically captured, and the simulation fidelity was limited. The framework introduced in this study leverages the outcomes of visual recognition (one masonry wall image) as a direct input for the rigid body dynamic simulation using the discrete element method (DEM) by developing 3D polyhedral discrete elements from the segmented brick images. Representing the discrete nature of the masonry walls is at the heart of this approach allowing for realistic simulation of large deformation of the masonry structure such as collapse and improves the estimation of the hazard vulnerability. The framework is composed of five steps: (i) the obtained image of a masonry wall is (ii) segmented into constituent bricks. A complementary code is developed to enhance the quality of image segmentation. Then (iii) all vertex coordinates of segmented bricks are captured with high fidelity. Two polygon approximation methods, Douglas-Peucker (DP) and splitting methods, are used to (iv) approximate the brick shapes into simpler polygons with a fewer number of vertices. This shape approximation is conducted to lower the computational cost required for DEM simulation while maintaining the overall geometry. This study demonstrates both methods can represent the original shape with much fewer vertices although the splitting method slightly outperforms the DP method. The approximated polygons are (v) exported to a free and open-source 3D computer graphics

software integrated with physics engines. The polygons are modeled as a set of 3D polyhedral discrete elements and the DEM simulation is conducted using the impulse-based dynamics approach. These days, the complex form of the masonry wall can be captured with laser scanning. While this study focuses on planar masonry walls, this image-based modeling-to-simulation frame can be extended for complex walls if the bricks in the laser scanned masonry image are properly segmented. The extension of this study for general 3D masonry structures is suggested for future research. The proposed image-based modeling-to-simulation framework will help the architectural engineers to better assess the hazard vulnerability of masonry structures.

CHAPTER 3 . IMAGE-BASED 3D MODELING-TO-SIMULATION OF SINGLE-WYTHE MASONRY STRUCTURE VIA REVERSE DESCRIPTIVE GEOMETRY

3.1 Introduction

Masonry structures represent a significant sub-population of the historic heritage, and constitute the largest proportion of the building stock worldwide (D'Ayala 2013). Single-wythe masonry structures are constructed with walls of one masonry unit thickness, and therefore, the masonry wall serves as structural system as well as exterior facing. Many masonry structures have been constructed as unreinforced single-wythe structures due to their relatively low construction cost, convenience of maintenance and reasonable structural stability (Weber 2013). For example, single-wythe masonry structures make up about 8% of all masonry structures in Sicily, Italy (Binda et al. 2006). In the 1990s, the price of wood increased (Martin and Darr 1997), thus the single-wythe load bearing masonry walls gained popularity (Jayasinghe 1998) and are still widely used these days due to the cost competitiveness. However, these single-wythe masonry structures are more vulnerable to hazards than multi-wythe structures (Al-Sakkaf et al. 2020). Many heritage masonry structures are single-wythe, and many of those have been severely damaged and are under the exposure to various hazards such as strength degradation, vibration caused by nearby traffic, wind and earthquakes, lack of maintenance, vandalism, etc. (D'Ayala 2013; Lourenço 2002). With its enormous value as heritage, it is of great importance to estimate the aggravating impact of these hazards on single-wythe masonry structures to better identify the preservation needs and preventive measures for damage mitigation.

Experimental investigations have been conducted for single-wythe masonry structures to estimate their vulnerability against various hazards including seismic performance, dynamic response against blast-induced loadings, behavior under axial compression and shear loading, traffic-induced vibration of masonry structures, and the impact of wind driven rain (Al-Fakih et al. 2020; Altunışık et al. 2021; Azzara et al. 2021; Banerjee et al. 2021; Cacciotti 2020; Pereira et al. 2015; Vasconcelos and Lourenço 2009; Zini et al. 2022). However, experimental studies on heritage single-wythe masonry structures have limitations in robustly estimating overall structural performance depending on the required test and structure size (Bui et al. 2019). Therefore, numerical analysis has been adopted in the research community as an alternative (Bui et al. 2019; Kayırga and Altun 2021; Malomo et al. 2020).

Numerical modeling has been made in two different approaches: continuum- or discontinuum-based methods, which targeted at macro- or micro-scale mechanical modeling respectively (Lemos 2007). The continuum-based approach, such as the finite element method (FEM), models the whole masonry structure as a continuous medium. Therefore, the structural behavior after the onset of failure may not be realistic (Smoljanović et al. 2013). On the other hand, the discontinuum-based approach, such as the discrete element method (DEM), simulates the discontinuous nature of masonry bricks by explicitly modeling the individual bricks and their interactions (Lourenço 2002). Therefore, DEM has been broadly adopted to investigate the behavior of masonry structures in the research community (Bui et al. 2017; Caliò et al. 2012; Chen et al. 2021; Dell'Endice et al. 2021; Gobbin et al. 2021; Kassotakis et al. 2020; Malomo et al. 2019; Masi et al. 2020; Occhipinti et al. 2022; Pulatsu et al. 2018; Smoljanović et al. 2013).

Nevertheless, discrete element modeling for large heritage single-wythe masonry structures is considered a difficult task (Kassotakis et al. 2020). A masonry structure may contain too many bricks to be modeled manually. Furthermore, a lot of those structures are rubble masonry, where the stone bricks have a non-rectangular shape. Therefore, manual discrete element modeling of these masonry structures may be impractical, and sometimes infeasible. The accuracy of the DEM simulation of masonry structures is also limited without the brick shapes being accurately modeled. To overcome these challenges, imaging techniques have been recently adopted to capture the ground truth brick geometry (Abu-Haifa and Lee 2022; Castellazzi et al. 2015; Ioannides et al. 2012; Kassotakis et al. 2020; Loverdos et al. 2021; Micelli and Cascardi 2020; Truong-Hong et al. 2013). For example, an innovative framework has been developed to use a single masonry image for streamlined image-based DEM modeling (Abu-Haifa and Lee 2022), but this approach is limited to modeling of a planar masonry wall. A framework that converts a large set of images into a whole 3D masonry structure of multiple walls has been proposed (Kassotakis et al. 2020). While this study provided a great insight, this method did not consider the actual geometry of brick shapes as it voxelized the masonry structure.

The objective of this study is to develop a streamlined image-based 3D modeling-to-simulation framework for the discrete element analysis of single-wythe masonry structures. This study is built upon the previous work presented in Abu-Haifa and Lee (2022) that focused on a planar masonry wall. The main difference from the previous work is the use of ‘reverse descriptive geometry’ that adopts a set of 2D wall images to digitally construct a 3D masonry structure model composed of multiple walls. One photographic image for each wall is needed for the 2D-to-3D modeling. The modeled 3D masonry structure is then

used for DEM analysis. The provided framework presents an integrated approach that incorporates image analysis, numerical modeling, and simulation methods to systematically assess the hazard vulnerability of single-wythe masonry structures. This comprehensive, cost-effective, and efficient approach aims to enhance the practice of risk assessment, allowing for more accurate estimation of the structures' vulnerability under different hazard scenarios. By implementing this approach, the resilience and preservation of single-wythe heritage masonry structures can be effectively enhanced. Section 3.2 introduces the proposed framework and demonstrates it using a virtual masonry structure as an example. In Section 3.3, this approach is specifically applied to a heritage single-wythe masonry structure.

3.2 Methodology

The core of the proposed framework in this study is a 2D-to-3D approach, which may be considered as an opposite concept of the conventional descriptive geometry (also known as the stereotomy) that represents a 3D object with multiple 2D geometric projections (Migliari 2012). The proposed framework uses a reverse descriptive geometry in the sense that the 2D projection images are used to digitally construct a 3D object.

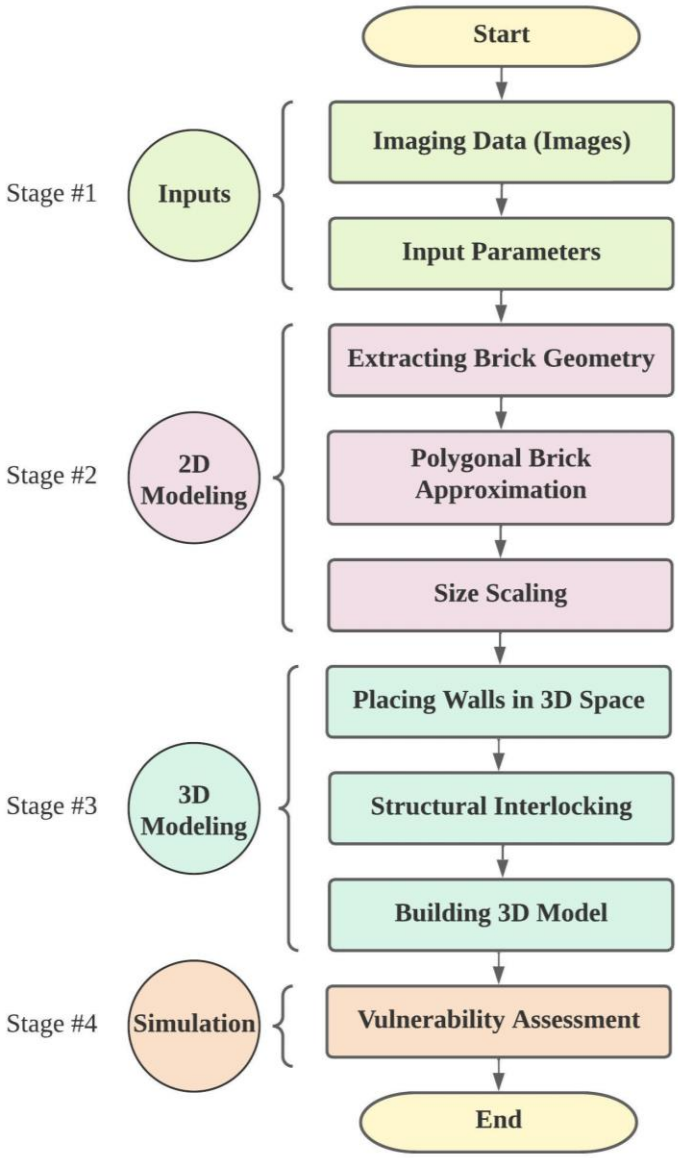

Figure 3.1 Overview of the proposed streamlined image-based 3D modeling-to-simulation framework for single-wythe masonry structure

An overview of the streamlined image-based 3D modeling-to-simulation framework for single-wythe masonry structure is presented in Figure 3.1, where the framework is divided to four stages and several steps in each stage: 1) Input acquisition – the 2D planar masonry wall images are obtained along with other identified input parameters; 2) 2D modeling – a

set of 2D planar masonry wall models is developed from each 2D masonry wall image; 3) 3D modeling – in this stage, the 2D planar wall models are placed in a 3D space and extruded. The adjoining wythes at the building corners are constructed taking account of a structural masonry bond pattern adopted for single-wythe masonry structures; and 4) Simulation – the 3D masonry model is simulated using the DEM to estimate the hazard vulnerability of the structure. MATLAB (MathWorks 2021d) is used to develop the bespoke codes to automate the imaging-to-simulation process. It is worth noting that the developed image-based modeling process is fully automatic. Once the binary images of the walls are obtained, and the input parameters are identified, the algorithm automatically builds the whole 3D DEM model of the structure. A free and open-source 3D computer graphics software, Blender (The Blender Foundation 2021b), and its integrated Bullet physics engine (Coumans 2020) are used for the DEM simulation of 3D masonry structure. The Bullet physics engine works on the impulse-based dynamics method that can be seen as a momentum-exchange method, which is a DEM (Augarde et al. 2021).

An example single-wythe masonry structure shown in Figure 3.2 is used in Section 3.2 to illustrate the procedures in the proposed framework. The model has six sides (walls), where each wall has a different height and width. The structure is composed of typical rectangular bricks with a size of 400 × 180 × 180 mm (width × depth × height), and a 10 mm mortar layer in-between. All walls are nearly half-brick thick. There is no particular reason for selecting the brick size, as the proposed method will work with any brick size. That being said, the chosen brick resembles the dimensions of the 8-inch thru-wall double monarch brick. The stretcher bond type is considered at the adjoining wythe, which is widely used for half-brick masonry walls (Smith 1972). Stretcher bond is a repeating pattern in which

each layer alternates with an offset of half a brick, preventing a straight joint across the layers (Bärtschi and Bonwetsch 2013).

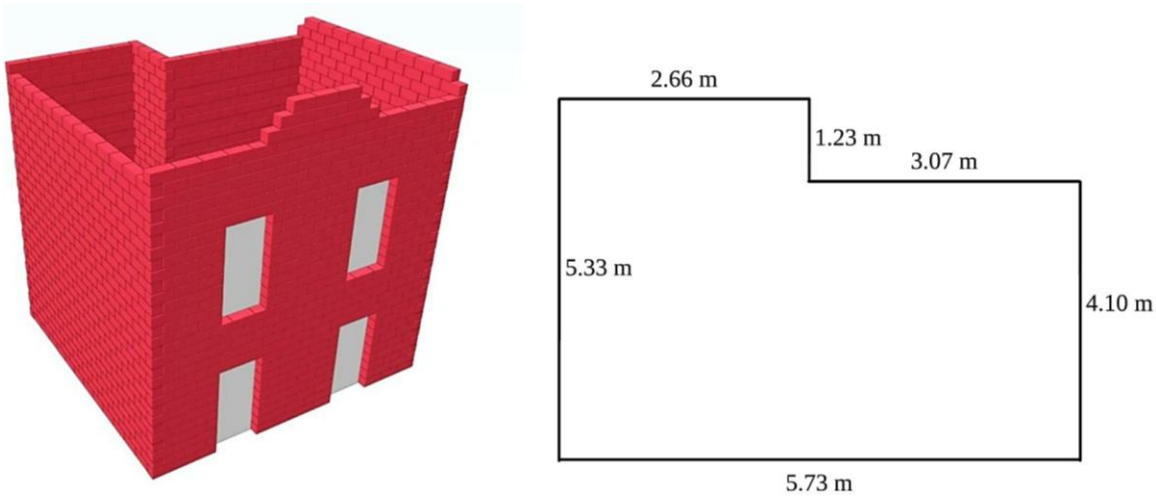

Figure 3.2. Virtual 3D single-wythe masonry structure as an example to demonstrate the image-based 3D modeling-to-simulation framework. The dimensions are shown on the plan view.

3.2.1 Inputs (Stage 1)

3.2.1.1 Input Images

One image for each side of the structure is going to be used as input for the modeling. The images may be stitched or cut to represent a wall in one image. Figure 3.3 presents all the input images for the example single-wythe masonry structure, in which each image represents a wall of the structure.

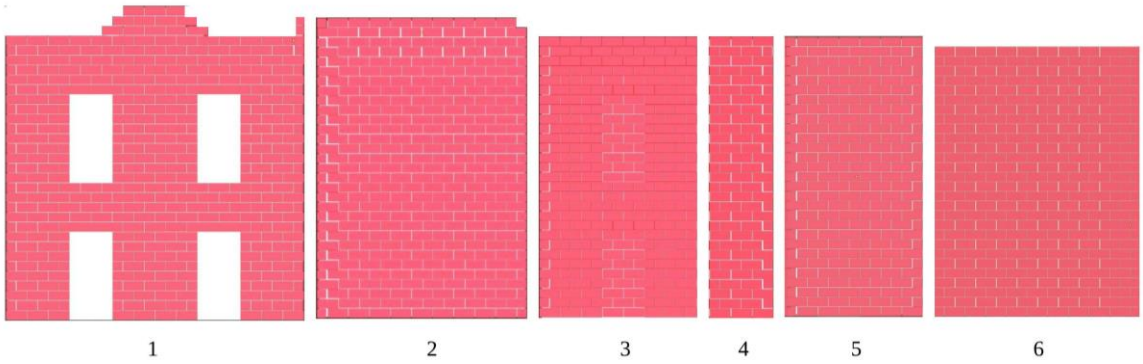

Figure 3.3. Input images from all sides of the single-wythe masonry structure (shown with the image numbers).

3.2.1.2 Input Parameters

The framework requires four input parameters as well as the input wall images: (i) dimension (width and height) of walls, (iii) orientation of walls, (iv) brick thickness, and (v) target number of vertices to represent each brick in modeling. The images are to be numbered in ascending order, starting from the front façade and moving counterclockwise as in Figure 3.3, where the wall images are numbered from 1 to 6. Table 3.1 shows the input parameters and their corresponding values. The orientation of the wall is determined counterclockwise from the global coordinate system (i.e., the global X-axis). In this study, X, Y, and Z refer to the global coordinates. For the example structure, the origin of the global coordinate system is set at the lower-left corner of the front wall (i.e., wall #1) as in Figure 3.4, and the orientation θ of all images (walls) can be defined counterclockwise as shown in Table 3.1. As a note, a target accuracy level can be used (instead of the target number of vertices) as an input to ensure the minimum accuracy required to represent all bricks. For simplicity, however, this study adopts the same number of vertices to represent all bricks, resulting in each brick being modeled with different accuracies.

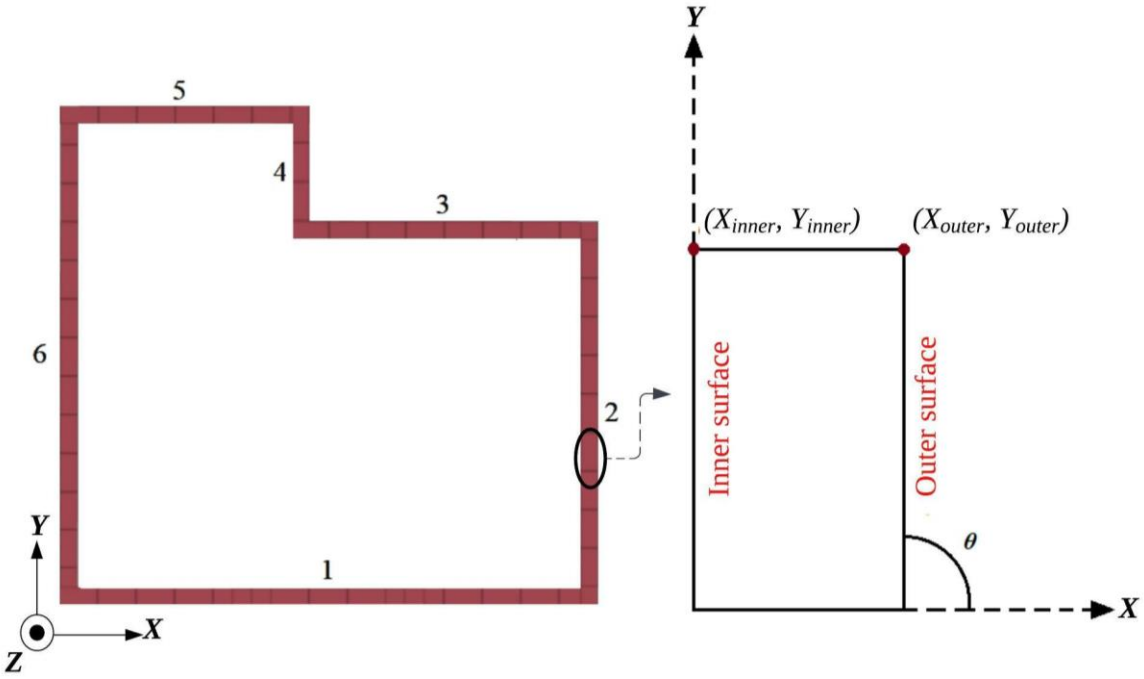

Figure 3.4. Plan view of the example single-wythe masonry structure; *X*, *Y*, and *Z* refer to the global coordinates.

Table 3.1. Input parameters considered for the example masonry structure.

	Wall				
Image *n*	Width W_n (m)	Height H_n (m)	Orientation θ_n (°)	Brick thickness (m)	Target # of vertices
1	5.73	6.07	0	0.18	5
2	4.10	5.88	90	0.18	5
3	3.07	5.50	180	0.18	5
4	1.23	5.50	90	0.18	5
5	2.66	5.50	180	0.18	5
6	5.33	5.31	270	0.18	5

3.2.2 2D Wall Modeling (Stage 2)

3.2.2.1 Extracting Brick Geometry

Image segmentation is required to distinguish bricks from mortar and to extract the brick geometries. Image segmentation is the process of translating a digital image into smaller meaningful subclasses or objects, for further analysis of the image (Cheng et al. 2001). Technically, the process labels every pixel in the image based on certain characteristics such as intensity, color, and texture. However, manual segmentation is time-consuming and impractical, considering a masonry structure may contain too many bricks to segment. Various automatic and semi-automatic algorithms were developed to facilitate this process (Ibrahim et al. 2019; Riveiro et al. 2016; Valero et al. 2018). The segmentation output is a converted black and white binary image, where the bricks can be represented as white pixels and the mortar is represented as black pixels. This study adopts the segmentation approach adopted by Abu-Haifa and Lee (2022). A binary image of wall #1 is shown as an example in Figure 3.5. The segmented wall images are shown in Figure 3.6, where the segmented bricks are colored randomly to illustrate that each brick is identified as an individual object.

While segmented, the bricks in the image are not polygons yet. To this end, the MATLAB boundary tracing function (MathWorks 2023a) is used to extract the geometry of each brick and present it as a polygon. The boundary of each segmented brick is traced, from which the boundary pixel locations are identified. The bricks are then converted into a set of polygons, where each boundary pixel is used to create the vertices of the polygon. This process typically results in polygons with a large number of vertices because each brick in

a segmented image is represented by many pixels. Table 3.2 shows the average number of vertices that represent each brick polygon, for which about 200 vertices are used. The average number of vertices is calculated by dividing the sum of V_j by k, where V_j is the number of vertices representing the brick j in a wall and k is the number of bricks in the wall. The developed brick polygons are shown in Figure 3.7 (highlighted in green).

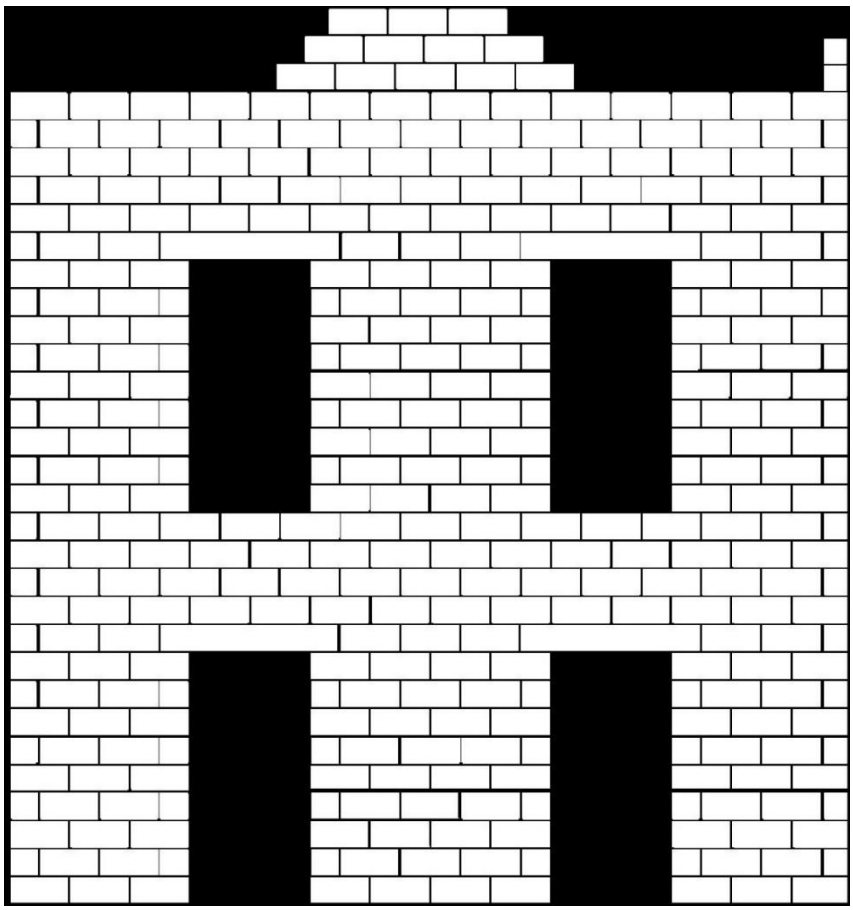

Figure 3.5. A binary image of wall #1.

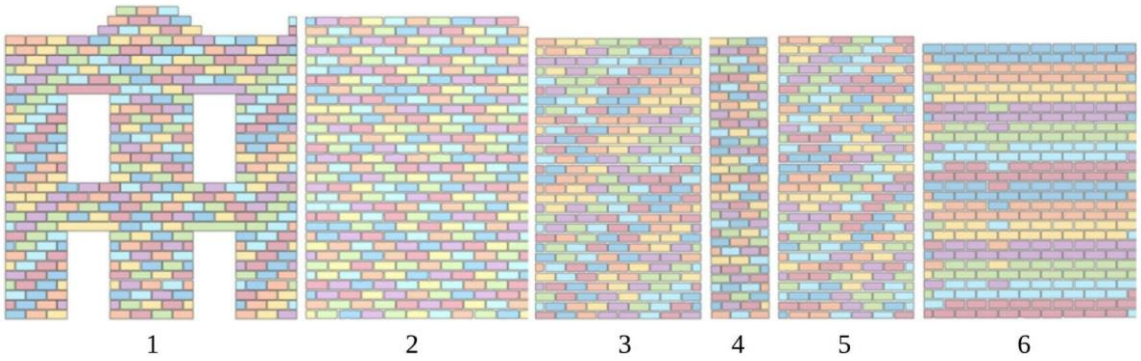

Figure 3.6. Segmentation results for the input images of the virtual single-wythe masonry structure.

Table 3.2. Average number of vertices to represent each brick polygon in all walls.

Wall image #	Average number of vertices for each brick polygon
1	237.37
2	235.94
3	186.59
4	220.90
5	184.14
6	234.08

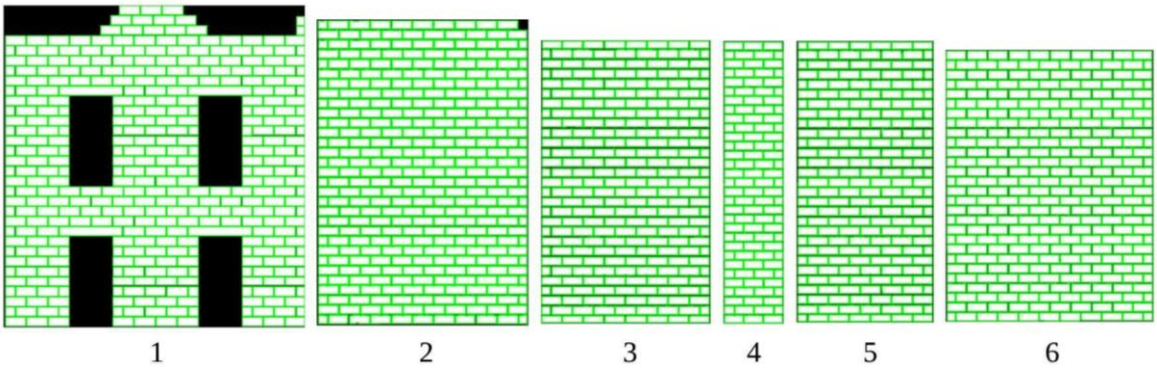

Figure 3.7. Developed brick polygons in all walls (shown in green lines).

3.2.2.2 Polygon Brick Approximation

Modeling a simple brick shape (e.g., a rectangle) with a polygon with about 200 vertices is clearly inefficient. Therefore, this step converts the polygons into simpler ones by eliminating redundant vertices, for which this study adopts the splitting method (Pikaz and

Dinstein 1995). By identifying a line that connects the two farthest points on the boundary, the splitting method iteratively splits the shape into two halves. The points that have the maximum perpendicular distance from the line are identified, forming the four boundary vertices. Virtual lines are built between these vertices, and the process is repeated until the polygon is simplified to the desired number of vertices. In the end, the simplified polygon is drawn by connecting the final vertices with lines.

Hypothetically, four vertices would be enough to represent the rectangular brick shape in the example structure, but a few more vertices would be needed to account for some geometric variation that may be available in brick shapes (Lelandais et al. 2014). Figure 3.8 shows an example. The brick polygon in Figure 3.8a obtained from a segmented image is nearly a rectangle, but not in an exact sense. Figure 3.8b and c present brick polygons approximated with four and five vertices, respectively. Clearly, Figure 3.8c better represents the overall shape than Figure 3.8b, where the geometric variation is accounted for.

A MATLAB code (Bone 2023) is employed to simplify polygon shapes in all walls. All brick shapes are simplified using five vertices. Although simplification can lead to reduced computational costs in subsequent simulation steps, it also results in a smooth surface that eliminates the inherent roughness of individual bricks. Consequently, to ensure the reliability of the simulation, a proper friction coefficient is assigned to each simplified polygon. Figure 3.9 shows the walls with simplified brick polygons.

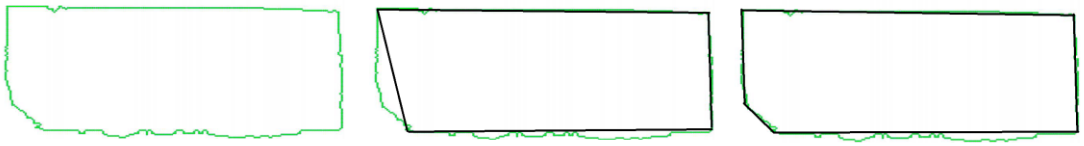

Figure 3.8. Polygon brick approximation: (a) brick polygon obtained from segmented wall image; (b) polygon approximated with 4 vertices; and (c) polygon approximated with 5 vertices.

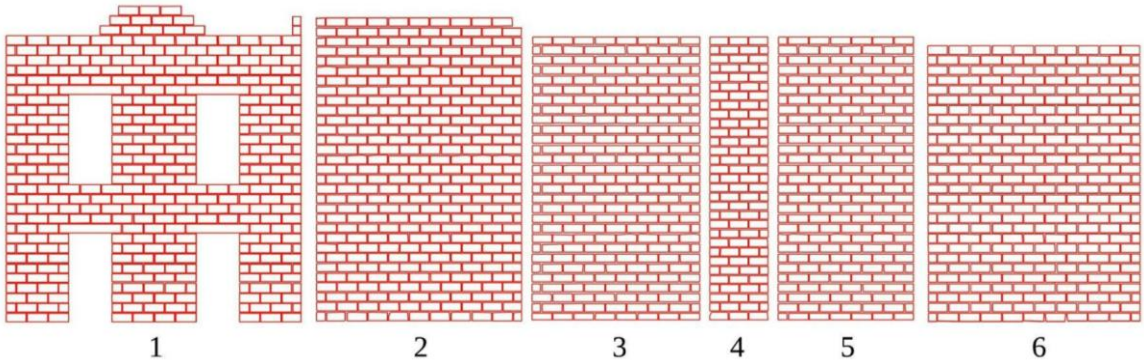

Figure 3.9. Simplified polygons with 5 vertices after applying splitting method on the input images.

3.2.2.3 Size Scaling

The image coordinates are defined in pixels and have their origin at the upper-left corner for the width (*w*) and height (*h*) of the wall image, respectively. Accordingly, the locations of all brick polygons inside a wall are defined in pixels. Therefore, the pixel-based coordinates are translated to a local Cartesian coordinate system, where the origin is at the lower-left corner of each wall, as shown in Figure 3.10. Please note that the lower cases (*x*, *y* and *z*) are used to indicate the local coordinate system, compared to the upper cases for the global coordinate system (as discussed in Section 3.2.1.2). The *y* coordinate is 0 as it is a 2D image. In this step, the coordinates of each vertex are scaled based on the actual wall dimensions (which are input parameters) using a scaling factor from pixels to a physical

length, e.g., meters. The *x*- and *z*-coordinates are scaled by the width and height ratios (*W/w*) and (*H/h*), respectively, where *W* and *H* are the actual wall width and height (as in Table 3.1). Then, the pixel-based *z*-coordinate is subtracted from *H* to invert it into the Cartesian coordinate with the origin at the lower left corner of the wall, as shown in Equation (2). The z_{pixel} and $z_{Cartesian}$ represent *z* coordinates in pixel and Cartesian-based coordinates, respectively.

$$z_{Cartesian} = H - z_{pixel} \times \frac{H}{h} \tag{2}$$

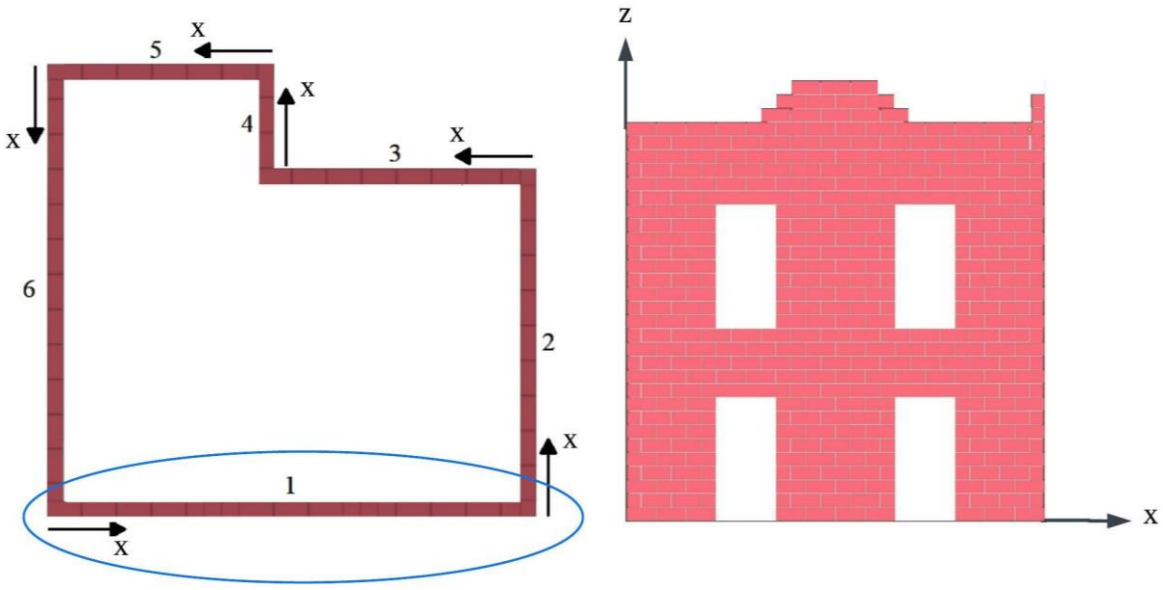

Figure 3.10. Local coordinate system in terms of *x* and *z* in Cartesian coordinate system. Example shown with wall #1

3.2.3 3D Structure Modeling (Stage 3)

This stage constructs the 3D model of the single-wythe masonry structure based on the processed data obtained from the previous stage to build the whole 3D DEM model.

3.2.3.1 Placing Walls in 3D Space

This step places the 2D walls (local coordinate) into 3D space (global coordinate), for which the relationship between the local and global coordinates is developed using a rotation matrix as in Equation (3). The *Z*-coordinate (global) equals its *z*-coordinate (local), and the *y*-coordinate (local) is always 0, so Equation (3) can be simplified to Equation (4). Please note that the subscript *outer* denotes the coordinates of the brick surface facing 'outward'. The subscript *inner* is reserved for a later step to indicate the coordinates of brick surface facing 'inward' (see Figure 3.4) after walls are extruded to the thickness direction (to be discussed in Section 3.2.3.3). Per user input, θ is the angle between the *X*-axis and *x*-axis of a wall, *n* is the wall number to compute the global coordinates, and W_n is the width of wall *n*. Therefore, $(X_{outer})_n$ denotes *X*-coordinates of the *outer* brick surface in the *n*-th wall. For wall #1, $n = 1$ (thus no summation is needed), and θ_1 is 0 (thus global *X* and local *x* coordinates coincide, while the *Y* coordinates are all 0). Once the global coordinates of all bricks are obtained, the wall surfaces of the structure can be constructed as in Figure 3.11, where the brick polygons (in green) are presented with 5 vertices as stated earlier.

$$\begin{bmatrix}(X_{outer})_n\\(Y_{outer})_n\end{bmatrix} = \begin{bmatrix}\cos\theta_n & -\sin\theta_n\\ \sin\theta_n & \cos\theta_n\end{bmatrix}\begin{bmatrix}(x_{outer})_n\\(y_{outer})_n = 0\end{bmatrix} + \begin{bmatrix}\sum_{i=1}^{n-1}(W_i\cos\theta_i)\\ \sum_{i=1}^{n-1}(W_i\sin\theta_i)\end{bmatrix} \tag{3}$$

$$\begin{bmatrix}(X_{outer})_n\\(Y_{outer})_n\end{bmatrix} = \begin{bmatrix}(x_{outer})_n\cos\theta_n + \sum_{i=1}^{n-1}(W_i\cos\theta_i)\\ (x_{outer})_n\sin\theta_n + \sum_{i=1}^{n-1}(W_i\sin\theta_i)\end{bmatrix} \tag{4}$$

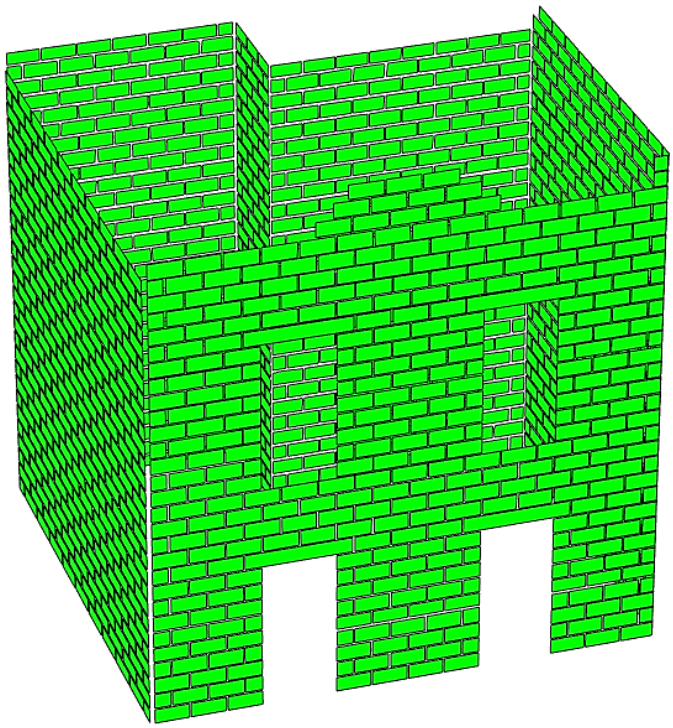

Figure 3.11. The outer wall surfaces of the example single-wythe masonry structure.

3.2.3.2 Structural Interlocking

Stretcher bond is considered for adjoining wythes, i.e., structural masonry interlocking between walls. If all polygons in Figure 3.11 are extruded to the thickness directions, overlapping occurs at the corners, as shown in Figure 3.12. A solution to this is to remove one of the neighboring bricks at the adjoining wythes, e.g., if the red polygon in Figure 3.12 is removed, then no overlapping occurs when the remaining polygon in the neighbor is extruded. Therefore, the polygons of a smaller size than a typical brick located at the corners, e.g., the yellow and green polygons in Figure 3.13, are removed to properly model the stretcher bond.

Figure 3.14 presents the flowchart to detect and remove the small polygons located at wall boundaries to model the stretcher bond. A threshold approach is adopted for this task

(Pauker and Kassirer 1980). It iteratively removes all polygons located between walls having an area approximately equal to a predefined threshold area (A_{th}). The area of a polygon and its center in the local coordinate system are determined. A corner polygon is detected if the *x*-coordinate of brick center is approximately equal to half of brick thickness (*t/2*) or located at the last half brick thickness of the wall width (*W* - *t/2*). All corner polygons having an approximately equal area to the threshold area are removed. Figure 3.15 shows the wall surfaces of the example single-wythe masonry structure with these small corner polygons removed.

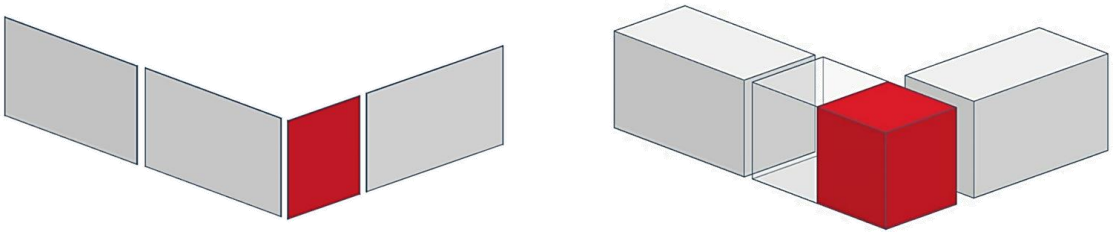

Figure 3.12. Overlapping occurs when all polygons are extruded to the thickness directions.

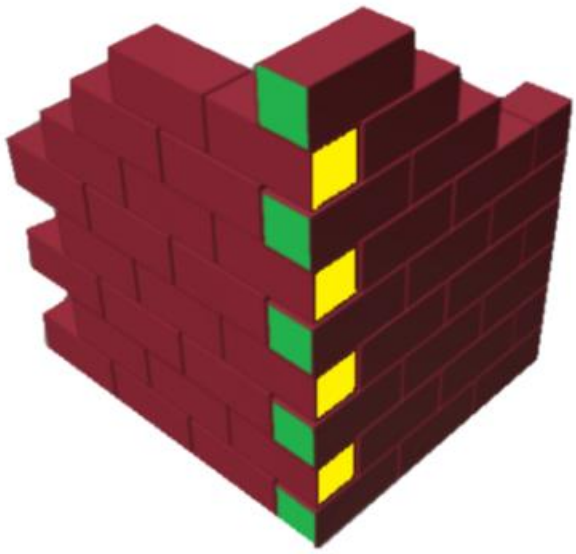

Figure 3.13. Stretcher bond in masonry brick construction.

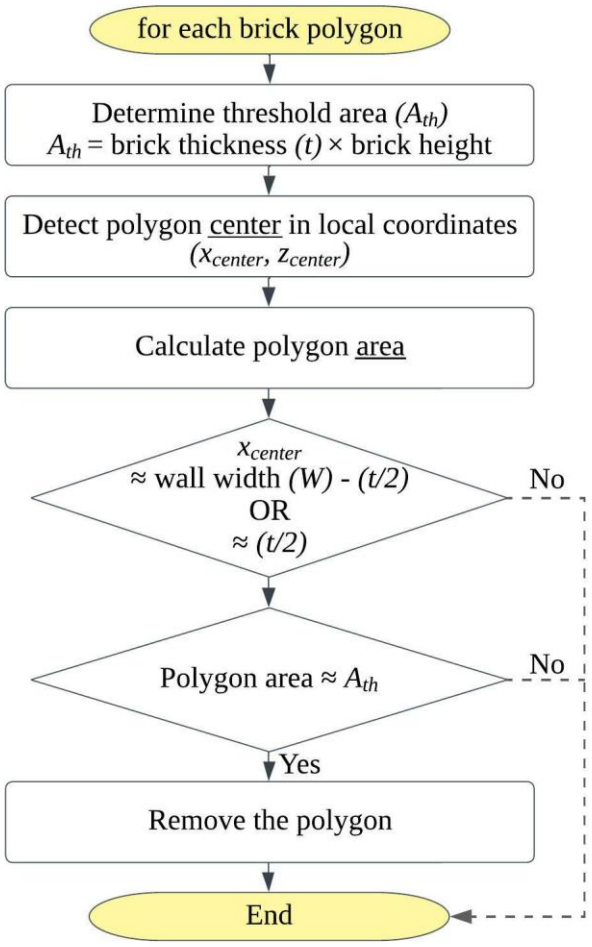

Figure 3.14. Flowchart for the threshold method adopted to consider the stretcher bond.

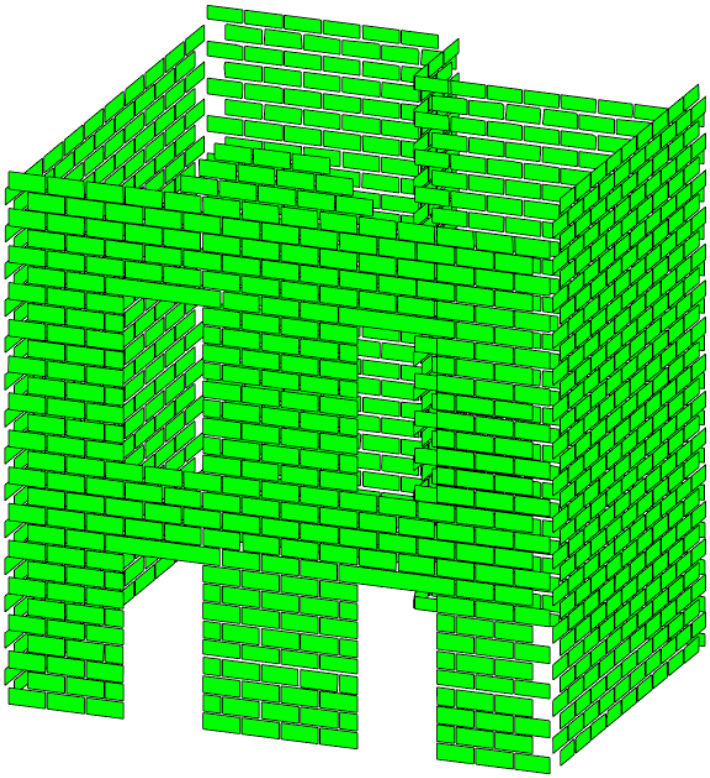

Figure 3.15. The outer wall surfaces of the example single-wythe masonry structure with the small corner bricks removed for modeling of structural interlocking between walls.

3.2.3.3 Building 3D Model

A 3D brick polyhedron is created from each brick polygon after extruded into the brick thickness direction. The *inner* wall coordinates can be found after the extrusion using Equation (5), where t_n is the brick thickness of the *n*-th wall, which is entered as an input parameter. The *Z*-coordinate of any inner vertex equals to its outer Z-coordinate ($Z_{inner} = Z_{outer}$). The 3D model of the single-wythe masonry structure is represented by 3D brick polyhedrons. The geometry of the 3D model is written in stereolithography (STL) file format.

$$\begin{bmatrix} (X_{inner})_n \\ (Y_{inner})_n \end{bmatrix} = \begin{bmatrix} \cos\theta_n & -\sin\theta_n \\ \sin\theta_n & \cos\theta_n \end{bmatrix} \begin{bmatrix} 0 \\ t_n \end{bmatrix} + \begin{bmatrix} (X_{outer})_n \\ (Y_{outer})_n \end{bmatrix} \quad (5)$$

3.2.4 DEM Simulation (Stage 4)

The 3D model is then used for DEM analysis of the building's vulnerability to hazards. Figure 3.16 shows the developed 3D single-wythe masonry structure modeled with brick polyhedrons. Blender is used to conduct the DEM simulation of the modeled structure subjected to hazards. The Blender is a free and open-source 3D computer graphics software (The Blender Foundation 2021b) that houses the Bullet physics engine (Coumans 2020) that simulates collisions between rigid bodies based on the impulse-based dynamics. It is worth noting that numerical methods satisfying the following two requirements can be referred to as DEM per Cundall and Hart (1992): (1) allowing for finite displacements and rotations of discrete bodies, including complete separation of the bodies; and (2) automatically identifying new contacts as the simulation progresses. The momentum-exchange method is one of the four kinds of DEM that comply with this definition. The Bullet physics engine dynamically simulates rigid polyhedral bodies using an impulse-based dynamics scheme that can be considered as a momentum-exchange method (Augarde et al. 2021). The impulse-based dynamic simulation method (i.e., velocity-based) is computationally far more efficient than the conventional (i.e., force/acceleration-based) DEM, and it was reported to show a speed up of almost two orders of magnitude with high simulation fidelity. Therefore, the impulse-based dynamics approach is well suited for a large-scale simulation of many bricks. Furthermore, this approach is more suitable for the image-based modeling-to-simulation of masonry structures due to its high tolerance for geometrical errors. The impulse-based dynamics approach considers relative velocity to resolve a collision between two bodies and therefore has a greater tolerance for any penetration error that may be potentially caused by inaccurate image processing, e.g.,

influenced by lighting, shadow, image resolution, etc. On the other hand, the conventional DEM considers the relative position between two bodies (i.e., penetration) to resolve a collision (whereby the contact force is computed), which therefore any small geometrical error may trigger spurious energy gain and numerical instability in the modeled system. A Bullet plug-in, Bullet Constraints Builder (BCB), is used to model the mortar effect by setting constraints between adjacent bricks (Kostack 2021). Constraints between bricks are aligned to the center-to-center line of both connected bricks. A detailed comparison between the conventional DEM and the impulse-based dynamic simulation method is provided in Lee and Hashash (2015). The constraint-based modeling for masonry structures is discussed in Abu-Haifa and Lee (2022). The mortar (constraint) between the bricks breaks once it reaches its breaking threshold. The breaking thresholds for the compressive, tensile, and shear strengths are used as the same values that were used in Abu-Haifa and Lee (2022). A synthetic magnitude 7 earthquake is applied for 10 seconds on the developed model. The collapse sequence of the modeled single-wythe masonry structure is realistically simulated, as shown in Figure 3.17.

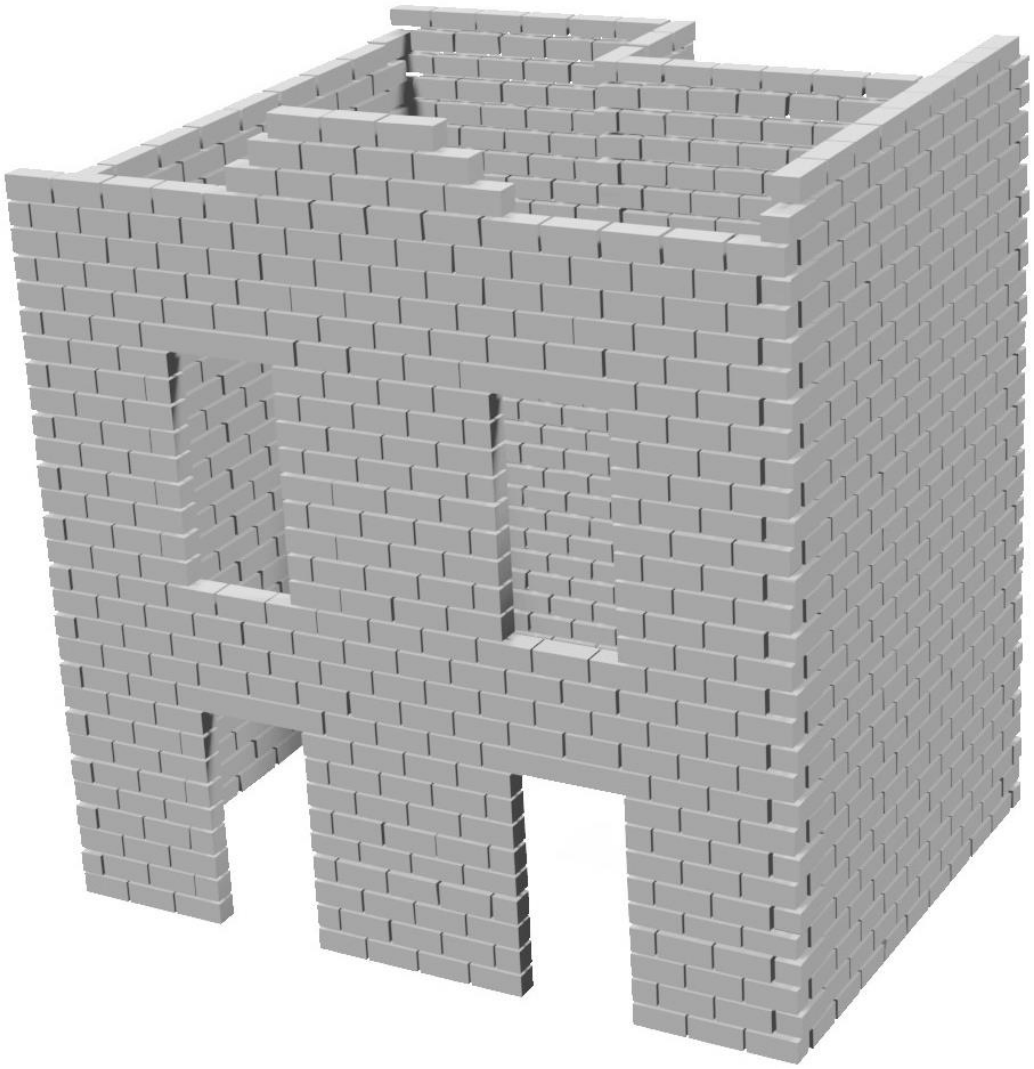

Figure 3.16. The developed 3D masonry structure with brick polyhedrons.

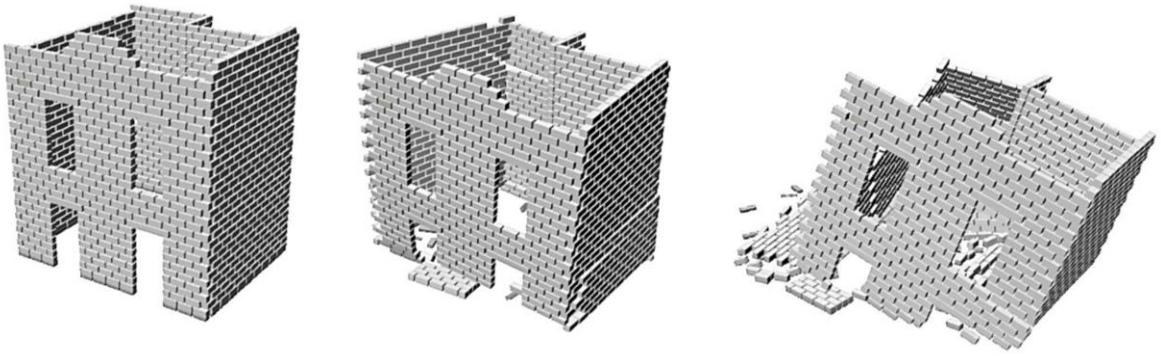

Figure 3.17. Collapse simulation of the example single-wythe masonry structure.

3.3 Application to a Heritage Single-Wythe Structure

A real-world single-wythe masonry structure shown in Figure 3.18 is considered as a case study to validate the developed image-based modeling-to-simulation framework. It is known as Stylite Tower, which is an ancient single-wythe masonry structure built during the Byzantine period at Umm ar-Rasas in Jordan, a UNESCO World Heritage Site. It is almost 13.5 m high (Clemente et al. 2019a), with a base dimension of 2.43 × 2.48 m. Stylite Tower is the only surviving tower of its kind in the world, thus it has enormous heritage value to preserve.

The brick shapes are rectangular with some variations. We measured the thickness of bricks, which ranges from 378 to 432 mm. For simplicity, all bricks are assumed to have the same thickness of 400 mm. One photo was taken for each side of the structure. These photos were taken at a standing human height, therefore there is perspective-related image distortion in the photos. Adobe Photoshop (2022a) is adopted to correct the image distortion, for which the perspective wrapping function is used. This function adjusts objects in an image by taking into account the surrounding environment for a pseudo-orthogonal projection. Figure 3.18b shows images of all four walls of Stylite Tower after correcting the distortion. It is worth mentioning that the minor visual obstruction (i.e., the steel fence around the structure), as shown in Figure 3.18, is also removed using Adobe Photoshop using the content-aware fill function (Adobe Photoshop 2022b).

The segmented and extracted geometries of all bricks are shown in Figure 3.19, where the boundaries of each brick are clearly identified and captured. Many bricks in the structure are overall rectangular but have variations, therefore more than 4 vertices are needed to

create a high-fidelity wall model. The Dice Similarity Coefficient (DSC), also known as Sørensen–Dice coefficient, is adopted to find the least number of vertices required to represent brick shapes with high accuracy. Developed by Sørensen (1948) and Dice (1945), DSC measures the similarity of two shapes in the range between 0 and 1, where 1 means that the two shapes match perfectly. The DSC is formulated as shown in Equation (6), where it compares the area of intersection between the brick's original shape ($A_{original}$) and the approximated polygon ($A_{approximated}$) to the sum of the two areas. When all bricks are approximated as 8-sided polygons, the average DSC value is 0.9845, which indicates that the approximated polygon shapes present a high geometric fidelity. Figure 3.20 shows the approximated polygons of the bricks in all images. Table 3.3 presents the input parameters used for image-based modeling of Stylite Tower.

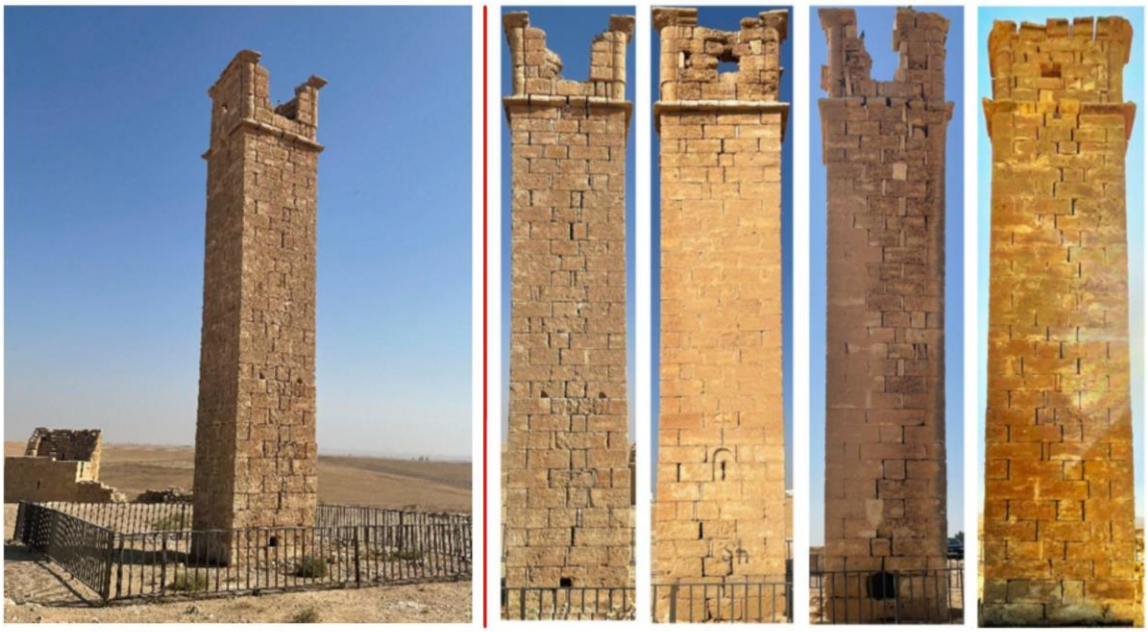

Figure 3.18. A heritage single-wythe masonry structure: (a) Stylite Tower in Jordan, (b) Image of each wall of the structure after image distortion corrected (images by Mohammad Abu-Haifa).

$$DSC = \frac{2|A_{original} \cap A_{approximated}|}{|A_{original}| + |A_{approximated}|} \quad (6)$$

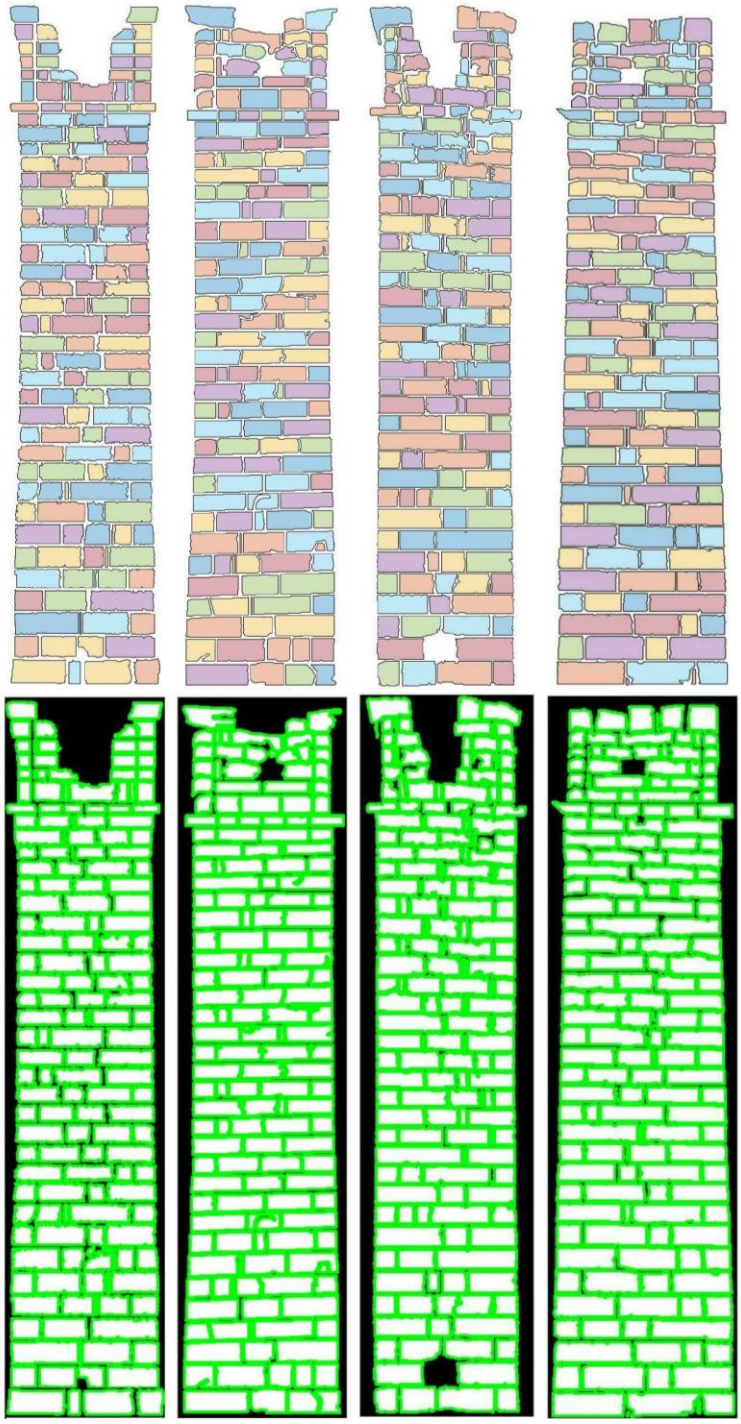

Figure 3.19. The segmented images and extracted brick geometries in Stylite Tower.

Table 3.3. Input parameters for the image-based modeling of Stylite Tower.

Image #	Wall			Brick thickness (m)	Target # of vertices
	Width W (m)	Height H (m)	Orientation θ (°)		
1	2.43	13.5	0	0.40	8
2	2.48	13.5	90	0.40	8
3	2.43	13.5	180	0.40	8
4	2.48	13.5	270	0.40	8

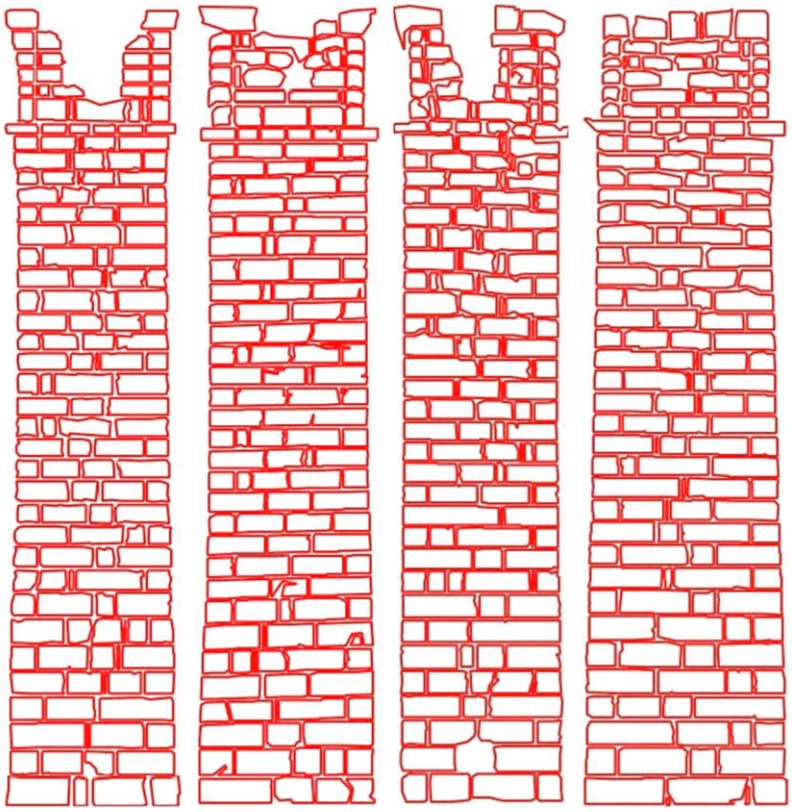

Figure 3.20. Simplified polygons with 8 vertices after applying splitting method on the input images.

The vertices of the simplified polygons are scaled based on the actual dimensions of the structure. The 3D model is then developed with consideration of the stretcher bond. The model is exported to Blender in STL format for DEM simulation. The entire process, which includes building the 3D DEM model of Stylite Tower from the binary images and

exporting the model in the required format, takes less than 20 seconds. Following the assignments of material properties, brick constraints, breaking thresholds, and the seismic load, the DEM simulation on the developed Stylite Tower model is conducted. Figure 3.21 shows the collapsing sequence of Stylite Tower after applying a synthetic earthquake of magnitude 7 for 10 seconds. A computer system running on a 64-bit Windows 11 operating system is employed for the simulation. The computer is equipped with a 3 GHz Intel Core i7-9700 processor and 24 GB of RAM. The simulation process runs for approximately 2 minutes in batch mode.

Previous studies have utilized the finite element method to assess the tower's capacity to withstand seismic events. While these studies highlighted the possibility of collapse if an intense seismic event were to occur in the area, the actual collapse was not simulated due to the limitations of the adopted simulation method (Clemente et al. 2019a; b; Koellisch 2008; Pierdicca et al. 2021). In contrast, our approach explicitly simulates the potential collapse in response to the given earthquake. It is worth noting that the mechanical properties used in the simulation (including brick and mortar properties) may not represent the actual properties of Stylite Tower. This study focuses on the development of a framework that streamlines the process from 2D imaging to 3D modeling (i.e., via reverse descriptive geometry) and DEM simulation. Therefore, determination of the actual mechanical properties of the tower is out of scope and suggested for future study.

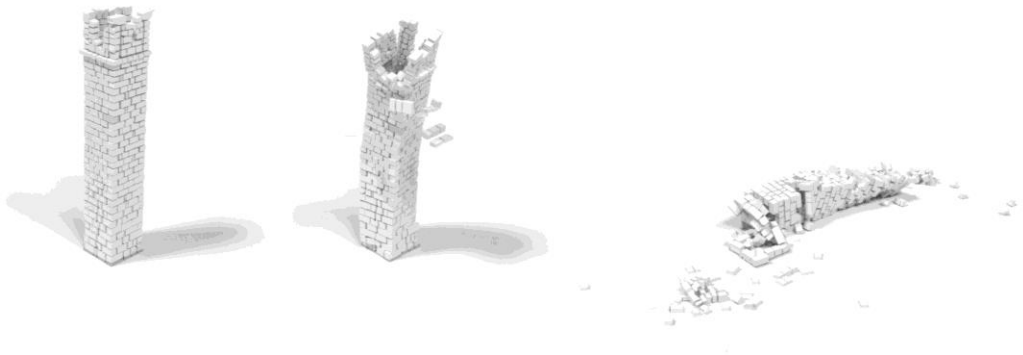

Figure 3.21. The 3D DEM simulation for Stylite Tower after applying a synthetic earthquake of magnitude 7 Richter.

3.4 Concluding Remarks

This study presents an image-based 3D modeling-to-simulation framework for assessing the hazard vulnerability of single-wythe masonry structures. A ‘reverse descriptive geometry’ concept is used for 2D-to-3D modeling, whereby a set of 2D images of planar walls are used as an input for 3D modeling of the single-wythe masonry structures and followed by simulation using the discrete element method (DEM). The 2D modeling stage involves the representation of all walls by segmenting and approximating each brick into simplified polygons. The framework then systematically builds the whole 3D DEM model from the 2D walls. The adjoining wythes at the building corners are modeled via an original bespoke method proposed in this study. The proposed framework is successfully applied to Stylite Tower, a heritage single-wythe masonry structure in Jordan. The results clearly showcased the applicability of the developed methodology, highlighting the streamlined process for assessing the vulnerability of single-wythe masonry structures. While the main focus of this study is on the walls of single-wythe masonry structures, the slab and roof may be easily added to the structure in future studies. It is worth noting that this study serves as an initial exploration, intended to assess the feasibility and effectiveness of the

proposed approach. The outcomes of this research will offer an insight and serve as a foundation for future advancements in the field. We invite the masonry structures research community to explore the potential of the proposed approach further with various single-wythe structures. The proposed framework may also be extended for multi-wythe masonry structures and complex brick shapes.

CHAPTER 4 . PHENOTYPIC TRAIT OF PAINTING CRACKS

4.1 Introduction

A painting is like our skin in some sense. Just as the genetic makeup leaves unique physical characteristics on our skin such as fingerprints, the painting cracks known as *craquelure* has been recognized as an important characteristic of painting that may serve as a unique identifier. The cracks naturally manifest on the surface of a painting due to (i) drying and (ii) aging (Krzemień et al. 2016). The drying (desiccation) cracks begin to form within the first few weeks after applying paint, as volatile solvents evaporate from the painted surface. This process is strongly influenced by factors such as adhesion to the sublayer, thickness and composition of the pictorial layers, etc. On the other hand, the aging cracks start to form after the pictorial layers are dried. The cracks develop over its lifetime, and as a result of the slow and gradual process, the formation is affected by many environmental factors (Giorgiutti-Dauphiné and Pauchard 2016). Therefore, the delicate and intricate cracks, shaped by the painter's choice of materials, techniques, and the way the artwork was stored, may exhibit unique characteristics that are common to the artist's paintings which differ from those of other artists. As such, analyzing the painting cracks has become an important part of art examination, offering valuable information about the painting's authenticity (Barron and Sharma 2020; Pauchard and Giorgiutti-Dauphiné 2020). Therefore, the crack analysis is considered to offer valuable information that can help determine the painting's origin and potentially establish a connection to a particular artist or period. (Sidorov and Yngve Hardeberg 2019).

Some descriptive methods have been developed in the art conservation community as an effort to characterize the crack patterns and link those to the origins of paintings. Bucklow (1997) is widely regarded as the seminal work that pioneered a systematic approach for quantifying crack patterns and establishing their connection to the origin of paintings. Bucklow adopted a set of statistical and classification techniques to develop a formal description of painting cracks. As a result of the study, a collection of descriptive terms was developed to associate the crack patterns with the origins of paintings. The descriptions include the predominant direction and orientation of cracks, smoothness and straightness of cracks, shape and size of islands (enclosed by the cracks), thickness of cracks, and regularity of cracks. This approach was demonstrated, as shown in Table 4.1, to differentiate Italian, Flemish, Dutch, and French paintings created from different historical periods. Bucklow (Bucklow 1998) also utilized a repertory grid approach to represent the structure of painting cracks in numerical ratings. This approach improved the quantitative aspect of the analysis and facilitated the comparison of crack patterns across different paintings and art-historical categories. Later, Bucklow (1999) introduced an image-based painting crack analysis whereby digitized crack images were segmented and converted into a set of Bezier curves for further analysis. The quantitative nature of this approach was recognized as a great advantage. However, a significant drawback was also highlighted: the prohibitive computational cost required for the image processing primarily due to the limited computing power available at the time of the research. Bucklow reported it took several months for the computer to represent 40 crack patterns, whereas it took 9 hours for the author to heuristically complete the representation of 528 crack patterns.

Since then, with significant advances in computing resources and algorithmic enhancements, image processing has become more feasible. In general, image processing involves the manipulation of digital images through mathematical algorithms with the goal of enhancing or extracting information from the image. Image segmentation is an image processing technique that partitions an image into meaningful segments or regions based on color information, texture, or intensity gradients of the image. It is considered a critical step in many image processing applications, such as object recognition, classification, and tracking, as it simplifies image data and enhances the accuracy of subsequent analysis. Image processing including segmentation has played a crucial role in the development of computer vision systems (Suri 2000). These advancements have transformed image-based crack analysis into a more systematic endeavor for 2D (Abas 2004; Spagnolo and Somma 2010) and 3D analyses (Kim et al. 2022). Recent studies in the image-based crack analysis have focused on representing the painting crack network as a graph (Sidorov and Yngve Hardeberg 2019; Zabari 2021) and/or employing image-based deep learning techniques to learn and identify the crack patterns for further classification (Sindel et al. 2021; Yuan et al. 2023).

Table 4.1. Summary of descriptive terms used for connections with painting origins (Bucklow 1997).

	Italian (14-15th century)	Flemish (15-16th century)	Dutch (17th century)	French (18-19th century)
Predominant Direction	Often have	Nearly always have	Usually have	Usually don't have
Orientation	Usually perpendicular to grain	Usually parallel to grain	Usually perpendicular to longest side	N/A

Island sizes	Usually small to medium	Usually very small	Usually medium	Usually large
Island shape	N/A	Usually square	Often square	Usually not square
Smoothness	Usually jagged	Usually straight	Usually jagged	Usually smooth
Straightness	N/A	Usually straight	N/A	Usually curved
Crack thickness	Sometimes distinct secondary cracks	Often uniform thickness of cracks	N/A	N/A
Regularity	N/A	Usually highly ordered cracks	N/A	N/A

Crack analysis is not exclusive to the field of paintings, but also an important research subject in geology and geological engineering, as existing cracks are a major factor that can impact the behavior of geo-materials such as rock and soil. For example, identification of fracture patterns in rock is important to better understand the geomechanical and hydrological behavior of the rock materials (Lei et al. 2017). In addition to being indicative of past stresses and strains, the physical crack properties such as the crack shape, size, roughness, and connectivity can have significant implications for the stability and functionality of the materials. Recently, image-based analysis has become increasingly popular in the fields for crack identification in tandem with the advances in imaging techniques (Liu et al. 2013). Since then, digital images have been heavily used to characterize the soil desiccation cracks (Bordoloi et al. 2020; Liu et al. 2020, 2022a; Zeng et al. 2022). Fractal analysis has been frequently conducted to assess the cracking characteristics. For example, Hirata (1989) demonstrated the fractal structure of rock fracture geometry by using a box method to obtain the fractal dimension. This involved dividing the intricate crack web into a series of smaller square boxes, each with a side

length of r. Hirata (1989) showed that r and the number of boxes $N(r)$ that crack enters follow a relation as in Equation (7), where d is the fractal dimension. When plotted on a log-log space, a linear relation is realized with a slope of $-d$. To be more specific, the presence of the linear graph in a log-log space signifies self-similarity across multiple scales. Mathematically, self-similarity manifests itself in a power law. As shown in Equation (8), a power function $f(x) = \beta x^d$ scales the argument x by a constant c will result in a proportionate scaling of the function itself (Newman 2005), thus having a self-similar nature across different scales. This self-similarity was observed in soil desiccation cracks (Baer et al. 2009; Goehring et al. 2015; Vallejo 2009), which was discussed as an indication of distinctive characteristics associated with soil.

$$N(r) \sim r^{-d} \tag{7}$$

$$f(cx) = \beta(cx)^d = c^d \beta x^d = c^d f(x) \propto f(x) \tag{8}$$

In view of this, two questions arise: (i) would the painting cracks also display self-similarity as in the soil desiccation cracks? and (ii) if so, could the characteristic self-similar trait of the cracks be used as an identifier in relation to the origins of the paintings? These questions are currently difficult to answer due to the limited evidence available within the research community. A few studies conducted the fractal analysis of painting cracks to identify the self-similarity. Eggert (2006) discussed the fractal geometries of cracks in artwork, which relate to glass rather than paintings. The objective of this study is to address the two questions above. Section 4.2 discusses the methodology. Section 4.3 examines the painting crack images presented in Bucklow (1997), focusing on the analysis of how the identified cracks from the methodology correlate with different paintings.

4.2 Methodology

4.2.1 Two approaches for crack analysis

When it comes to analyzing cracks, there are two possible approaches that can be employed. The first approach involves focusing on the crack network, while the second approach involves considering the characteristics of individual islands enclosed by the painting cracks. Figure 4.1 illustrates an example of an island. The first approach is more conventional, which has been adopted in most crack analyses, e.g., representing a crack network as a graph. On the other hand, the second approach is far less common. To the best knowledge, Freeman et al. (2013) is the only study attempted to analyze the island geometries in painting cracks. Our study will adopt the second approach, drawing an analogy between the discrete islands in painting cracks and the discrete soil clods (i.e., distinct clumps or aggregates of soil) in desiccation cracks. To this end, a methodology proposed by Lee et al. (2022) is employed, which was originally developed to analyze the geometries of soil particles. To be more specific, it was to characterize the *phenotypic trait* of the particles, and the study evidenced the phenotypic trait of the particle geometries exhibits self-similarity across scales as observed by the observed power law. In light of the findings, this study aims to characterize the phenotypic trait of the islands by adapting the methodology in Lee et al. (2022) to answer the afore-stated two questions. It is worth noting that the phenotypic trait is a geometry concept beyond shape and size; it extends to the underlying properties associated with shape and size. As an analogy, people of a race may have some variations in their appearances but share a phenotypic trait due to a common genetic origin and biological history. For example, while every Korean woman possesses

a distinct facial appearance from one another, they also share a common phenotypic trait that stems from their shared genetic origin. This phenotypic trait sets them apart from Japanese women, who have a different genetic background and exhibit their own unique set of characteristics. Likewise, mineral particles that originate from the same geologic origin and experienced the same history possess a shared phenotypic trait, despite exhibiting variations in their shapes and sizes. Similarly, the painting cracks and the islands created within them share a common origin attributed to the use of specific materials and painting techniques, as well as the history of drying and aging. Given the similarities, we may hypothesize the existence of a common phenotypic trait behind the formation of islands in paintings created by the same artist. Then, how can we capture the underlying phenotypic trait?

Figure 4.1. Example of an island separated by painting cracks (Image courtesy of Jeronimo Perez Roca - South Florida Art Conservation LLC (Roca 2013)).

4.2.2 Phenotypic trait of 3D geometries

Lee et al. (2022) reported that a power law relationship exists between the surface area-to-volume ratio (A_s/V) and the volume (V) for a family of particles having a common geologic origin and history. Graphically, the data points realize a linear relationship between A_s/V and V in a log-log space, suggesting a self-similar nature across multiple length scales. This

discovery indicates the presence of a phenotypic trait of the 3D particle geometries. An example is shown in Figure 4.2. The particle set contains 100 Florida limestone particles (Tripathi et al. 2023). Two different groups of particles, originating from distinct sources, are ‘randomly’ mixed (Figure 4.2a), yet their distinct identities elude the naked eye. However, a power regression analysis on the A_s/V and V geometry data brings to light the presence of two coherent data clusters. These data clusters exhibit two distinct linear relationships in the log-log space (Figure 4.2b). They are positioned at dissimilar locations with different variations. The coefficient of determination (R^2) for each group is calculated as 0.73 and 0.94, respectively. The dataset located in the upper region of the plot, characterized by larger values of V, corresponds to the larger particles, while the data in the lower region represent smaller particles. The data orientations, as represented by the power regression slopes, depend on the relationship between particle shape and size of each group. These serve as identifiers that unveil two distinct phenotypic traits exhibited by the particles, much like genetic footprints. This suggests that this group comprises a mixture of two different kinds of particles.

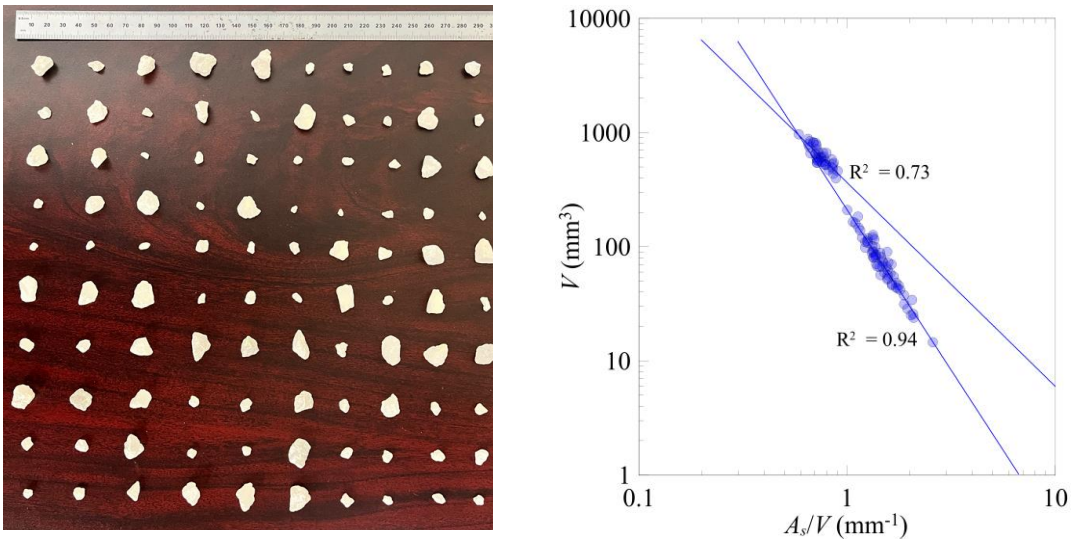

(a) (b)

Figure 4.2. The methodology to undercover the phenotypic traits: (a) 100 Florida limestone particles, and (b) Two phenotypic traits of particle geometries realized in terms of A_s/V and V.

4.2.3 Phenotypic trait of 2D geometries

The methodology by Lee et al. (2022) was originally developed to analyze the 3D geometry. Therefore, this study adapts and develops a 2D equivalent concept to reveal the phenotypic trait of the island geometries, whereby the island area (A) is used in the place of particle volume (V), and the length of island perimeter (P) is used in the place of particle surface area (A_s). This study therefore examines whether the P/A and A data demonstrates a self-similar phenotypic trait that can be correlated with the painting origins.

Another modification in this study is the utilization of bivariate ellipses to comprehensively represent the location and variation of the data. For consistency in utilizing the bivariate ellipse, the eigenvector of the ellipse is also employed to indicate the orientation of the data, avoiding the need for a separate adoption of a power regression line as in Lee et al. (2022) and as illustrated in the example above (Figure 4.2b). Although the slope of the

eigenvector may exhibit a slight difference compared to that of the power regression, both remain proportionate. Therefore, it is deemed suitable for the purpose of this study.

4.3 Analysis

4.3.1 Images of painting cracks

This study analyzes the crack images of Italian, Flemish, Dutch, and French paintings from 14^{th} to 19^{th} centuries collected by and presented in Bucklow (1997).

Table 4.2 presents a summary of the origins and descriptions of all seventeen images in Bucklow (1997). Please note that the figures in Bucklow (1997) are referred to as 'Image' while the figures in this study are labeled as 'Figure' to avoid any confusion. The specified horizontal dimension in the table indicates the length scale of each image. The qualitative description by Bucklow is also presented in the table.

Table 4.2. Descriptions of all seventeen images presented in Bucklow (1997).

Image #	Origin	Painter	Painting	Horizontal dimension d_h (cm)	Description of craquelure pattern
1	French	Nicolas de Largilliere	'Study of Hands'	7	No direction
2	Flemish	Hieronymus Bosch	'Christ Mocked'	4.5	Parallel to the wood grain
3	Italian	Paolo Uccello	'The Battle of San Romano'	4.5	Perpendicular to the wood grain
4	Dutch	Frans Hals	'Portrait of Woman with a Fan'	7	Jagged and straight cracks with square islands
5	French	Alexander Gabriel Decamps	'The Caravan'	7	Smooth and curved cracks, and not square islands
6	Italian	Sandro Botticelli	'Four Scenes from the Early Life of St Zenobius'	4.5	Small islands

7	Italian	Master of the Fogg Pieta	‘St Lawrence’	4.5	Large islands
8	French	Francois Boucher	‘Venus Asks Vulcan for Arms for Aeneas’	7	Cracks of uniform thickness
9	Italian	Paolo Uccello	‘The Battle of San Romano’	4.5	Secondary network
10	Dutch	Johannes Lingelbach	‘The Army of Charles II’	7	Connected network
11	Italian	Duccio	‘Annunciation’	7	Broken network
12	Flemish	Master of St Giles	‘Saint Giles’	4.5	Ordered network
13	French	Francois Boucher	‘Diana Bathing’	7	Random network
14	Italian	Lorenzo Monaco	‘The Coronation of the Virgin’	4.5	Typical pattern for an Italian $14^{th}/15^{th}$ -century painting on panel
15	Flemish	Robert Campin	'Virgin and Child before a Firescreen'	4.5	Typical pattern for a Flemish $15^{th}/16^{th}$-century painting on panel
16	Dutch	Jan van de Cappelle	'River Scene with a Large Ferry'	7	Typical pattern for a Dutch 17^{th}-century painting on canvas
17	French	Jean Simeon Chardin	‘The House of Cards’	7	Typical French eighteenth-century painting on canvas

4.3.2 Analysis procedure

The workflow adopted for this study is shown in Figure 4.3. First, in Step 1, the quality of the images presented in Bucklow (1997) is enhanced using an artificial intelligence (AI)-based photo editing platform (Pickwish 2023). The purpose of this enhancement is to clearly depict the boundaries of the islands, aiming to facilitate a smoother image segmentation process.

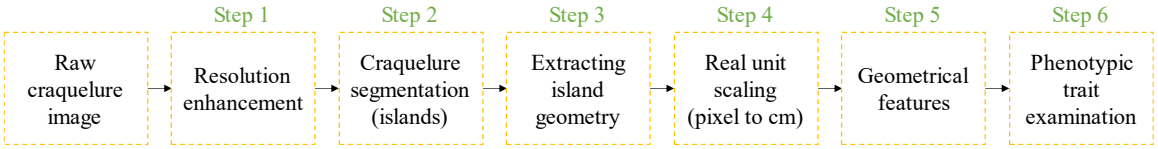

Figure 4.3. Overview of the workflow used to examine the phenotypic trait in craquelure images.

The image segmentation process (Step 2) involves converting all craquelure images to binary images. The converted black and white binary images are shown in Figure 4.4, where the islands are represented as white pixels and the cracks is represented as black pixels. Image Segmenter app (MathWorks 2021e), a MATLAB image processing toolkit, is then utilized for segmenting the crack images, thereby identifying the individual islands within each image. The effectiveness of this segmentation procedure using the Image Segmenter app has been demonstrated in Abu-Haifa and Lee (2022). Figure 4.5 shows the segmentation results for all images, where the segmented islands are randomly colored.

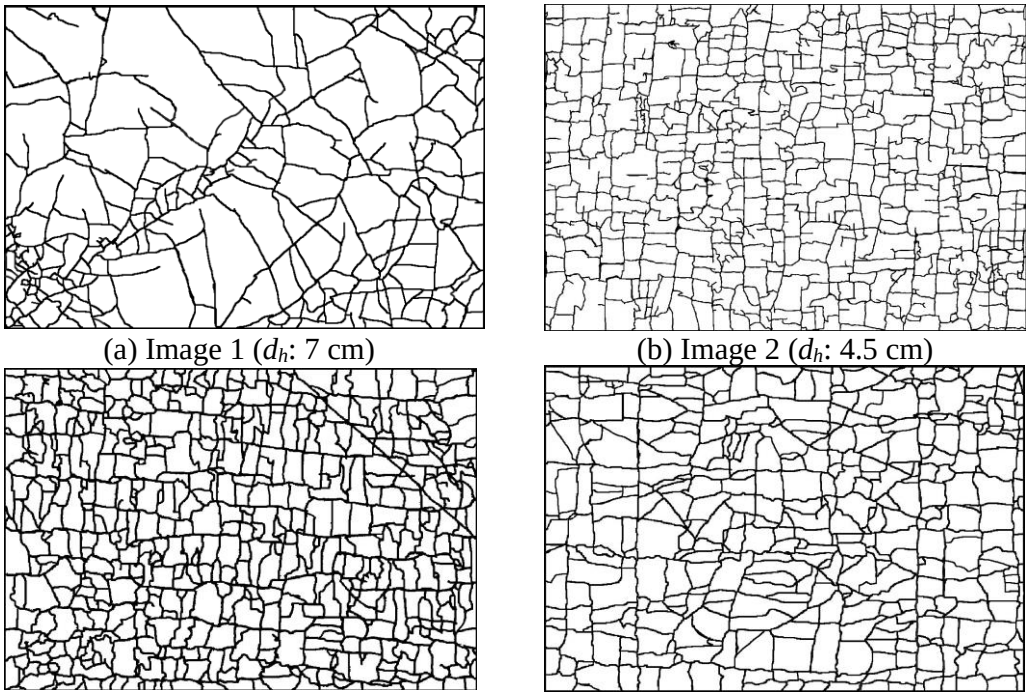

(a) Image 1 (d_h: 7 cm)

(b) Image 2 (d_h: 4.5 cm)

(c) Image 3 (d_h: 4.5 cm)

(d) Image 4 (d_h: 7 cm)

(e) Image 5 (d_h: 7 cm)

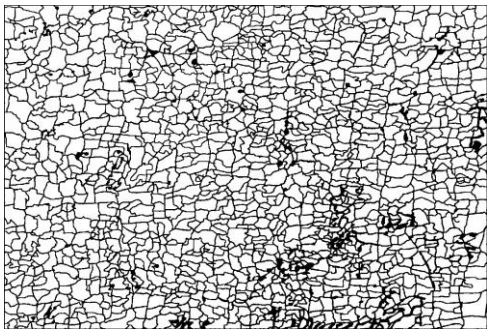

(f) Image 6 (d_h: 4.5 cm)

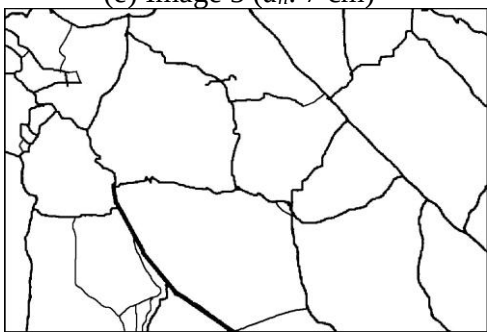

(g) Image 7 (d_h: 4.5 cm)

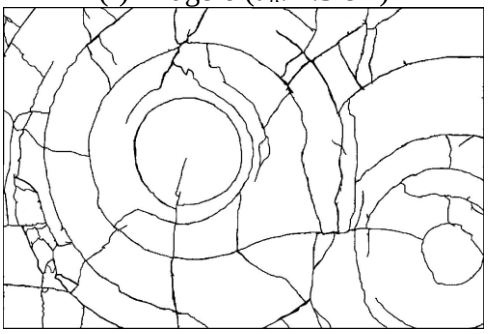

(h) Image 8 (d_h: 7 cm)

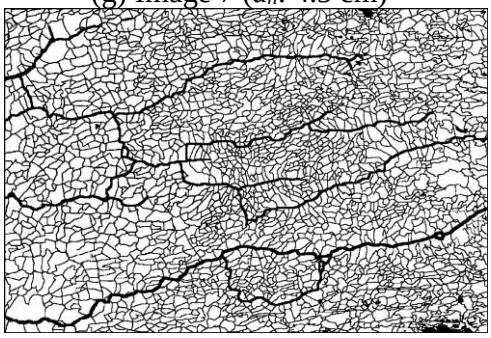

(i) Image 9 (d_h: 4.5 cm)

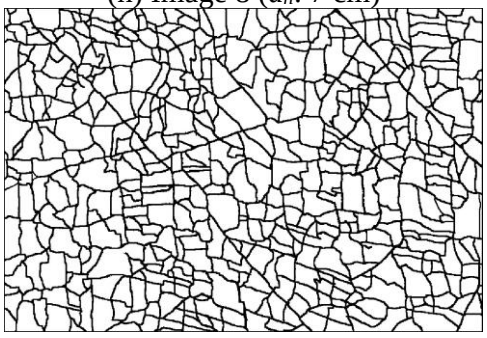

(j) Image 10 (d_h: 7 cm)

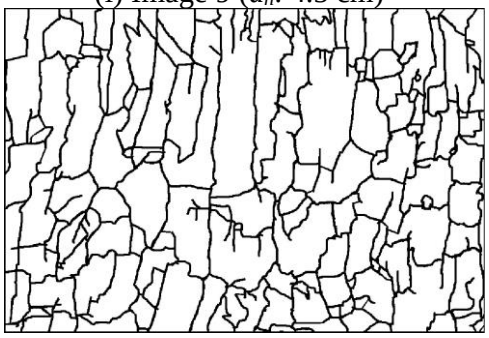

(k) Image 11 (d_h: 7 cm)

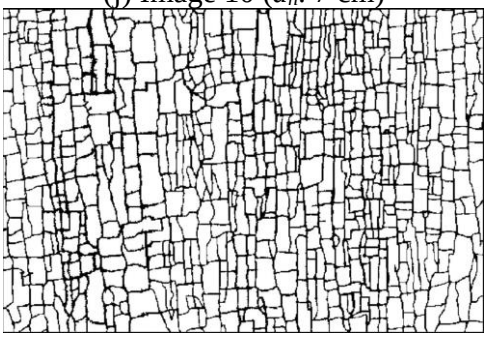

(l) Image 12 (d_h: 4.5 cm)

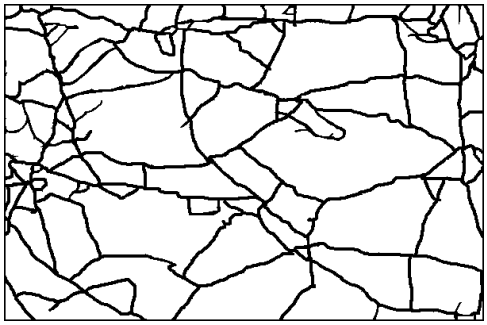

(m) Image 13 (d_h: 7 cm)

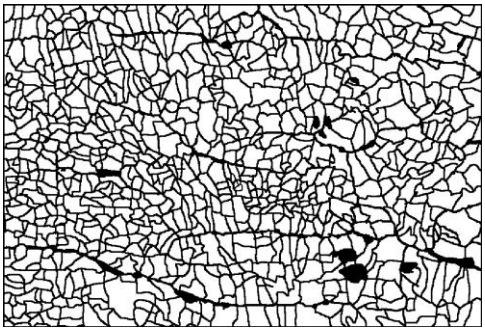

(n) Image 14 (d_h: 4.5 cm)

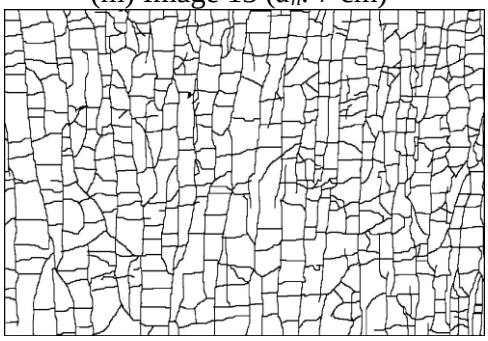

(o) Image 15 (d_h: 4.5 cm)

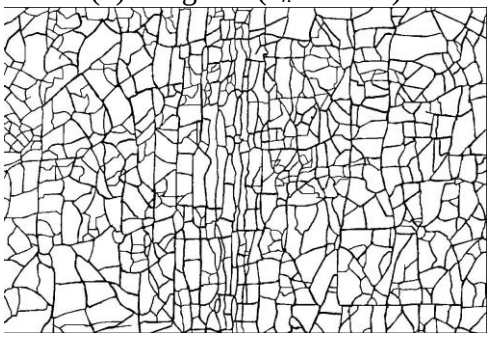

(p) Image 16 (d_h: 7 cm)

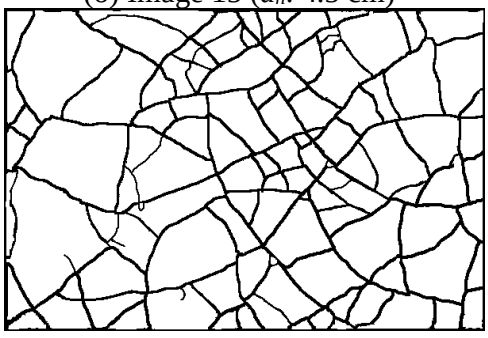

(q) Image 17 (d_h: 7 cm)

Figure 4.4. Binary crack images, where d_h indicates the horizontal dimension of image.

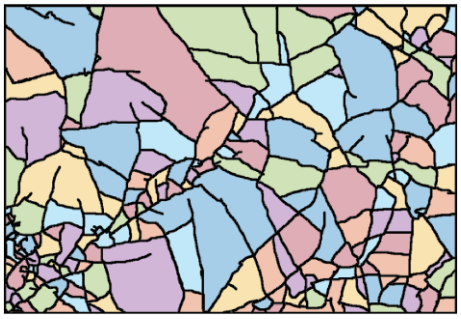

(a) Image 1

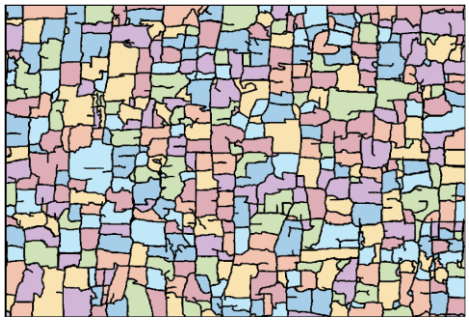

(b) Image 2

(c) Image 3

(d) Image 4

(e) Image 5

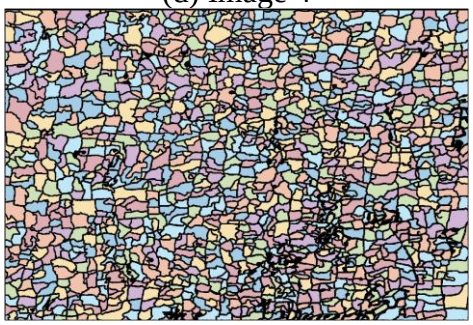

(f) Image 6

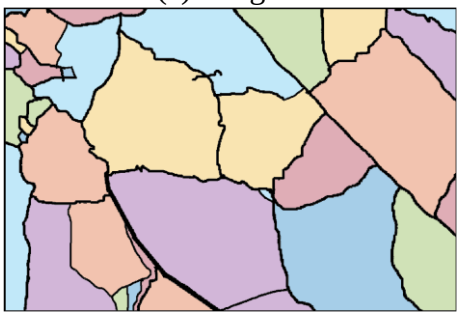

(g) Image 7

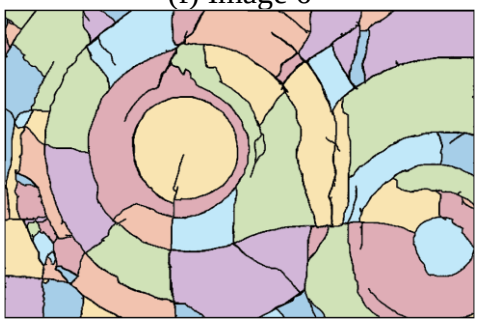

(h) Image 8

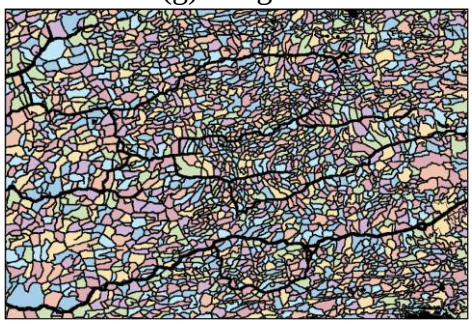

(i) Image 9

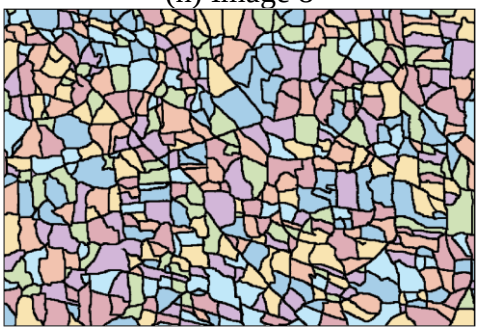

(j) Image 10

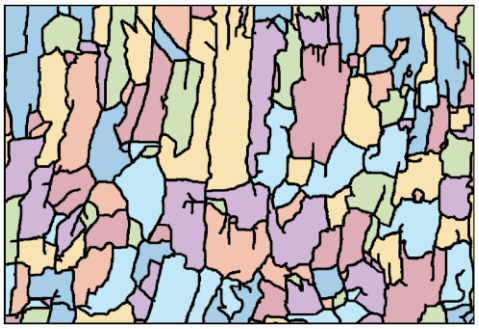

(k) Image 11

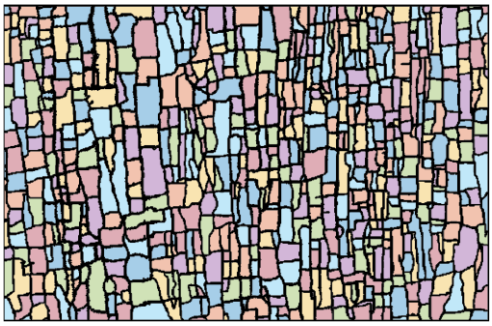

(l) Image 12

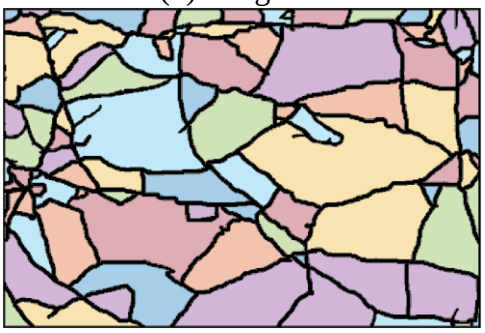

(m) Image 13

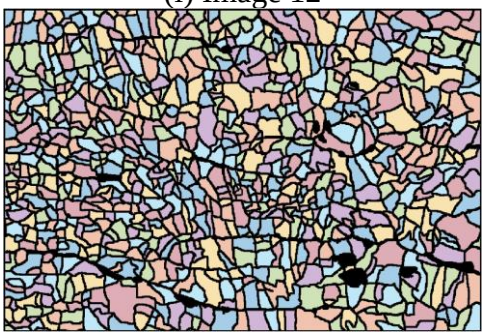

(n) Image 14

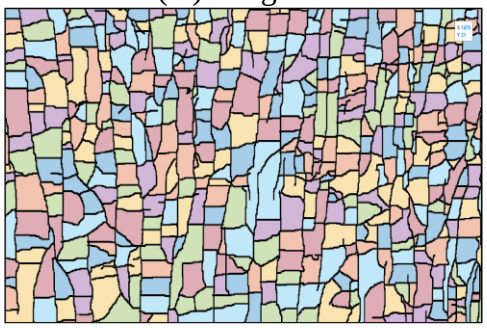

(o) Image 15

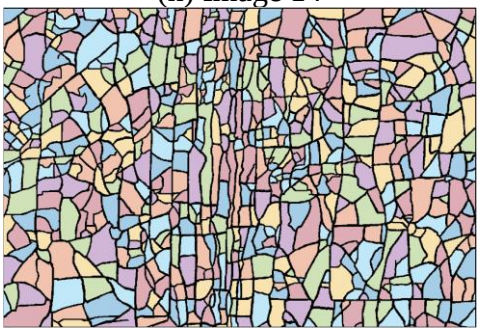

(p) Image 16

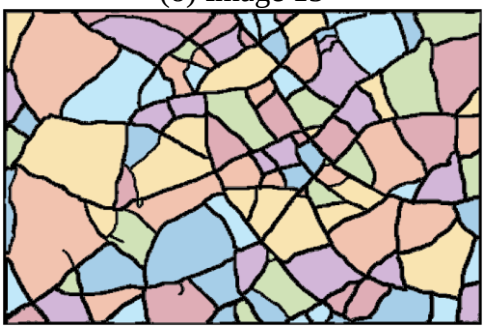

(q) Image 17

Figure 4.5. Segmented craquelure images.

The geometry (boundary) of each segmented island is then captured using the MATLAB boundary tracing function (MathWorks 2023a), which is represented as a polygon (Step

3). The vertices of the polygon, representing the boundaries of the polygonal islands, are given in pixels, resulting in a sufficient number of vertices for each island. In Step 4, the islands are scaled to their actual length (i.e., pixels are converted to cm) based on the horizontal dimension provided in

Table 4.2.

In Step 5, the geometrical information (i.e., area *A* and perimeter *P*) for each island is determined from the polygons using the built-in MATLAB functions *polyarea* and *perimeter* (MathWorks 2023b; c). In case a partial crack is present within an island, as illustrated in Figure 4.6a, a threshold crack width of 2 pixels is utilized to determine whether the partial crack should be included as part of the boundary. If the width of the partial crack is at least 2 pixels, it is considered part of the boundary and included (Figure 4.6b), otherwise not included (Figure 4.6c). Lastly, the phenotypic trait is analyzed in terms of the *P*/*A* and *A* data (Step 6).

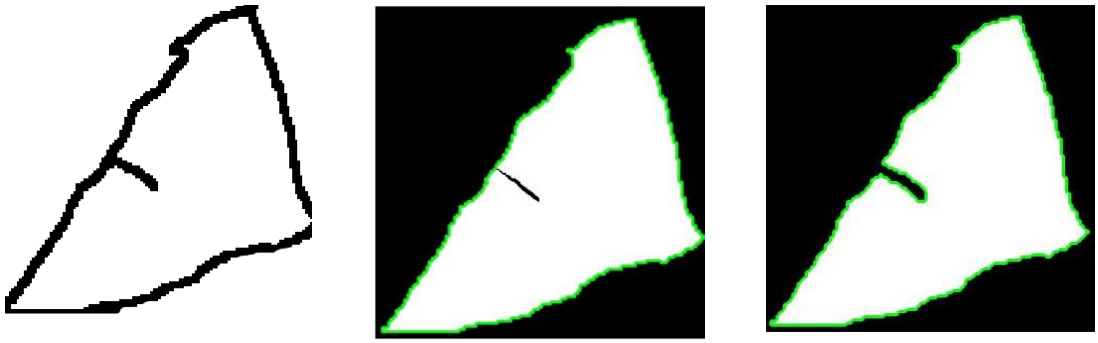

(a) (b) (c)

Figure 4.6. Determination of island boundary: (a) Presence of a partial crack; (b) A partial crack is considered part of the boundary (in green) if the width is at least 2 pixels; and (c) A small crack is not considered as part of the boundary.

4.3.3 Results and discussion

The phenotypic traits of painting cracks in all 17 images are shown in Figure 4.7, presented by the *P*/*A* and *A* data of the islands within each image. As shown in the figure, the data points, each representing the geometry of an island, align in a coherent linear relation within the log-log space. This observation confirms that the painting cracks display a self-similar nature across scales, addressing the first research question posed in this study. Please note the values along each axis are presented on a logarithmic scale with a base of 10. For example, 0 in the axes indicates the numerical value 1 (= 10^0). The scale range is set to be sufficiently large, ensuring consistency across all images. The length units are cm, so the unit of *P*/*A* is cm^{-1}.

Bivariate ellipse is plotted to provide a comprehensive representation of the data's location, variance, and orientation (Van Houwelingen et al. 1993). All bivariate ellipses in this study are constructed with the estimations performed at a 99% confidence level. The eigenvector of the ellipse is also plotted to enhance the visualization of the orientation. The bivariate ellipses are then used to address the second research question posed in this study. Specifically, this investigation explores whether the phenotypic trait exhibited by the *P*/*A* and *A* data can serve as identifying characteristics associated with the provenances of the paintings.

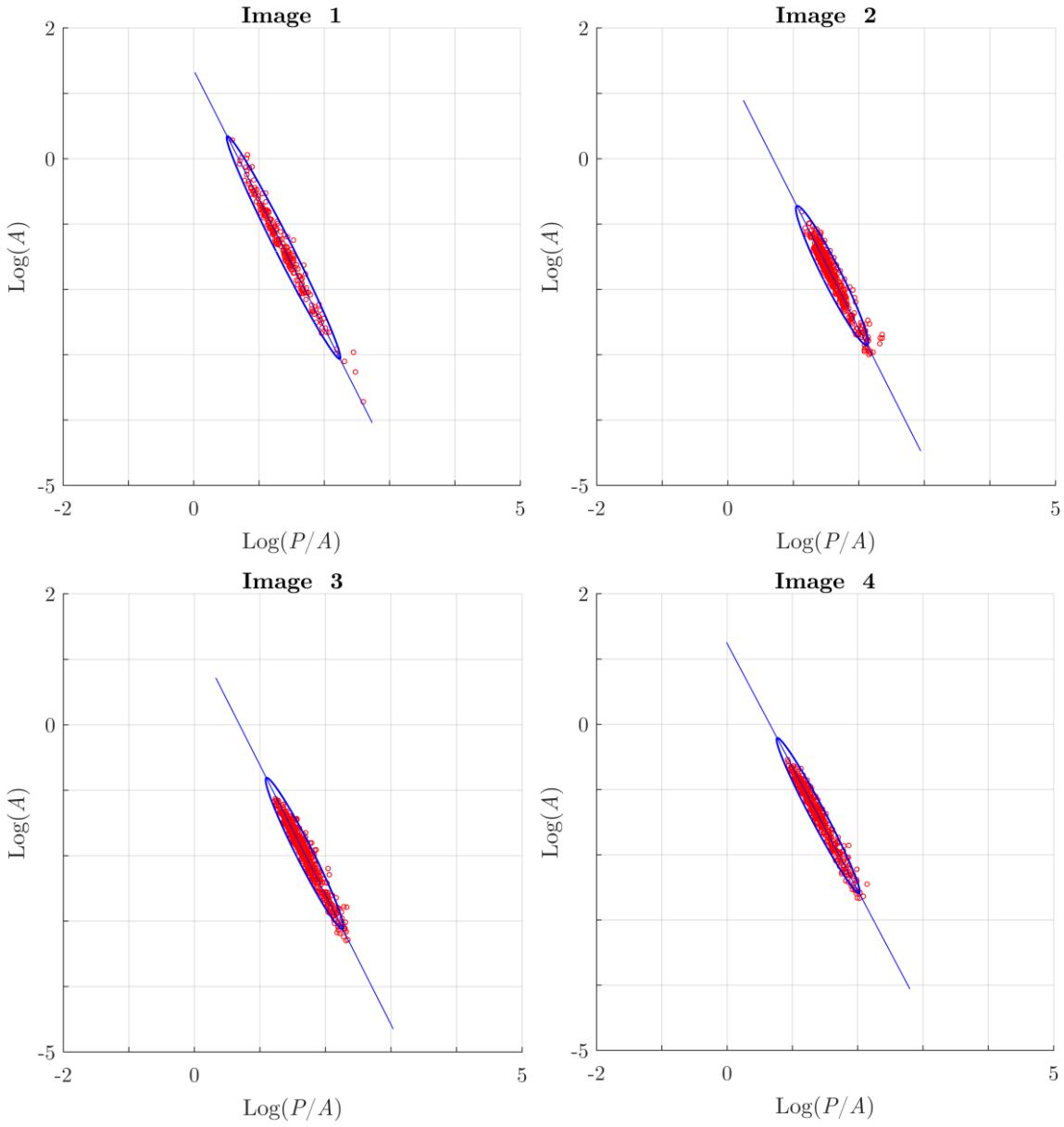
Image 1
Image 2
Image 3
Image 4
Log(A)
Log(P/A)
2
0
-5
-2
0
5

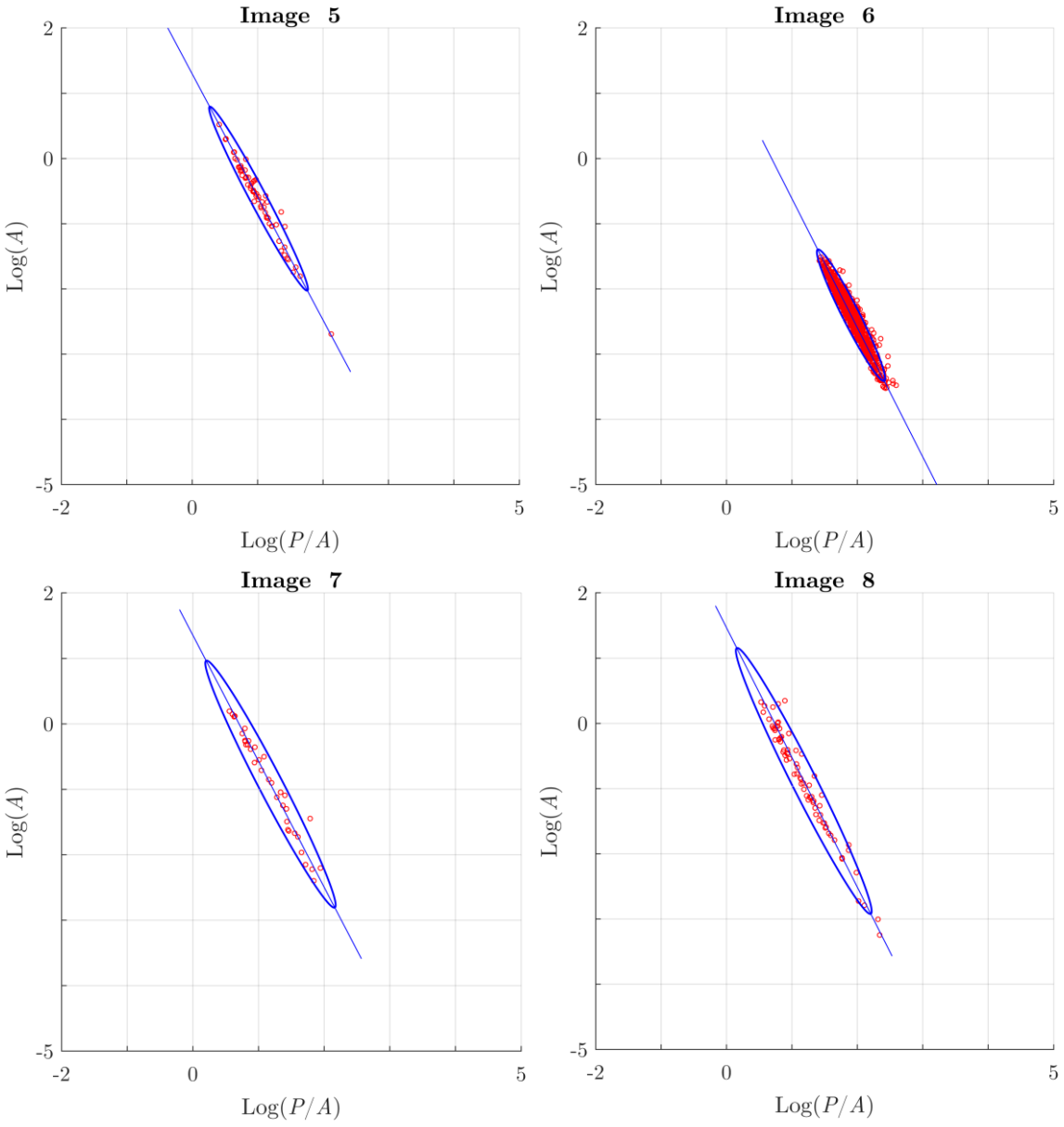
Image 5
Image 6
Image 7
Image 8
Log(A)
Log(P/A)
2
0
-5
-2
0
5

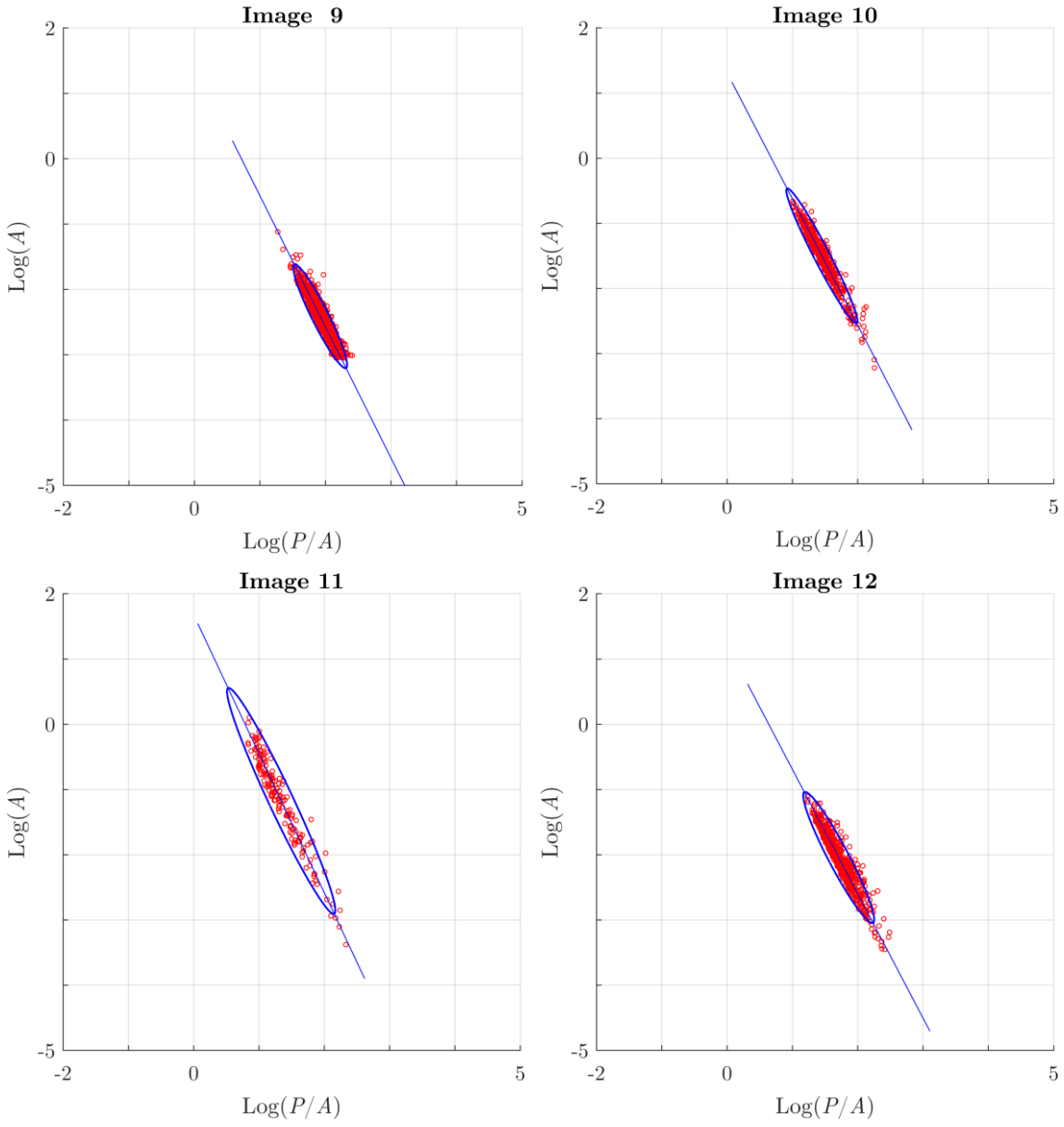
Image 9
Image 10
Image 11
Image 12
Log(A)
Log(P/A)
2
0
-5
-2
0
5

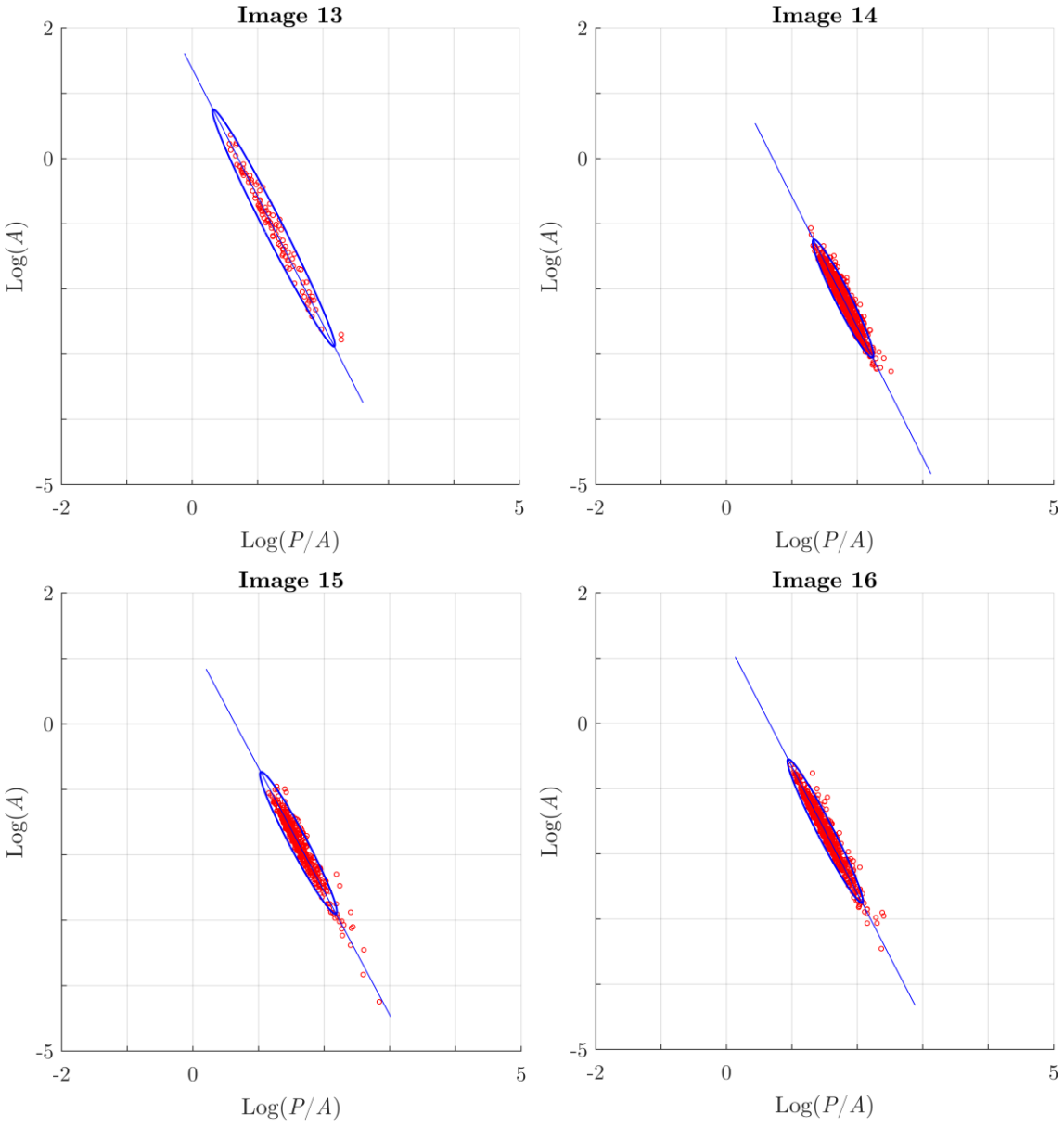
Image 13
Image 14
Image 15
Image 16
Log(A)
Log(P/A)
2
0
-5
-2
0
5

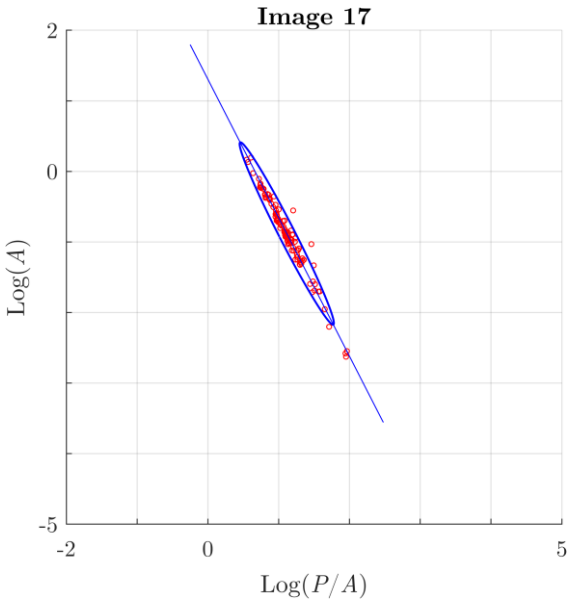

Figure 4.7. Phenotypic traits of painting cracks that are presented by the *P*/*A* and *A* data.

Figure 4.8 illustrates the ellipses estimated for the crack images from Flemish paintings (Images 2, 12, and 15). Figure 4.9 presents those for Dutch paintings (Images 4, 10, and 16) and Figure 4.10 shows the ellipses estimated for the crack images from Italian paintings (Images 3, 6, 7, 9, 11, and 14). Those for French paintings (Images 1, 5, 8, 13, and 17) are presented in Figure 4.11. Figure 4.8 evidences the presence of comparable ellipses for the Flemish paintings. Similarly, Figure 4.9 also supports this finding by demonstrating that paintings originating from the same source exhibit comparable ellipses, suggesting the presence of shared phenotypic traits influenced by the provenance of the paintings.

On the other hand, Figure 4.10 reveals the presence of three distinct sub-groups, indicating that the phenotypic traits of painting cracks within each sub-group are comparable, while differing from those in other sub-groups. The physical characteristics of the painting cracks exhibit clear differences among the sub-groups as shown in Figure 4.4. It is evident that Images 6 and 9 commonly have the smallest islands among all Italian paintings. In contrast,

Images 7 and 11 display much larger islands with some instances of a broken crack network. Please note the horizontal dimension d_h of Image 11 is 7 cm that is larger than the other. Images 3 and 14 demonstrate cracks perpendicular to the wood grain with islands characterized by intermediate sizes. These sub-groups effectively represent the distinct traits exhibited by the painting cracks.

While these paintings have Italian origins, the observed variations in cracks can be attributed to various factors. These include the age of paintings, the specific materials used, the painting techniques employed by the artists, as well as the environmental conditions present during the creation and preservation stages (Elkhuizen et al. 2019; Flores 2018; Maev et al. 2020). For example, Images 7 and 11 correspond to paintings created in the 14th centuries, while Images 3 and 14 represent paintings from the 15th century (Bucklow 1997; Fehm 1976; Griffiths 1978; Robb 1936). The similarity within each sub-group can be also attributed to factors such as painting technique. For example, both 'Four Scenes from the Life of Saint Zenobius' (Image 6) and 'The Battle of San Romano' (Image 9) were painted in the Florentine Gothic style, which emerged in the 13th century in Florence, Italy (Higgitt and White 2005; Roy and Gordon 2001; Uccello et al. 1964). This style is characterized using vibrant colors, ornate decorations, and stylized figures (Covi 1963). Also, both paintings utilize the same painting medium, specifically 'tempera on wood panel.' (The National Gallery 2023a; b). Unlike oil paints that utilize oils or encaustic paints that use beeswax to attach the color pigments, tempera uses an emulsion of water, egg yolks, or entire eggs, and sometimes with a little adhesive such as honey or milk (Thompson 1962). Therefore, while Images 6 and 9 belong to paintings created during the 15th century (Dunkerton and Roy 1996; Griffiths 1978), these exhibit the distinct

characteristics that differentiate those from other paintings of the same period. For instance, Image 14 followed a style referred to as the International Gothic (Higgitt and White 2005). This could possibly result in different reactions to fluctuations in temperature and humidity, leading to variations in the creation of cracks. Another possible reason for these similarities is the place of restoration and cleaning conditions. For example, paintings of Images 6 and 9 were restored in the National Gallery, London and had underwent similar preservation practices (The National Gallery 2023b; a).

In French paintings, it is observed that the cracks exhibit larger islands compared to paintings of different origins, as shown in Figure 4.4, thus resulting in data with a correspondingly large area *A*. Consequently, the ellipses representing those islands cover the plot space associated with high *A* values (Figure 4.11). The French paintings also have sub-groups. The cracks in Images 1, 8, and 13 show similar phenotypic traits, resulting in comparable ellipses. Likewise, Images 5 and 17 also exhibit comparable traits and ellipses. Similarly, the observed trend suggests that paintings created within the same century tend to exhibit similar traits in the cracks. Images 1, 8, and 13 correspond to paintings created in the 18^{th} century (Ledbury and Hyde 2006; Louvre Museum 1742; Meyer 1995) , while Images 5 and 17 represent paintings from the 19^{th} and 18^{th} century, respectively (Bucklow 1997). However, in addition to the age factor, other reasons also explain the difference between the two sub-groups. For example, the painting medium for paintings of Images 5 and 17 is ‘oil on canvas’ (Bucklow 1997; The National Gallery 2023c), while the painting of Image 8 is created using ‘pen and brown ink and brown wash over black chalk’ (Getty Museum Collection 2023).

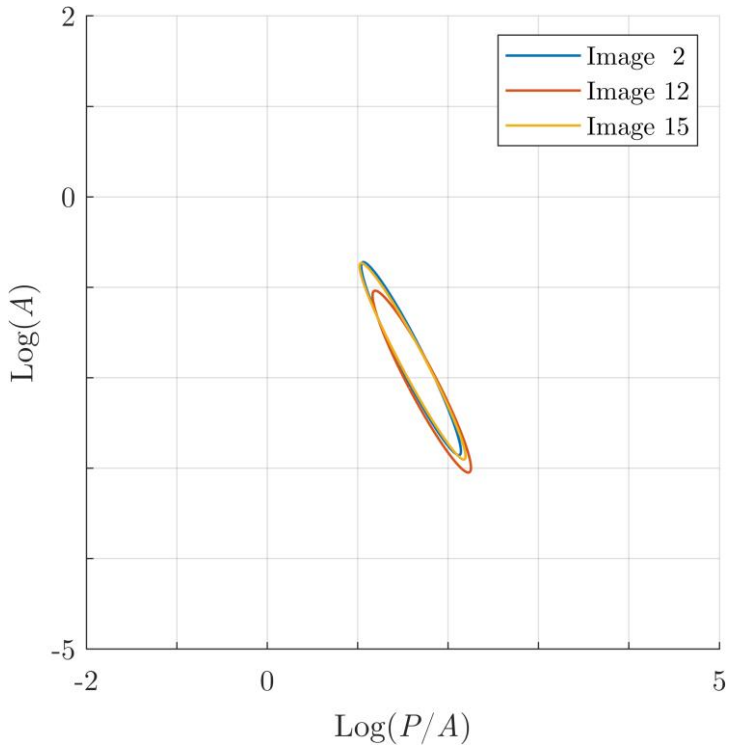

Figure 4.8. Bivariate ellipses estimated for the crack images from the Flemish Paintings.

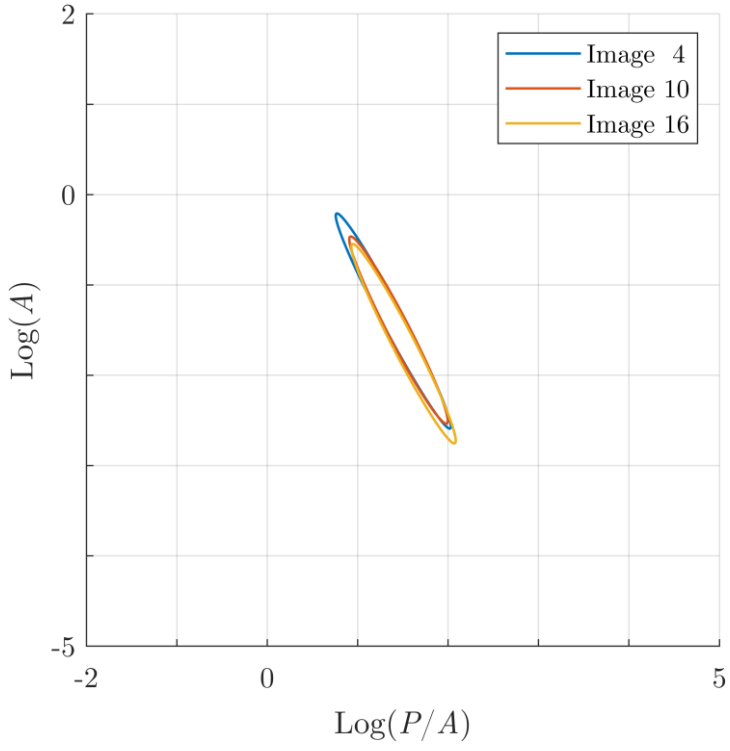

Figure 4.9. Bivariate ellipses estimated for the crack images from the Dutch Paintings.

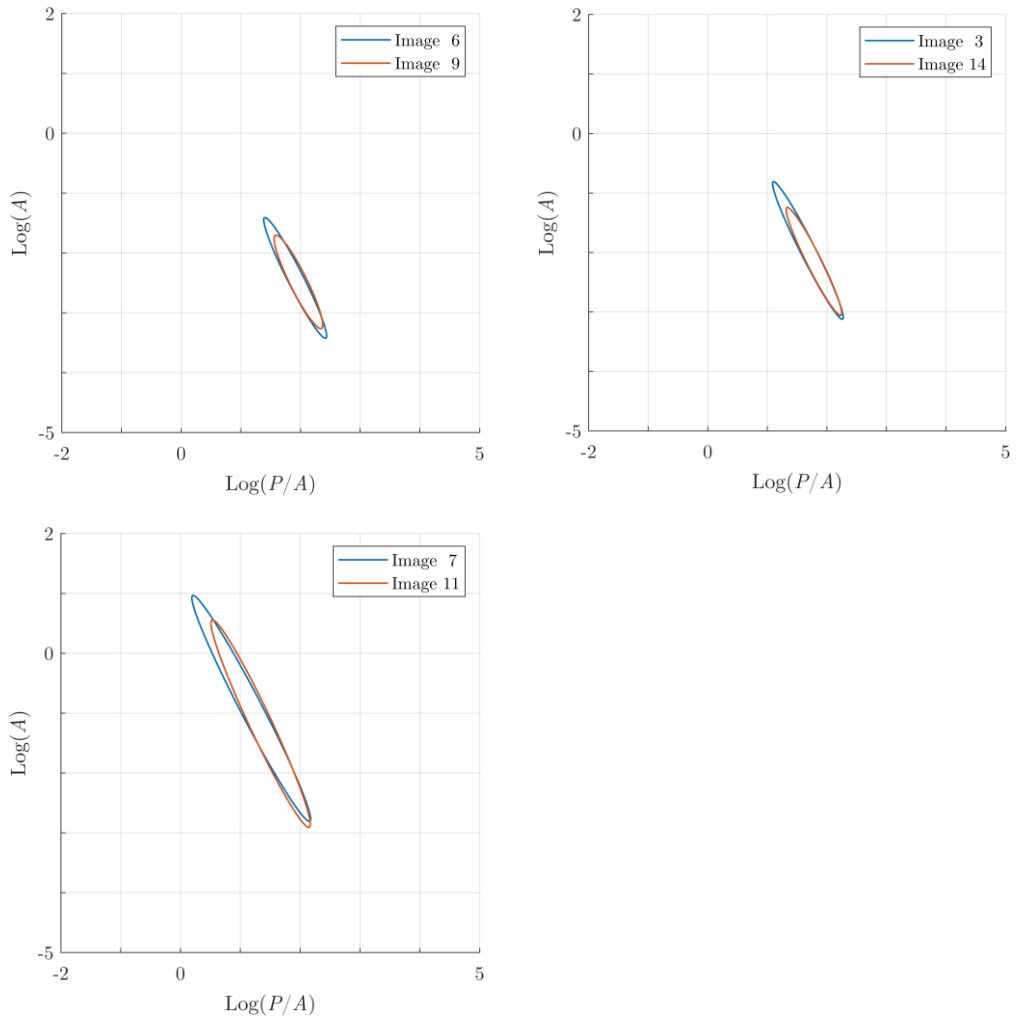

Figure 4.10. Comparable bivariate ellipses within each sub-group of Italian paintings.

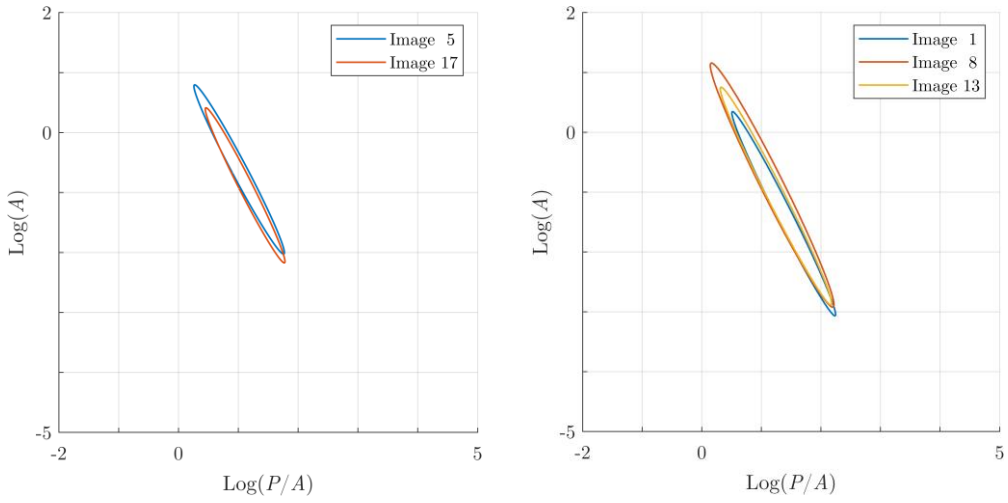

Figure 4.11. Comparable bivariate ellipses within each sub-group of French paintings.

4.4 Concluding Remarks

This study introduces a new perspective on the painting cracks, also known as craquelure, investigating two questions: (i) Do painting cracks exhibit self-similarity? and (ii) If so, can the characteristic self-similarity of these cracks be utilized as an identifier that can be correlated with the origins of paintings? To this end, we employ the concept of the phenotypic trait of painting cracks, with a specific focus on analyzing the characteristics of islands enclosed by cracks. A set of crack images from French, Italian, Flemish, and Dutch paintings spanning the 14^{th} to 19^{th} centuries is analyzed. Digital image analysis techniques, including image segmentation and boundary detection, are utilized to extract the 2D geometrical features from the images. This study evidences a power-law relation between perimeter-to-area (P/A) and area (A) data of the islands in a log-log space. This power-law relation highlights the inherent self-similar nature present behind the various crack patterns. Bivariate ellipses and their eigenvectors are employed as a comprehensive representation of the location, variance, and orientation of the island geometry data. The study finds that comparable ellipses emerge when the cracks exhibit similar phenotypic traits, particularly in case paintings share the origin, employ similar painting techniques, and undergo common preservation practices. Therefore, these phenotypic traits appear to serve as identifying characteristics that can be associated with the provenances of the paintings. It is important to note that establishing a universal measure to directly determine the origin of a painting solely based on its cracks remains a challenge. This difficulty arises due to variations in preservation practices, including storing and handling, which can influence the development of aging cracks over time, even among works by the same artist. Nevertheless, the comparative study presented in this study provides compelling evidence

supporting the validity of the proposed approach that utilizes the P/A and A data of islands. We invite the research community to further explore the approach to unlock the potential for elucidating the phenotypic traits of painting cracks.

In addition to the field of scientific examination of artworks, the findings in this study have far-reaching significance. The approach employed in this study introduces a new paradigm for crack analysis, emphasizing the examination of islands formed within cracks. Therefore, this approach has the potential to be extended beyond the realm of art, e.g., to analyze the characteristics of soil clods to better understand the formation of desiccation cracks. By shifting the focus from the crack network itself, this approach offers a departure from conventional crack analyses, and will open up new avenues for understanding the physical characteristics and underlying mechanisms of cracks

CHAPTER 5 . CONCLUDING REMARKS AND RECOMMENDATIONS

5.1 Concluding Remarks

The objectives of this PhD dissertation have been thoroughly outlined and achieved in an innovative and efficient manner. By utilizing a single image per masonry wall as input and analyzing the outcomes of image processing techniques, this study leads to a novel approach in the digital reconstruction of 3D masonry structures and preservation practice. The implementation of polyhedron reconstruction and impulse-based dynamics, considerably enhances computational efficiency, which is crucial for the preservation practice of hazard vulnerability assessment of unreinforced masonry structures and has significant implications for retaining the historic masonry heritage of the country. Furthermore, the maintenance of computational efficiency by simplifying brick geometries and providing a new method of craquelure pattern analysis through image processing techniques directly contributes to enhancing the simulation accuracy and prediction of painting provenance, respectively. Overall, this PhD dissertation makes a valuable contribution to the field, paving the way for future research and innovation in the preservation of historic masonry structures. In addition, the analysis of craquelure patterns using image processing techniques showed that historic paintings are most likely to share similar craquelure behavior if they belong to the same origin and time period.

To sum up, the major findings from this study are summarized below:

- The study introduced a streamlined framework for modeling and simulating single-wythe masonry structures based on image analysis. This framework offers a significant improvement in accurately assessing the vulnerability of such structures

to hazards. Moreover, it demonstrates notable computational efficiency, ensuring efficient analysis and evaluation processes.

- Masonry wall images were used as inputs with some other input parameters, like brick size and wall dimensions and orientations, for 3D discrete element modeling and analysis, where individual bricks are directly detected from the image, and the interactions of the bricks are explicitly considered in the numerical simulation of the masonry wall.
- The proposed framework (for both planar walls and single-wythe masonry structures) consists of four main stages; i) defining the inputs, ii) 2D modeling of the walls, iii) 3D reconstruction of the wall or structure, and iv) conducting the discrete element simulation for hazard vulnerability assessment.
- The image-based modeling-to-simulation framework can estimate collapse scenarios from input masonry wall images and proposes a prototype that transforms visual images into critical domain knowledge that would be useful for disaster preparedness.
- The 2D modeling stage mainly includes image segmentation to convert the image into a binary image, where the bricks are presented in white and the mortar layer in black, and the analysis of the resulted binary image to capture brick geometries and approximate their shapes into simplified polygons.
- Splitting and Douglas-Peuker methods showed their capabilities in simplifying brick shapes into simplified polygons with a much lower number of vertices, maintaining high fidelity. However, the splitting method slightly outperforms Douglas-Peuker method.

- The proposed frameworks for single-wythe masonry structures were automatically capable of considering the stretcher bond between adjoining walls.
- Image processing is an effective method that helps in the analysis of craquelure patterns of historic paintings for their dating and provenance.
- Analyzing the geometrical features of the painting islands, such as their areas, perimeters, and shapes, showed that paintings have a phenotypic trait (like mineral particles), which can help historians preserve historic paintings.

5.2 Recommendations for Future Research

Based on the findings of the dissertation, there are several recommendations for future studies that can build upon the proposed image-based frameworks for evaluating the seismic vulnerability of masonry structures and characterizing craquelure patterns of historic paintings. Here are some recommendations for future research:

- Future studies can explore the possibility of integrating other non-destructive techniques, such as X-ray imaging, acoustic emission testing (AET), or infrared thermology (IRT) with image-based modeling to improve the accuracy and reliability of the framework, resulting in a more comprehensive understanding of the tested material's internal structure, which would aid researchers in identifying and analyzing potential flaws and defects.
- It would also be interesting to investigate the possibility of developing the proposed image-based method for evaluating the seismic vulnerability of multiple-wythes masonry structures, offering potential advancement and improvements to more types of unreinforced masonry structures.

- The proposed framework's potential for predictive reconstruction of invisible masonry walls and assessment of entire masonry structures' hazard vulnerability can be further explored as a potential solution for overcoming image-based analysis obstacles when structures are in close proximity, making clear imaging of some masonry walls difficult.
- The potential of the proposed framework can be further developed by considering additional bonding types for adjoining masonry walls, which would enhance the accuracy of image-based modeling and improve the approach's overall effectiveness by making it applicable for more types of masonry structures.
- Further research can be conducted to investigate the potential of the proposed framework in assessing the hazard vulnerability of other types of masonry structures, such as cavity walls and reinforced masonry structures, and compare the results with other modeling approaches in identifying and analyzing potential vulnerabilities, which will open up a new avenue for research.
- Future research could further evaluate the performance of different image segmentation methods to determine how effectively they can i) capture the geometrical features of a masonry wall, ii) enhance the DEM simulation results, and iii) accurately identify and characterize the craquelure patterns of historic paintings. This exploration could bring about further advancements and improvements to image-based modeling methodologies and can result in finding the optimal segmentation method that best suits the intended goal of the analysis.
- Future studies can explore the possibility of using machine learning algorithms with larger dataset of paintings, to automatically recognize and classify the types of

paintings and the different styles of painters from digital images. This exploration could provide new insights into establishing both the provenance and history of paintings.

REFERENCES

Abas, F. (2004). “Analysis of craquelure patterns for content-based retrieval.” University of Southampton.

Abdelrahman, M. A., Said, S. A. M., and Ahmad, A. (1993). “A comparison of energy consumption and cost-effectiveness of four masonry materials in Saudi Arabia.” *Energy*, Elsevier, 18(11), 1181–1186.

Abu-Haifa, M., and Lee, S. J. (2022). “Image-Based Modeling-to-Simulation of Masonry Walls.” *Journal of Architectural Engineering*, 28(4), 06022001.

Abu-Haifa, M., and Lee, S. J. (2023). “Image-based 3D modeling-to-simulation of single-wythe masonry structure via reverse descriptive geometry.” *Journal of Building Engineering*, Elsevier, 76(10), 107125.

Adobe Photoshop. (2022a). “Adobe Photoshop (version 24.0.0).” *Preuzeto*, 2022.

Adobe Photoshop. (2022b). “Remove objects from your photos with Content-Aware Fill.” *Adobe*, <https://helpx.adobe.com/photoshop/using/content-aware-fill.html> (Nov. 7, 2022).

Ahiwale, D. D., Kontoni, D.-P. N., Jadhav, A. V, and Bawale, A. B. (2023). “FEM analysis of the effect of various brick bond patterns on masonry walls under in-plane cyclic loading.” *Asian Journal of Civil Engineering*, Springer, 1–15.

Al-Fakih, A., Wahab, M. M. A., Mohammed, B. S., Liew, M. S., Zawawi, N. A. W. A., and As’ ad, S. (2020). “Experimental study on axial compressive behavior of rubberized interlocking masonry walls.” *Journal of Building Engineering*, Elsevier, 29, 101107.

Al-Sakkaf, A., Zayed, T., and Bagchi, A. (2020). “A sustainability based framework for evaluating the heritage buildings.” *International Journal of Energy Optimization and Engineering (IJEOE)*, IGI Global, 9(2), 49–73.

Alecci, V., Fagone, M., Rotunno, T., and De Stefano, M. (2013). “Shear strength of brick masonry walls assembled with different types of mortar.” *Construction and Building Materials*, Elsevier, 40, 1038–1045.

Almeida, C., Guedes, J. P., Arêde, A., and Costa, A. (2016). “Geometric indices to quantify textures irregularity of stone masonry walls.” *Construction and Building Materials*, Elsevier, 111, 199–208.

Altunışık, A. C., Önalan, F., and Sunca, F. (2021). “Experimental, numerical and analytical investigation on blast response of brick walls subjected to TNT explosive.” *Journal of Structural Engineering*, 4(1), 28–45.

Angiolilli, M., Pathirage, M., Gregori, A., and Cusatis, G. (2021). “Lattice discrete particle model for the simulation of irregular stone masonry.” *Journal of Structural Engineering*, American Society of Civil Engineers, 147(9), 4021123.

Archtoolbox. (2023). “Typical Brick Bonds.” *Archtoolbox website*, <https://www.archtoolbox.com/brick-bonds/> (Jun. 5, 2023).

Asteris, P. G., Moropoulou, A., Skentou, A. D., Apostolopoulou, M., Mohebkhah, A., Cavaleri, L., Rodrigues, H., and Varum, H. (2019). “Stochastic vulnerability assessment of masonry structures: concepts, modeling and restoration aspects.” *Applied Sciences*, MDPI, 9(2), 243.

Augarde, C. E., Lee, S. J., and Loukidis, D. (2021). “Numerical modelling of large deformation problems in geotechnical engineering: A state-of-the-art review.” *Soils and Foundations*, 61(6), 1718–1735.

Azzara, R. M., Girardi, M., Iafolla, V., Lucchesi, D. M., Padovani, C., and Pellegrini, D. (2021). “Ambient vibrations of age-old masonry towers: Results of long-term dynamic monitoring in the historic centre of Lucca.” *International Journal of Architectural Heritage*, Taylor & Francis, 15(1), 5–21.

Baer, J. U., Kent, T. F., and Anderson, S. H. (2009). “Image analysis and fractal geometry to characterize soil desiccation cracks.” *Geoderma*, Elsevier, 154(1–2), 153–163.

Bakeer, T. (2016). “Empirical estimation of the load bearing capacity of masonry walls under buckling–Critical remarks and a new proposal for the Eurocode 6.” *Construction and Building Materials*, Elsevier, 113, 376–394.

Banerjee, S., Nayak, S., and Das, S. (2021). “Adjudging efficacy of geonet reinforcement on the seismic performance of brick masonry structures: an experimental study.” *Materials and Structures*, Springer, 54(6), 1–24.

Baraldi, D., Reccia, E., and Cecchi, A. (2018). “In plane loaded masonry walls: DEM and FEM/DEM models. A critical review.” *Meccanica*, Springer, 53, 1613–1628.

Barron, I. R., and Sharma, G. (2020). “Toward CanvasChain: A Block Chain and Craquelure Hash Based System For Authenticating and Tracking Fine Art Paintings.” *Electronic Imaging*, Society for Imaging Science and Technology, 32, 1–6.

Bärtschi, R., and Bonwetsch, T. (2013). “A stretcher bond with defects applied to a hyperboloid.” *Advances in Architectural Geometry 2012*, Springer, 37–42.

Basha, S. H., Guo, Z.-X., and Xie, X. (2022). “Effect of Structural Bonding Patterns on Mechanical Characteristics of Clay Brick Masonry under Different Loadings Using Digital Image Correlation Technique.” *Journal of Materials in Civil Engineering*, American Society of Civil Engineers, 34(11), 4022302.

Batar, O. S., Tercan, E., and Emsen, E. (2021). “Ayvalıkemer (Sillyon) historical masonry arch bridge: a multidisciplinary approach for structural assessment using point cloud data obtained by terrestrial laser scanning (TLS).” *Journal of Civil Structural Health Monitoring*, Springer, 11(5), 1239–1252.

Belemmi, G. (2012). “Construction materials: Stone and Ceramics.” <https://www.edu.xunta.gal/centros/espazoAbalar/aulavirtual/pluginfile.php/1319/mod_imscp/content/1/construction_materials_stone_and_ceramics.html> (May 23, 2021).

Bender, J., Erleben, K., and Trinkle, J. (2014). “Interactive Simulation of Rigid Body Dynamics in Computer Graphics.” *Computer Graphics Forum*, 33(1), 246–270.

Binda, L., Modena, C., Baronio, G., and Abbaneo, S. (1997). “Repair and investigation techniques for stone masonry walls.” *Construction and Building Materials*, Elsevier, 11(3), 133–142.

Binda, L., Pina-Henriques, J., Anzani, A., Fontana, A., and Lourenço, P. B. (2006). “A contribution for the understanding of load-transfer mechanisms in multi-leaf masonry walls: Testing and modelling.” *Engineering Structures*, Elsevier, 28(8), 1132–1148.

Biscarini, C., Catapano, I., Cavalagli, N., Ludeno, G., Pepe, F. A., and Ubertini, F. (2020). “UAV photogrammetry, infrared thermography and GPR for enhancing structural and material degradation evaluation of the Roman masonry bridge of Ponte Lucano in Italy.” *NDT & E International*, Elsevier, 115, 102287.

Błaszczak-Bąk, W., Suchocki, C., Janicka, J., Dumalski, A., Duchnowski, R., and Sobieraj-Żłobińska, A. (2020). “Automatic threat detection for historic buildings in dark places based on the modified OPTD method.” *ISPRS International Journal of Geo-Information*, Multidisciplinary Digital Publishing Institute, 9(2), 123.

Bone, P. (2023). “Polygon simplification.” *MATLAB Central File Exchange*, <https://www.mathworks.com/matlabcentral/fileexchange/45342-polygon-simplification> (Mar. 18, 2021).

Boni, C., Ferretti, D., Lenticchia, E., and Tasora, A. (2019). “DEM modelling of masonry vaults: influence of brick pattern and infill on stability during supports displacements.” *Proceedings of IASS Annual Symposia*, International Association for Shell and Spatial Structures (IASS), 1–8.

Bordoloi, S., Ni, J., and Ng, C. W. W. (2020). “Soil desiccation cracking and its characterization in vegetated soil: A perspective review.” *Science of the Total Environment*, Elsevier, 729, 138760.

Bowler, J., Brown, C., Capsimalis, M., Cohn, R., Cole, L. D., and others. (2001). “Scalable vector graphics (svg) 1.0 specification.” *World Wide Web Consortium*.

Brocken, H., and Nijland, T. G. (2004). “White efflorescence on brick masonry and concrete masonry blocks, with special emphasis on sulfate efflorescence on concrete blocks.” *Construction and Building Materials*, Elsevier, 18(5), 315–323.

Bruneau, M. (1994). “Seismic evaluation of unreinforced masonry buildings—A state-of-the-art report.” *Canadian Journal of Civil Engineering*, NRC Research Press Ottawa, Canada, 21(3), 512–539.

Brunelli, A., De Silva, F., Piro, A., Parisi, F., Sica, S., Silvestri, F., and Cattari, S. (2021). “Numerical simulation of the seismic response and soil–structure interaction for a monitored masonry school building damaged by the 2016 Central Italy earthquake.” *Bulletin of Earthquake Engineering*, Springer, 19(2), 1181–1211.

Bucklow, S. (1997). “The Description of Craquelure Patterns.” *Studies in Conservation*, 42(3), 129.

Bucklow, S. (1998). “A stylometric analysis of craquelure.” *Computers and the Humanities*, Springer, 31, 503–521.

Bucklow, S. (1999). “The description and classification of craquelure.” *Studies in conservation*, Taylor & Francis, 44(4), 233–244.

Bucklow, S. (2020). “The classification of craquelure patterns.” *Conservation of easel paintings*, Routledge, 295–301.

Bui, T. T., Limam, A., and Sarhosis, V. (2019). “Failure analysis of masonry wall panels subjected to in-plane and out-of-plane loading using the discrete element method.” *European Journal of Environmental and Civil Engineering*, Taylor & Francis, 25(5), 876–892.

Bui, T. T., Limam, A., and Sarhosis, V. (2021). “Failure analysis of masonry wall panels subjected to in-plane and out-of-plane loading using the discrete element method.” *European Journal of Environmental and Civil Engineering*, Taylor & Francis, 25(5), 876–892.

Bui, T. T., Limam, A., Sarhosis, V., and Hjiaj, M. (2017). “Discrete element modelling of the in-plane and out-of-plane behaviour of dry-joint masonry wall constructions.” *Engineering Structures*, 136, 277–294.

Buzzle. (2021). “What is Ashlar Masonry? Fine Stonework in the Making.” <https://historyplex.com/what-is-ashlar-masonry>.

Cacciotti, R. (2020). “Brick masonry response to wind driven rain.” *Engineering Structures*, Elsevier, 204, 110080.

Caliò, I., Marletta, M., and Pantò, B. (2012). "A new discrete element model for the evaluation of the seismic behaviour of unreinforced masonry buildings." *Engineering Structures*, Elsevier, 40, 327–338.

Castellazzi, G., D'Altri, A., Bitelli, G., Selvaggi, I., and Lambertini, A. (2015). "From Laser Scanning to Finite Element Analysis of Complex Buildings by Using a Semi-Automatic Procedure." *Sensors*, 15(8), 18360–18380.

Cavalagli, N., Cluni, F., and Gusella, V. (2013). "Evaluation of a statistically equivalent periodic unit cell for a quasi-periodic masonry." *International Journal of Solids and Structures*, Elsevier, 50(25–26), 4226–4240.

Cavalagli, N., Gioffrè, M., Grassi, S., Gusella, V., Pepi, C., and Volpi, G. M. (2020). "On the accuracy of UAV photogrammetric survey for the evaluation of historic masonry structural damages." *Procedia Structural Integrity*, Elsevier, 29, 165–174.

Cavaleri, L., Failla, A., La Mendola, L., and Papia, M. (2005). "Experimental and analytical response of masonry elements under eccentric vertical loads." *Engineering Structures*, Elsevier, 27(8), 1175–1184.

Chaiyasarn, K., Khan, W., Ali, L., Sharma, M., Brackenbury, D., and DeJong, M. (2018). "Crack detection in masonry structures using convolutional neural networks and support vector machines." *ISARC. Proceedings of the International Symposium on Automation and Robotics in Construction*, IAARC Publications, 1–8.

Chaiyasarn, K., Mahat, S., and Prukpratin, S. (2021). "The Application of 3D Image-Based Photogrammetry in Thai Heritage Sites: A Case Study of Wat Chai Wattanaram." *International Conference on Protection of Historical Constructions*, Springer, Cham, 477–488.

Chen, X., Wang, X., Wang, H., Agrawal, A. K., Chan, A. H. C., and Cheng, Y. (2021). "Simulating the failure of masonry walls subjected to support settlement with the combined finite-discrete element method." *Journal of Building Engineering*, Elsevier, 43, 102558.

Cheng, H.-D., Jiang, X. H., Sun, Y., and Wang, J. (2001). "Color image segmentation: advances and prospects." *Pattern recognition*, Elsevier, 34(12), 2259–2281.

Chiang, K.-Y., Chien, K.-L., and Hwang, S.-J. (2008). "Study on the characteristics of building bricks produced from reservoir sediment." *Journal of Hazardous Materials*, Elsevier, 159(2–3), 499–504.

Civil, I., Michalski, S. W., and Murray, A. (2002). "Cracking the 'matter paintings' of Antoni Tàpies: the role of artistic intent, deterioration and underlying mechanical causes." *th Triennial Meeting Rio de Janeiro: ICOM Committee for Conservation: Preprints (Vol.1), September 22-27*, Rio de Janeiro, Brazil.

Clayton, P., Zalachoris, G., Rathje, E., Bheemasetti, T., Caballero, S., Yu, X., and Bennett, S. (2016). “The geotechnical aspects of the September 3, 2016 M 5.8 Pawnee, Oklahoma earthquake.” *GEER Association, Berkeley, California, doi*, 10, G69885.

Clemente, P., Delmonaco, G., Puzzilli, L., and Saitta, F. (2019a). “Seismic analysis of the Stylite Tower at Umm ar-Rasas.” *Structural analysis of historical constructions*, Springer, 1780–1788.

Clemente, P., Delmonaco, G., Puzzilli, L., and Saitta, F. (2019b). “Stability and seismic vulnerability of the Stylite Tower at Umm ar-Rasas.” *Annals of Geophysics*, 62(3).

Coumans, E. (2020). “Bullet Physics.”

Covi, D. A. (1963). “Lettering in Fifteenth Century Florentine Painting.” *The Art Bulletin*, Taylor & Francis, 45(1), 1–17.

Cundall, P. A., and Hart, R. D. (1992). “Numerical Modelling OF Discontinua.” *Engineering Computations*, 9(2), 101–113.

Cundall, P. A., and Strack, O. D. L. (1979). “A discrete numerical model for granular assemblies.” *Géotechnique*, Thomas Telford, 29(1), 47–65.

Cuong, N. H., Shin, J., Kim, J. H., Luat, N.-V., and Lee, K. (2022). “Compressive and shear behavior of brick masonry assemblages strengthened with polyurea coating: Experiment and DEM investigations.” *Construction and Building Materials*, Elsevier, 348, 128534.

D’Altri, A. M., Milani, G., de Miranda, S., Castellazzi, G., and Sarhosis, V. (2018). “Stability analysis of leaning historic masonry structures.” *Automation in Construction*, Elsevier, 92, 199–213.

D’Altri, A. M., Sarhosis, V., Milani, G., Rots, J., Cattari, S., Lagomarsino, S., Sacco, E., Tralli, A., Castellazzi, G., and de Miranda, S. (2020). “Modeling strategies for the computational analysis of unreinforced masonry structures: review and classification.” *Archives of computational methods in engineering*, Springer, 27, 1153–1185.

D’Amato, M., and Sulla, R. (2021). “Investigations of masonry churches seismic performance with numerical models: Application to a case study.” *Archives of Civil and Mechanical Engineering*, Springer, 21, 1–26.

D’Ayala, D. (2013). “Assessing the seismic vulnerability of masonry buildings.” *Handbook of seismic risk analysis and management of civil infrastructure systems*, Elsevier, 334–365.

Dais, D., Bal, I. E., Smyrou, E., and Sarhosis, V. (2021). “Automatic crack classification and segmentation on masonry surfaces using convolutional neural networks and transfer learning.” *Automation in Construction*, Elsevier, 125, 103606.

DeJong, M. J., and Vibert, C. (2012). “Seismic response of stone masonry spires: Computational and experimental modeling.” *Engineering Structures*, 40, 566–574.

Dell’Endice, A., Iannuzzo, A., DeJong, M. J., Van Mele, T., and Block, P. (2021). “Modelling imperfections in unreinforced masonry structures: Discrete element simulations and scale model experiments of a pavilion vault.” *Engineering Structures*, 228, 111499.

Dice, L. R. (1945). “Measures of the amount of ecologic association between species.” *Ecology*, JSTOR, 26(3), 297–302.

Diz, S., Costa, A., and Costa, A. A. (2015). “Efficiency of strengthening techniques assessed for existing masonry buildings.” *Engineering Structures*, Elsevier, 101, 205–215.

Dizhur, D., and Ingham, J. M. (2015). *Seismic Improvement of Loadbearing Unreinforced Masonry Cavity Walls*. BRANZ.

Dorji, J., Zahra, T., Thambiratnam, D., and Lee, D. (2021). “Strength assessment of old masonry arch bridges through moderate destructive testing methods.” *Construction and Building Materials*, Elsevier, 278, 122391.

Douglas, D. H., and Peucker, T. K. (1973). “Algorithms for the reduction of the number of points required to represent a digitized line or its caricature.” *Cartographica: the international journal for geographic information and geovisualization*, University of Toronto Press, 10(2), 112–122.

Dunkerton, J., and Roy, A. (1996). “The Materials of a Group of Late Fifteenth-century Florentine Panel Paintings.” *National Gallery Technical Bulletin*, 17, 20–31.

Dunphy, K., and Sadhu, A. (2022). “Autonomous crack detection approach for masonry structures using artificial intelligence.” *Recent Developments in Structural Health Monitoring and Assessment–Opportunities and Challenges: Bridges, Buildings and Other Infrastructures*, World Scientific, 253–283.

Eggert, G. (2006). “To Whom the Cracks Tell.” *Studies in Conservation*, 51(1), 69–75.

Elkhuizen, W. S., Callewaert, T. W. J., Leonhardt, E., Vandivere, A., Song, Y., Pont, S. C., Geraedts, J. M. P., and Dik, J. (2019). “Comparison of three 3D scanning techniques for paintings, as applied to Vermeer’s ‘Girl with a Pearl Earring.’” *Heritage Science*, SpringerOpen, 7(1), 1–22.

Ellenberg, A., Kontsos, A., Bartoli, I., and Pradhan, A. (2014). “Masonry crack detection application of an unmanned aerial vehicle.” *Computing in Civil and Building Engineering - Proceedings of the 2014 International Conference on Computing in Civil and Building Engineering*.

Ellenberg, A., Kontsos, A., Moon, F., and Bartoli, I. (2016). “Bridge related damage quantification using unmanned aerial vehicle imagery.” *Structural Control and Health Monitoring*, Wiley Online Library, 23(9), 1168–1179.

Erleben, K., Sporring, J., Henriksen, K., and Dohlmann, H. (2005). *Physics-based Animation*. Charles River Media.

Falsone, G., and Lombardo, M. (2007). “Stochastic representation of the mechanical properties of irregular masonry structures.” *International Journal of Solids and Structures*, Elsevier, 44(25–26), 8600–8612.

Fang, D. L., Napolitano, R. K., Michiels, T. L., and Adriaenssens, S. M. (2018). “Assessing the stability of unreinforced masonry arches and vaults: a comparison of analytical and numerical strategies.” *International Journal of Architectural Heritage*, Taylor & Francis.

Fehm, S. A. (1976). “Luca di Tommè’s Influence on Three Sienese Masters: The Master of the Magdalen Legend, the Master of the Panzano Triptych, and the Master of the Pietà.” *Mitteilungen des Kunsthistorischen Institutes in Florenz*, 20. Bd.(H. 3), 333–350.

Ferreira, T. M., Vicentea, R., and Varum, H. (2014). “Seismic vulnerability assessment of masonry facade walls: development, application and validation of a new scoring method.” *Structural Engineering and Mechanics*, Techno-Press, 50(4), 541–561.

Flores, J. C. (2018). “Entropy Signature for crack networks in old paintings: saturation prospectus.” *Entropy*, MDPI, 20(10), 772.

Foraboschi, P. (2019). “Masonry does not limit itself to only one structural material: Interlocked masonry versus cohesive masonry.” *Journal of Building Engineering*, Elsevier, 26, 100831.

Freeman, A., Doutre, M., Bevan, G., and Murray, A. (2013). “Craquelure Documentation and Analysis: A Preliminary Process Using Reflectance Transformation Imaging and ImageJ.” *UCLA/Getty Program in Archaeological and Ethnographic Conservation*, Association of North American Graduate Programs in Conservation, 15.

Furtado, A., Rodrigues, H., Arêde, A., and Varum, H. (2020). “Mechanical properties characterization of different types of masonry infill walls.” *Frontiers of Structural and Civil Engineering*, Springer, 14, 411–434.

Getty Museum Collection. (2023). “Venus Receiving from Vulcan the Arms of Aeneas.” <https://www.getty.edu/art/collection/object/103R5V>.

Ghaboussi, J. (1988). “Fully deformable discrete element analysis using a finite element approach.” *Computers and Geotechnics*, 5(3), 175–195.

Ghiassi, B., Vermelfoort, A. T., and Lourenço, P. B. (2019). “Masonry mechanical properties.” *Numerical modeling of masonry and historical structures*, Elsevier, 239–261.

Giorgiutti-Dauphiné, F., and Pauchard, L. (2016). “Painting cracks: A way to investigate the pictorial matter.” *Journal of Applied Physics*, 120(6), 065107.

Gobbin, F., de Felice, G., and Lemos, J. V. (2021). “Numerical procedures for the analysis of collapse mechanisms of masonry structures using discrete element modelling.” *Engineering Structures*, Elsevier, 246, 113047.

Goehring, L., Nakahara, A., Dutta, T., Kitsunezaki, S., and Tarafdar, S. (2015). *Desiccation Cracks and their Patterns: Formation and Modelling in Science and Nature*. Wiley.

Gonen, S., Pulatsu, B., Soyoz, S., and Erdogmus, E. (2021). “Stochastic discontinuum analysis of unreinforced masonry walls: Lateral capacity and performance assessments.” *Engineering Structures*, Elsevier, 238, 112175.

Green, S., Bevan, A., and Shapland, M. (2014). “A comparative assessment of structure from motion methods for archaeological research.” *Journal of Archaeological Science*, Elsevier, 46, 173–181.

Griffiths, G. (1978). “The Political Significance of Uccello’s Battle of San Romano.” *Journal of the Warburg and Courtauld Institutes*, 41(1), 313–316.

Gupta, H., Ghosh, D., and Mittal, A. K. (2022). “Identification of Defects in Masonry Structure Using Infrared Thermography.” *Advances in Non Destructive Evaluation: Proceedings of NDE 2020*, Springer, 329–340.

Ham, Y., Lee, S. J., and Chowdhury, A. G. (2017). “Imaging-to-simulation framework for improving disaster preparedness of construction projects and neighboring communities.” *Computing in Civil Engineering 2017*, 230–237.

Hendry, A. W. (2001). “Masonry walls: materials and construction.” *Construction and Building materials*, Elsevier, 15(8), 323–330.

Higgitt, C., and White, R. (2005). “Analyses of paint media: new studies of Italian paintings of the fifteenth and sixteenth centuries.” *National Gallery Technical Bulletin*, NATIONAL GALLERY PUBLICATIONS, LONDON, 26, 89.

Hirata, T. (1989). “Fractal dimension of fault systems in Japan: Fractal structure in rock fracture geometry at various scales.” *Pure and Applied Geophysics PAGEOPH*, 131(1–2), 157–170.

Hossain, M. A., Totoev, Y., and Masia, M. J. (2016). “Friction on mortar-less joints in semi interlocking masonry.” *Proc. 16th International Brick and Block Masonry Conference (IBMAC 2016) Padova (Italy)*, 1635–1643.

Van Houwelingen, H. C., Zwinderman, K. H., and Stijnen, T. (1993). “A bivariate approach to meta-analysis.” *Statistics in medicine*, Wiley Online Library, 12(24), 2273–2284.

Ibrahim, Y., Nagy, B., and Benedek, C. (2019). “CNN-Based Watershed Marker Extraction for Brick Segmentation in Masonry Walls.” *International Conference on Image Analysis and Recognition*, 332–344.

Iglhaut, J., Cabo, C., Puliti, S., Piermattei, L., O’Connor, J., and Rosette, J. (2019). “Structure from motion photogrammetry in forestry: A review.” *Current Forestry Reports*, Springer, 5, 155–168.

Ioannides, M., Fritsch, D., Leissner, J., Davies, R., Remondino, F., and Caffo, R. (2012). *Progress in Cultural Heritage Preservation: 4th International Conference, EuroMed 2012, Lemessos, Cyprus, October 29--November 3, 2012, Proceedings*. Springer Science & Business Media.

Ismaiel, M., Chen, Y., Cruz-Noguez, C., and Hagel, M. (2022). “Thermal resistance of masonry walls: a literature review on influence factors, evaluation, and improvement.” *Journal of Building Physics*, SAGE Publications Sage UK: London, England, 45(4), 528–567.

Jayasinghe, M. T. R. (1998). “Loadbearing construction with local bricks.” Institution of Engineers: Colombo.

Juhásová, E., Sofronie, R., and Bairrao, R. (2008). “Stone masonry in historical buildings—Ways to increase their resistance and durability.” *Engineering Structures*, Elsevier, 30(8), 2194–2205.

Kappos, A. J., Penelis, G. G., and Drakopoulos, C. G. (2002). “Evaluation of simplified models for lateral load analysis of unreinforced masonry buildings.” *Journal of structural Engineering*, American Society of Civil Engineers, 128(7), 890–897.

Kassotakis, N., and Sarhosis, V. (2021). “Employing non-contact sensing techniques for improving efficiency and automation in numerical modelling of existing masonry structures: A critical literature review.” *Structures*, Elsevier, 1777–1797.

Kassotakis, N., Sarhosis, V., Peppa, M.-V., and Mills, J. P. (2022). “Semi-automated discrete-element modelling of arch structures incorporating SfM photogrammetry.” *Proceedings of the Institution of Civil Engineers-Engineering History and Heritage*, Thomas Telford Ltd, 176(1), 3–17.

Kassotakis, N., Sarhosis, V., Peppa, M. V, and Mills, J. (2021). “Quantifying the effect of geometric uncertainty on the structural behaviour of arches developed from direct measurement and Structure-from-Motion (SfM) photogrammetry.” *Engineering Structures*, Elsevier, 230, 111710.

Kassotakis, N., Sarhosis, V., Riveiro, B., Conde, B., D’Altri, A. M., Mills, J., Milani, G., de Miranda, S., and Castellazzi, G. (2020). “Three-dimensional discrete element modelling of rubble masonry structures from dense point clouds.” *Automation in Construction*, Elsevier, 119, 103365.

Kaya, A., Adanur, S., Bello, R. A., Genç, A. F., Okur, F. Y., Sunca, F., Günaydin, M., Altunişik, A. C., and Sevim, B. (2023). “Post-earthquake damage assessments of unreinforced masonry (URM) buildings by shake table test and numerical visualization.” *Engineering Failure Analysis*, Elsevier, 143, 106858.

Kayırga, O. M., and Altun, F. (2021). “Investigation of earthquake behavior of unreinforced masonry buildings having different opening sizes: Experimental studies and numerical simulation.” *Journal of Building Engineering*, Elsevier, 40, 102666.

Kemp, B. J. (2006). *Ancient Egypt: anatomy of a civilization*. Psychology Press.

Kim, S., Park, S. M., Bak, S., Kim, G. H., Kim, C.-S., Jun, J., Kim, C. E., and Kim, K. (2022). “Investigation of craquelure patterns in oil paintings using precise 3D morphological analysis for art authentication.” *Plos one*, Public Library of Science San Francisco, CA USA, 17(7), e0272078.

Klusáček, L., Nečas, R., Požár, M., Pěkník, R., and Svoboda, A. (2021). “Transverse prestressing and reinforced concrete as the key to restoration of masonry arch bridges.” *Engineering Structures*, Elsevier, 245, 112898.

Koellisch, W. (2008). “Umm er Rasas, a World Heritage site, mysterious and hidden. Preventive measures against damage from earthquakes and heavy rains.” *Heritage at Risk*, 73–77.

Kostack, K. (2021). “Bullet Constraints Builder for Blender.”

Koutsoudis, A., Vidmar, B., Ioannakis, G., Arnaoutoglou, F., Pavlidis, G., and Chamzas, C. (2014). “Multi-image 3D reconstruction data evaluation.” *Journal of cultural heritage*, Elsevier, 15(1), 73–79.

Krentowski, J. R., Knyziak, P., Pawłowicz, J. A., and Gavardashvili, G. (2023). "Historical masonry buildings' condition assessment by non-destructive and destructive testing." *Engineering Failure Analysis*, Elsevier, 146, 107122.

Krzemień, L., Łukomski, M., Bratasz, Ł., Kozłowski, R., and Mecklenburg, M. F. (2016). "Mechanism of craquelure pattern formation on panel paintings." *Studies in Conservation*, Taylor & Francis, 61(6), 324–330.

Kumar, S. L., Aravind, H. B., and Hossiney, N. (2019). "Digital image correlation (DIC) for measuring strain in brick masonry specimen using Ncorr open source 2D MATLAB program." *Results in Engineering*, Elsevier, 4, 100061.

Lawrence, S. J., and Gnanakrishnan, N. (1987). "The fire resistance of masonry walls-an overview." *First National Structural Engineering Conference 1987: Preprints of Papers: Preprints of Papers*, Institution of Engineers, Australia Barton, ACT, 431–437.

Ledbury, M., and Hyde, M. L. (2006). *Rethinking Boucher*. Getty Research Institute.

Lee, J., and Kang, H. (2010). "Flood fill mean shift: A robust segmentation algorithm." *International Journal of Control, Automation and Systems*, Springer, 8(6), 1313–1319.

Lee, S. J. (2014). "Developments in Large Scale Discrete Element Simulations with Polyhedral Particles." University of Illinois at Urbana-Champaign, Urbana.

Lee, S. J., and Hashash, Y. M. A. (2015). "iDEM: An impulse-based discrete element method for fast granular dynamics." *International Journal for Numerical Methods in Engineering*, 104(2), 79–103.

Lee, S. J., Shin, M., Lee, C. H., and Tripathi, P. (2022). "Phenotypic trait of particle geometries." *Granular Matter*, 24(3), 79.

Lei, Q., Latham, J.-P., and Tsang, C.-F. (2017). "The use of discrete fracture networks for modelling coupled geomechanical and hydrological behaviour of fractured rocks." *Computers and Geotechnics*, 85, 151–176.

Lei, T., Liu, P., Jia, X., Zhang, X., Meng, H., and Nandi, A. K. (2019). "Automatic fuzzy clustering framework for image segmentation." *IEEE Transactions on Fuzzy Systems*, IEEE, 28(9), 2078–2092.

Lelandais, B., Gardin, I., Mouchard, L., Vera, P., and Ruan, S. (2014). "Dealing with uncertainty and imprecision in image segmentation using belief function theory." *International Journal of Approximate Reasoning*, Elsevier, 55(1), 376–387.

Lemos, J. V., and Campos Costa, A. (2016). “Simulation of Shake Table Tests on Out-Of-Plane Masonry Buildings. Part (V): Discrete Element Approach.” *International Journal of Architectural Heritage*, 1–8.

Lemos, J. V. (2007). “Discrete element modeling of masonry structures.” *International Journal of Architectural Heritage*, Taylor & Francis, 1(2), 190–213.

Lindenbergh, R., and Pietrzyk, P. (2015). “Change detection and deformation analysis using static and mobile laser scanning.” *Applied Geomatics*, Springer, 7(2), 65–74.

Liu, B., Zhu, C., Tang, C.-S., Xie, Y.-H., Yin, L.-Y., Cheng, Q., and Shi, B. (2020). “Bio-remediation of desiccation cracking in clayey soils through microbially induced calcite precipitation (MICP).” *Engineering Geology*, 264, 105389.

Liu, C., Tang, C.-S., Shi, B., and Suo, W.-B. (2013). “Automatic quantification of crack patterns by image processing.” *Computers & Geosciences*, Elsevier, 57, 77–80.

Liu, R., Vail, M., Koohbor, B., Zhu, C., Tang, C.-S., Xu, H., and Shi, X.-C. (2022a). “Desiccation cracking in clay-bottom ash mixtures: insights from crack image analysis and digital image correlation.” *Bulletin of Engineering Geology and the Environment*, 81(4), 139.

Liu, Z., Brigham, R., Long, E. R., Wilson, L., Frost, A., Orr, S. A., and Grau-Bové, J. (2022b). “Semantic segmentation and photogrammetry of crowdsourced images to monitor historic facades.” *Heritage Science*, SpringerOpen, 10(1), 1–17.

Lourenço, P. B. (2002). “Computations on historic masonry structures.” *Progress in Structural Engineering and Materials*, Wiley Online Library, 4(3), 301–319.

Louvre Museum. (1742). “Diane coming out of the bath.” Paris, France.

Loverdos, D., and Sarhosis, V. (2022). “Automatic image-based brick segmentation and crack detection of masonry walls using machine learning.” *Automation in Construction*, Elsevier, 140, 104389.

Loverdos, D., Sarhosis, V., Adamopoulos, E., and Drougkas, A. (2021). “An innovative image processing-based framework for the numerical modelling of cracked masonry structures.” *Automation in Construction*, Elsevier, 125, 103633.

Luo, D., Wang, S., Du, X., Zhao, P., Lu, T., Yang, H., and Frank Chen, Y. (2021). “Health detection techniques for historic structures.” *Materials Testing*, De Gruyter, 63(9), 855–864.

Maev, R. G., Baradarani, A., and Taylor, J. R. B. (2020). “New concept for art and antiquities identification based on craquelure pattern analysis.” *Insight-Non-Destructive Testing and Condition Monitoring*, The British Institute of Non-Destructive Testing, 62(3), 134–138.

Malomo, D., DeJong, M. J., and Penna, A. (2019). “Distinct element modelling of the in-plane cyclic response of URM walls subjected to shear-compression.” *Earthquake Engineering & Structural Dynamics*, 48(12), 1322–1344.

Malomo, D., Pinho, R., and Penna, A. (2020). “Numerical modelling of the out-of-plane response of full-scale brick masonry prototypes subjected to incremental dynamic shake-table tests.” *Engineering Structures*, Elsevier, 209, 110298.

Marques, R., and Lourenço, P. B. (2014). “Unreinforced and confined masonry buildings in seismic regions: Validation of macro-element models and cost analysis.” *Engineering Structures*, Elsevier, 64, 52–67.

Martin, R. M., and Darr, D. R. (1997). “Market responses to the US timber demand-supply situation of the 1990s: Implications for sustainable forest management.” *Forest Products Journal*, Forest Products Society, 47(11/12), 27.

Martínez-Soto, F., Ávila, F., Puertas, E., and Gallego, R. (2021). “Spectral analysis of surface waves for non-destructive evaluation of historic masonry buildings.” *Journal of Cultural Heritage*, Elsevier, 52, 31–37.

Masi, F., Stefanou, I., Maffi-Berthier, V., and Vannucci, P. (2020). “A Discrete Element Method based-approach for arched masonry structures under blast loads.” *Engineering Structures*, 216, 110721.

MathWorks. (2021a). “MATLAB.”

MathWorks. (2021b). “Image Segmenter.” MATLAB (No. R2021a).

MathWorks. (2021c). “Fill image regions and holes - MATLAB imfill.” <https://www.mathworks.com/help/images/ref/imfill.html> (May 24, 2021).

MathWorks. (2021d). “MATLAB R2021a.” Natick, Massachusetts, United States.

MathWorks. (2021e). “Image Segmenter - MATLAB R2021a.” *Image Processing Toolbox*, MATLAB R2021a.

MathWorks. (2023a). “Trace region boundaries in binary image - MATLAB bwboundaries.” <https://www.mathworks.com/help/images/ref/bwboundaries.html> (Feb. 24, 2023).

MathWorks. (2023b). “Area of polygon - MATLAB polyarea.” <https://www.mathworks.com/help/matlab/ref/polyarea.html> (May 3, 2023).

MathWorks. (2023c). “Perimeter of polyshape - MATLAB perimeter.” <https://www.mathworks.com/help/matlab/ref/polyshape.perimeter.html> (Aug. 3, 2023).

Meyer, A. (1995). “Re-dressing Classical Statuary: The Eighteenth-Century ‘Hand-in-Waistcoat’ Portrait.” *The Art Bulletin*, 77(1), 45.

Micelli, F., and Cascardi, A. (2020). “Structural assessment and seismic analysis of a 14th century masonry tower.” *Engineering Failure Analysis*, Elsevier, 107, 104198.

Migliari, R. (2012). “Descriptive geometry: From its past to its future.” *Nexus Network Journal*, Springer, 14(3), 555–571.

Moret, W. (2014). “Vulnerability assessment methodologies: A review of the literature.” *Washington, DC: FHI*, 360.

Muhit, I. B., Raihan, M. T., and Nuruzzaman, M. D. (2014). “Determination of mortar strength using stone dust as a partially replaced material for cement and sand.” *Advances in concrete construction*, Techno-Press, 2(4), 249.

National Park Service. (2014). “Keeping Watch on Surging Seas.” *Experience Your America*.

Nayak, S., and Dutta, S. C. (2016). “Failure of masonry structures in earthquake: A few simple cost effective techniques as possible solutions.” *Engineering Structures*, Elsevier, 106, 53–67.

Newman, M. (2005). “Power laws, Pareto distributions and Zipf’s law.” *Contemporary Physics*, 46(5), 323–351.

Nghiem, H. L., Al Heib, M., and Emeriault, F. (2015). “Method based on digital image correlation for damage assessment in masonry structures.” *Engineering Structures*.

Nowak, R., Kania, T., Rutkowski, R., and Ekiert, E. (2022). “Research and TLS (LiDAR) Construction Diagnostics of Clay Brick Masonry Arched Stairs.” *Materials*, Multidisciplinary Digital Publishing Institute, 15(2), 552.

Nowak, R., Orłowicz, R., and Rutkowski, R. (2020). “Use of TLS (LiDAR) for building diagnostics with the example of a historic building in Karlino.” *Buildings*, Multidisciplinary Digital Publishing Institute, 10(2), 24.

Occhipinti, G., Caliò, I., D’Altri, A. M., Grillanda, N., de Miranda, S., Milani, G., and Spacone, E. (2022). “Nonlinear finite and discrete element simulations of multi-storey masonry walls.” *Bulletin of Earthquake Engineering*, Springer, 20(4), 2219–2244.

Paine, D. J. (2018). “Brown concrete wall photo – Free Brick Image on Unsplash.” *Unsplash*.

Paris, V., Pizzigoni, A., and Adriaenssens, S. (2020). “Statics of self-balancing masonry domes constructed with a cross-herringbone spiraling pattern.” *Engineering Structures*, Elsevier, 215, 110440.

Park, H.-J., Ha, J.-G., Kim, S.-H., and Jo, S.-S. (2019). “Seismic Performance of Ancient Masonry Structures in Korea Rediscovered in 2016 M 5.8 Gyeongju Earthquake.” *Sustainability*, 11(6), 1565.

Pauchard, L., and Giorgiutti-Dauphiné, F. (2020). “Craquelures and pictorial matter.” *Journal of Cultural Heritage*, 46, 361–373.

Pauker, S. G., and Kassirer, J. P. (1980). “The threshold approach to clinical decision making.” *New England Journal of Medicine*, Mass Medical Soc, 302(20), 1109–1117.

Pellegrini, D., Barontini, A., Girardi, M., Lourenço, P. B., Masciotta, M. G., Mendes, N., Padovani, C., and Ramos, L. F. (2023). “Effects of temperature variations on the modal properties of masonry structures: An experimental-based numerical modelling approach.” *Structures*, Elsevier, 595–613.

Peng, B., Zhang, L., and Yang, J. (2009). “Iterated graph cuts for image segmentation.” *Asian Conference on Computer Vision*, 677–686.

Penna, A., Senaldi, I. E., Galasco, A., and Magenes, G. (2016). “Numerical simulation of shaking table tests on full-scale stone masonry buildings.” *International Journal of Architectural Heritage*, Taylor & Francis, 10(2–3), 146–163.

Pepe, M., and Costantino, D. (2020). “Techniques, Tools, Platforms and Algorithms in Close Range Photogrammetry in Building 3D Model and 2D Representation of Objects and Complex Architectures.” *Comput. Aided Des. Appl*, 18, 42–65.

Pepe, M., and Costantino, D. (2021). “UAV Photogrammetry and 3D Modelling of Complex Architecture for Maintenance Purposes: the Case Study of the Masonry Bridge on the Sele River, Italy.” *Periodica Polytechnica Civil Engineering*, 65(1), 191–203.

Pepe, M., Pingaro, M., Trovalusci, P., Reccia, E., and Leonetti, L. (2020). “Micromodels for the in-plane failure analysis of masonry walls: Limit Analysis, FEM and FEM/DEM approaches.” *Frattura e Integrità Strutturale*, 14(51), 504–516.

Pereira, J. M., Campos, J., and Lourenço, P. B. (2015). “Masonry infill walls under blast loading using confined underwater blast wave generators (WBWG).” *Engineering Structures*, Elsevier, 92, 69–83.

Petersen, R. B. (2009). “In-plane shear behaviour of unreinforced masonry panels strengthened with fibre reinforced polymer strips.” University of Newcastle.

Peterson, C. E. (1934). “Distant View of Tower - Fort Jefferson, Key West, FL.” Library of Congress.

Petroman, I., Sava, C., Văduva, L., Marin, D., and Petroman, C. (2020). "Modern forms of historical cultural tourism-case study." *Quaestus*, Dimitrie Cantemir Christian University, Faculty of Management in Tourism and …, (16), 91–104.

Pickwish. (2023). "AI Photo Editor | Free Online Photo Editing Tools." <https://picwish.com/> (Feb. 1, 2023).

Pierdicca, R., Intrigila, C., Piccinini, F., Malinverni, E. S., Giannetti, I., and Caruso, G. (2021). "Multidisciplinary approach for the analysis of structural heritage at risk: the case study of stylite tower at Umm ar-Rasas (Jordan)." *International Journal of Architectural Heritage*, Taylor & Francis, 1–25.

Pikaz, A., and Dinstein, I. hak. (1995). "An algorithm for polygonal approximation based on iterative point elimination." *Pattern Recognition Letters*, Elsevier, 16(6), 557–563.

Pla-Rucki, G. F., and Eberhard, M. O. (1995). "Imaging of reinforced concrete: State-of-the-art review." *Journal of infrastructure systems*, American Society of Civil Engineers, 1(2), 134–141.

Polak, A., Kelman, T., Murray, P., Marshall, S., Stothard, D. J. M., Eastaugh, N., and Eastaugh, F. (2017). "Hyperspectral imaging combined with data classification techniques as an aid for artwork authentication." *Journal of Cultural Heritage*, Elsevier, 26, 1–11.

Popovics, J. S. (2003). "NDE techniques for concrete and masonry structures." *Progress in Structural Engineering and Materials*, Wiley Online Library, 5(2), 49–59.

Praseeda, K. I., Reddy, B. V. V., and Mani, M. (2015). "Embodied energy assessment of building materials in India using process and input–output analysis." *Energy and Buildings*, Elsevier, 86, 677–686.

Pulatsu, B., Bretas, E. M., and Lourenco, P. B. (2016). "Discrete element modeling of masonry structures: Validation and application." Techno Press.

Pulatsu, B., Erdogmus, E., and Bretas, E. M. (2018). "Parametric Study on Masonry Arches Using 2D Discrete-Element Modeling." *Journal of Architectural Engineering*, 24(2), 04018005.

Pulatsu, B., Erdogmus, E., Lourenço, P. B., Lemos, J. V, and Hazzard, J. (2020). "Discontinuum analysis of the fracture mechanism in masonry prisms and wallettes via discrete element method." *Meccanica*, Springer, 55, 505–523.

Pulatsu, B., Erdogmus, E., Lourenço, P. B., and Quey, R. (2019). "Simulation of uniaxial tensile behavior of quasi-brittle materials using softening contact models in DEM." *International Journal of Fracture*, Springer, 217, 105–125.

Pulatsu, B., Kim, S., Erdogmus, E., and Lourenço, P. B. (2021). "Advanced analysis of masonry retaining walls using mixed discrete–continuum approach." *Proceedings of the Institution of Civil Engineers-Geotechnical Engineering*, Thomas Telford Ltd, 174(3), 302–314.

Pushkar, A., Senthilvel, M., and Varghese, K. (2018). "Automated progress monitoring of masonry activity using photogrammetric point cloud." *ISARC. Proceedings of the International Symposium on Automation and Robotics in Construction*, IAARC Publications, 1–7.

Qiu, Q. (2020). "Imaging techniques for defect detection of fiber reinforced polymer-bonded civil infrastructures." *Structural Control and Health Monitoring*, Wiley Online Library, 27(8), e2555.

Radi, K., Jauffrès, D., Deville, S., and Martin, C. L. (2019). "Elasticity and fracture of brick and mortar materials using discrete element simulations." *Journal of the Mechanics and Physics of Solids*, Elsevier, 126, 101–116.

Reid, D. A. (2004). "Teaching Mathematics through Brick Patterns." *Nexus Network Journal*, Springer, 6, 113–123.

Riveiro, B., Lourenço, P. B., Oliveira, D. V., González-Jorge, H., and Arias, P. (2016). "Automatic Morphologic Analysis of Quasi-Periodic Masonry Walls from LiDAR." *Computer-Aided Civil and Infrastructure Engineering*, 31(4), 305–319.

Robb, D. M. (1936). "The Iconography of the Annunciation in the Fourteenth and Fifteenth Centuries." *The Art Bulletin*, 18(4), 480–526.

Roca, J. P. (2013). "I noticed several cracks on my painting. Should I call a conservator? (Part I)." *South Florida Art Conservation LLC*.

Roca, P., Cervera, M., Gariup, G., and Pela', L. (2010). "Structural analysis of masonry historical constructions. Classical and advanced approaches." *Archives of computational methods in engineering*, Springer, 17, 299–325.

Roy, A., and Gordon, D. (2001). "Uccello's Battle of San Romano." *National Gallery Technical Bulletin*, NATIONAL GALLERY PUBLICATIONS, LONDON, 22, 4–17.

Russo, S., and Sciarretta, F. (2013). "Masonry exposed to high temperatures: Mechanical behaviour and properties—An overview." *Fire Safety Journal*, Elsevier, 55, 69–86.

Santini, S., Baggio, C., Sabbatini, V., and Sebastiani, C. (2022). "Seismic Assessment of Roman Concrete Groin Vaults through UAV, NDT and 3D Analyses." *Heritage*, Multidisciplinary Digital Publishing Institute, 5(1), 311–331.

Sarangapani, G., Venkatarama Reddy, B. V, and Jagadish, K. S. (2005). “Brick-mortar bond and masonry compressive strength.” *Journal of materials in civil engineering*, American Society of Civil Engineers, 17(2), 229–237.

Sauer, J., and Schömer, E. (1998). “A constraint-based approach to rigid body dynamics for virtual reality applications.” *Proceedings of the ACM symposium on Virtual reality software and technology*, 153–162.

Schonberger, J. L., and Frahm, J.-M. (2016). “Structure-from-motion revisited.” *Proceedings of the IEEE conference on computer vision and pattern recognition*, 4104–4113.

Schwanghart, W. (2021). “Line Simplification.” *MATLAB Central File Exchange.*, <https://www.mathworks.com/matlabcentral/fileexchange/21132-line-simplification>.

Sejnoha, J., Sejnoha, M., Zeman, J., Sykora, J., and Vorel, J. (2008). “Mesoscopic study on historic masonry.” *arXiv preprint arXiv:0804.3262*.

Shabani, A., Kioumarsi, M., and Zucconi, M. (2021). “State of the art of simplified analytical methods for seismic vulnerability assessment of unreinforced masonry buildings.” *Engineering Structures*, Elsevier, 239, 112280.

Shaun. (2020). “Wall bricks rustic - free photo on pixabay.” <https://pixabay.com/fr/photos/mur-briques-rustique-maçonnerie-5508929/> (May 23, 2021).

Sidorov, O., and Yngve Hardeberg, J. (2019). “Craquelure as a graph: Application of image processing and graph neural networks to the description of fracture patterns.” *Proceedings of the IEEE/CVF International Conference on Computer Vision Workshops*, 0.

Sindel, A., Maier, A., and Christlein, V. (2021). “Craquelurenet: Matching The Crack Structure In Historical Paintings For Multi-Modal Image Registration.” *2021 IEEE International Conference on Image Processing (ICIP)*, IEEE, 994–998.

Smith, S. (1972). “Bonding.” *Brickwork*, Springer, 15–25.

Smoljanović, H., Živaljić, N., and Nikolić, Ž. (2013). “A combined finite-discrete element analysis of dry stone masonry structures.” *Engineering structures*, Elsevier, 52, 89–100.

Sorensen, T. A. (1948). “A method of establishing groups of equal amplitude in plant sociology based on similarity of species content and its application to analyses of the vegetation on Danish commons.” *Biol. Skar.*, 5, 1–34.

Spagnolo, G. S., and Somma, F. (2010). “Virtual restoration of cracks in digitized image of paintings.” *Journal of Physics: Conference Series*, 249, 012059.

Stavroulaki, M. E., Riveiro, B., Drosopoulos, G. A., Solla, M., Koutsianitis, P., and Stavroulakis, G. E. (2016). “Modelling and strength evaluation of masonry bridges using terrestrial photogrammetry and finite elements.” *Advances in Engineering Software*, Elsevier, 101, 136–148.

Stork, D. G. (2009). “Computer vision and computer graphics analysis of paintings and drawings: An introduction to the literature.” *Computer Analysis of Images and Patterns: 13th International Conference, CAIP 2009, Münster, Germany, September 2-4, 2009. Proceedings 13*, Springer, 9–24.

Suchocki, C., Katzer, J., and Rapiński, J. (2018). “Terrestrial laser scanner as a tool for assessment of saturation and moisture movement in building materials.” *Periodica Polytechnica Civil Engineering*, 62(3), 694–699.

Suri, J. S. (2000). “Computer vision, pattern recognition and image processing in left ventricle segmentation: The last 50 years.” *Pattern Analysis & Applications*, Springer, 3(3), 209–242.

Taylor, J. R. B., Baradarani, A., and Maev, R. G. (2015). “Art forgery detection via craquelure pattern matching.” *Computational Forensics: 5th International Workshop, IWCF 2012, Tsukuba, Japan, November 11, 2012 and 6th International Workshop, IWCF 2014, Stockholm, Sweden, August 24, 2014, Revised Selected Papers*, Springer, 176–187.

The Blender Foundation. (2021a). “Blender.”

The Blender Foundation. (2021b). “Blender - a 3D modelling and rendering package.” Amsterdam, Netherlands.

The National Gallery. (2023a). “Four Scenes from the Early Life of Saint Zenobius | NG3918.” <https://www.nationalgallery.org.uk/paintings/sandro-botticelli-four-scenes-from-the-early-life-of-saint-zenobius>.

The National Gallery. (2023b). “Paolo Uccello | The Battle of San Romano | NG583.” <https://www.nationalgallery.org.uk/paintings/paolo-uccello-the-battle-of-san-romano>.

The National Gallery. (2023c). “Jean-Siméon Chardin | The House of Cards | NG4078.” <https://www.nationalgallery.org.uk/paintings/jean-simeon-chardin-the-house-of-cards>.

Theodossopoulos, D., and Sinha, B. (2013). “A review of analytical methods in the current design processes and assessment of performance of masonry structures.” *Construction and Building Materials*, Elsevier, 41, 990–1001.

Thompson, D. V. (1962). *The practice of tempera painting*. Courier Corporation.

Tóth, A. R., Orbán, Z., and Bagi, K. (2009). "Discrete element analysis of a stone masonry arch." *Mechanics Research Communications*, 36(4), 469–480.

Trigger, B. G., Kemp, B. J., O'Connor, D., and Lloyd, A. B. (1983). *Ancient Egypt: a social history*. Cambridge University Press.

Tripathi, P., Lee, S. J., Shin, M., and Lee, C. H. (2023). "Replication Data: 3D Geometry Characterization of Florida and Virginia Mineral Particles." US National Science Foundation (NSF) Designsafe-CI.

Truong-Hong, L., Laefer, D. F., Hinks, T., and Carr, H. (2013). "Combining an angle criterion with voxelization and the flying voxel method in reconstructing building models from LiDAR data." *Computer-Aided Civil and Infrastructure Engineering*, Wiley Online Library, 28(2), 112–129.

Tumialan, J. G., Micelli, F., and Nanni, A. (2001). "Strengthening of masonry structures with FRP composites." *Structures 2001: A Structural Engineering Odyssey*, 1–8.

Tzamtzis, A. D., and Asteris, P. G. (2003). "Finite element analysis of masonry structures: part I-review of previous work." *North American Masonry Conference, Clemson, South Carolina*.

Uccello, P., Berti, L., and Berti, L. (1964). *Paolo Uccello*. Fabbri.

Valero, E., Bosché, F., and Forster, A. (2018). "Automatic segmentation of 3D point clouds of rubble masonry walls, and its application to building surveying, repair and maintenance." *Automation in Construction*, Elsevier, 96, 29–39.

Valero, E., Forster, A., Bosché, F., Hyslop, E., Wilson, L., and Turmel, A. (2019). "Automated defect detection and classification in ashlar masonry walls using machine learning." *Automation in construction*, Elsevier, 106, 102846.

Vallejo, L. E. (2009). "Fractal analysis of temperature-induced cracking in clays and rocks." *Géotechnique*, 59(3), 283–286.

Valluzzi, M. R., and Sbrogiò, L. (2019). "Vulnerability of architectural heritage in seismic areas: Constructive aspects and effect of interventions." *Cultural Landscape in Practice: Conservation vs. Emergencies*, Springer, 203–218.

Vasconcelos, G., and Lourenço, P. B. (2009). "Experimental characterization of stone masonry in shear and compression." *Construction and Building Materials*, Elsevier, 23(11), 3337–3345.

Vemuri, J., Ehteshamuddin, S., and Kolluru, S. (2018). “Numerical simulation of soft brick unreinforced masonry walls subjected to lateral loads.” *Cogent Engineering*, Taylor & Francis, 5(1), 1551503.

Verstrynge, E., Lacidogna, G., Accornero, F., and Tomor, A. (2021). “A review on acoustic emission monitoring for damage detection in masonry structures.” *Construction and Building Materials*, Elsevier, 268, 121089.

Vicente, R., Lagomarsino, S., Ferreira, T. M., Cattari, S., and Mendes da Silva, J. A. R. (2018). “Cultural heritage monuments and historical buildings: conservation works and structural retrofitting.” *Strengthening and retrofitting of existing structures*, Springer, 25–57.

Wang, C., Sarhosis, V., and Nikitas, N. (2018a). “Strengthening/retrofitting techniques on unreinforced masonry structure/element subjected to seismic loads: A literature review.” *Open Construction and Building Technology Journal*, Bentham Open, 12(1), 251–268.

Wang, L., Chang, Y., Wang, H., Wu, Z., Pu, J., and Yang, X. (2017). “An active contour model based on local fitted images for image segmentation.” *Information sciences*, Elsevier, 418, 61–73.

Wang, N., Zhao, Q., Li, S., Zhao, X., and Zhao, P. (2018b). “Damage classification for masonry historic structures using convolutional neural networks based on still images.” *Computer-Aided Civil and Infrastructure Engineering*, Wiley Online Library, 33(12), 1073–1089.

Wang, N., Zhao, X., Zhao, P., Zhang, Y., Zou, Z., and Ou, J. (2019a). “Automatic damage detection of historic masonry buildings based on mobile deep learning.” *Automation in Construction*, Elsevier, 103, 53–66.

Wang, N., Zhao, X., Zhao, P., Zhang, Y., Zou, Z., and Ou, J. (2019b). “Automatic damage detection of historic masonry buildings based on mobile deep learning.” *Automation in Construction*, Elsevier, 103(July 2018), 53–66.

Weber, R. A. (2013). “Building envelope design guide—Masonry wall systems.” *Athena Sustainable Materials Institute*, <https://www.wbdg.org>.

Wilmers, W. (2012). “Restoration of masonry arch bridges.” *Proceedings of the Institution of Civil Engineers-Bridge Engineering*, Thomas Telford Ltd, 135–146.

Yi, T., Moon, F. L., Leon, R. T., and Kahn, L. F. (2006). “Lateral load tests on a two-story unreinforced masonry building.” *Journal of Structural Engineering*, American Society of Civil Engineers, 132(5), 643–652.

Yuan, Q., He, X., Han, X., and Guo, H. (2023). “Automatic recognition of craquelure and paint loss on polychrome paintings of the Palace Museum using improved U-Net.” *Heritage Science*, 11(1), 65.

Zabari, N. (2021). “Analysis of craquelure patterns in historical painting using image processing along with neural network algorithms.” *Optics for Arts, Architecture, and Archaeology VIII*, R. Groves and H. Liang, eds., SPIE, 5.

Zampieri, P., Simoncello, N., Gonzalez-Libreros, J., and Pellegrino, C. (2020). “Evaluation of the vertical load capacity of masonry arch bridges strengthened with FRCM or SFRM by limit analysis.” *Engineering Structures*, Elsevier, 225, 111135.

Zedan, M. F., Al-Sanea, S., Al-Mujahid, A., and Al-Suhaibani, Z. (2016). “Effect of thermal bridges in insulated walls on air-conditioning loads using whole building energy analysis.” *Sustainability*, MDPI, 8(6), 560.

Zeng, H., Tang, C.-S., Zhu, C., Vahedifard, F., Cheng, Q., and Shi, B. (2022). “Desiccation cracking of soil subjected to different environmental relative humidity conditions.” *Engineering Geology*, 297, 106536.

Zhang, S., and Beyer, K. (2019). “Numerical investigation of the role of masonry typology on shear strength.” *Engineering Structures*, Elsevier, 192, 86–102.

Zhang, X., Chiu, Y.-W., and Hao, H. (2022). “Dynamic Tensile Properties of Clay Bricks.” *Mechanics of Materials*, Elsevier, 165, 104157.

Zhang, Y., Tubaldi, E., Macorini, L., and Izzuddin, B. A. (2018). “Mesoscale partitioned modelling of masonry bridges allowing for arch-backfill interaction.” *Construction and Building Materials*, Elsevier, 173, 820–842.

Zini, G., Betti, M., and Bartoli, G. (2022). “Experimental analysis of the traffic-induced-vibration on an ancient lodge.” *Structural Control and Health Monitoring*, Wiley Online Library, 29(3), e2900.

VITA

MOHAMMAD IBRAHIM ABU-HAIFA

Born, Muscat, Oman

2013-2017	B.E., Civil Engineering Jordan University of Science and Technology Irbid, Jordan
2017-2019	M.S., Civil Engineering (Structural Engineering) Jordan University of Science and Technology Irbid, Jordan
2020-2023	Teaching and Research Assistant Florida International University Miami, Florida, USA
2020-2022	Doctoral Candidate, Civil Engineering (Structural Engineering) Florida International University Miami, Florida, USA
2022	UGS Doctoral Evidence Acquisition Fellow Florida International University Miami, Florida, USA
2023	UGS Dissertation Year Fellow Florida International University Miami, Florida, USA

PUBLICATIONS AND PRESENTATIONS

Abu-Haifa, M. and Lee, S.J., 2022. Image-based modeling-to-simulation of masonry walls. *Journal of Architectural Engineering*, *28*(4), p.06022001. https://doi.org/10.1061/(ASCE)AE.1943-5568.0000569

Abu-Haifa, M. and Lee, S.J., 2023. Image-Based 3D Modeling-to-Simulation of Single-wythe Masonry Structure Via Reverse Descriptive Geometry. *Journal of Building Engineering*, 76(10), p.107125. https://doi.org/10.1016/j.jobe.2023.107125

Abu-Haifa, M., Lee, S.J. and Zhu, C., 2023. Phenotypic Trait of Painting Cracks. *Studies in Conservation*. (Under Review).

Abu-Haifa, M. and Lee, S.J., June 9, 2023. An image-based modeling-to-simulation framework for hazard vulnerability assessment of unreinforced masonry structures. *ASCE Engineering Mechanics Institute,* Atlanta, Georgia.

Abu-Haifa, M. and Lee, S.J., April 5, 2022. Image-based modeling-to-simulation framework for hazard vulnerability assessment of un-reinforced masonry structures with typical and irregular bricks. *Graduate Students Appreciation Week,* FIU, Miami, Florida.